

From Core to Detail: Unsupervised Disentanglement with Entropy-Ordered Flows

Daniel Galperin¹ Ullrich Köthe¹

Abstract

Learning unsupervised representations that are both semantically meaningful and stable across runs remains a central challenge in modern representation learning. We introduce entropy-ordered flows (EOFFlows), a normalizing-flow framework that orders latent dimensions by their explained entropy, analogously to PCA’s explained variance. This ordering enables adaptive injective flows: after training, one may retain only the top C latent variables to form a compact core representation while the remaining variables capture fine-grained detail and noise, with C chosen flexibly at inference time rather than fixed during training. EOFFlows build on insights from Independent Mechanism Analysis, Principal Component Flows and Manifold Entropic Metrics. We combine likelihood-based training with local Jacobian regularization and noise augmentation into a method that scales well to high-dimensional data such as images. Experiments on the CelebA dataset show that our method uncovers a rich set of semantically interpretable features, allowing for high compression and strong denoising.

1. Introduction

This paper investigates the unsupervised learning of semantically meaningful features that are stable across training runs and datasets. While feature computation in principle requires only an encoder — as, for example, in self-supervised learning — we study this problem in a normalizing-flow framework in order to leverage exact likelihoods and information-theoretic tools. Specifically, we introduce *entropy-ordered flows* (EOFs), which sort latent dimensions according to their “explained entropy”, analogously to how classical PCA orders components by explained variance. The ordering allows us to construct *adap-*

¹Heidelberg University. Correspondence to: Daniel Galperin <daniel.galperin@iwr.uni-heidelberg.de>, Ullrich Köthe <ullrich.koethe@iwr.uni-heidelberg.de>.

Preprint. Under review.

tive injective flows by keeping only the $C < \dim(Z)$ most important variables. They constitute the *core* subspace of the representation, whereas the remaining features form the *detail* subspace. Crucially, suitable values of C can be determined after training at *inference* time. This sets our concept apart from β -VAEs (Burgess et al., 2018), rectangular flows (Caterini et al., 2021), or \mathcal{M} -flows (Brehmer & Cranmer, 2020), which must fix C as a training hyperparameter.

In order to construct meaningful orderings, our method rests on a key insight from Independent Mechanism Analysis (IMA, [Gresele et al., 2021](#); [Ghosh et al., 2023](#)): Features are statistically independent (i.e. disentangled) when the Jacobian of the decoder has orthogonal columns everywhere. This is approximately achieved when ordinary maximum likelihood training is regularized with the *local IMA contrast*. Indeed, [Reizinger et al. \(2022\)](#) have shown that standard β -VAEs implicitly train for IMA. In their pioneering work on *principal component flows*, [Cunningham et al. \(2022\)](#) designed IMA-based learning strategies for normalizing flows. We propose crucial improvements to their method, most notably the use of noise augmentation according to the *inflation-deflation* principle, which was studied in [Horvat & Pfister \(2022; 2023\)](#) for normalizing flows on lower dimensional manifolds. Interestingly, we find that a substantial amount of noise must be added to achieve stable disentanglement when the intrinsic dimension is much lower than the embedding dimension, as in images.

Entropy-ordered flows admit a natural geometric interpretation. If we view the latent space as a Cartesian coordinate system, the mapping of the core dimensions through the decoder defines an orthogonal curvilinear coordinate system on the C -dimensional reconstruction manifold, capturing the essential structure of the data. The mapping of the detail dimensions similarly defines a curvilinear coordinate system for the residual degrees of freedom, which are lost under dimensionality reduction. In case of a linear map, this corresponds exactly to the null space, and EOFs provide a nonlinear generalization of this decomposition. Following [Galperin & Koethe \(2025\)](#), these curvilinear coordinate systems form the basis for our entropy estimates, which in turn determine the ordering of features by importance.

The entropy spectrum induced by the ordering saturates at

the (natural or augmented) noise entropy of the data. Our experiments show that this often happens at relatively small values of C . This suggests a natural cut-off between core and detail features and provides a practical estimate of the intrinsic dimension of the data. From this perspective, intrinsic dimension is not an absolute quantity, but is fundamentally limited by measurement accuracy: geometric structure below the noise level is statistically indistinguishable from noise, regardless of the true generative dimensionality.

EOFFlows also enable an elegant resolution of the three-way trade-off between rate, distortion, and perception studied in [Blau & Michaeli \(2019\)](#). When reconstructing data from only the C most important features, one may either set the remaining latent variables to zero before decoding, which approximates the optimal distortion at the given rate, or sample them from the latent prior, which guarantees exact recovery of the data distribution and thus optimal perception. [Blau & Michaeli \(2019\)](#) show that the latter increases the distortion by at most a factor of two relative to the former, a bound we verify empirically in Appendix (E.5.8).

Contributions:

- We introduce an information-theoretic framework unifying density estimation, manifold Learning, and feature disentanglement on the basis of normalizing flows. Our training objective, **Maximum Manifold Likelihood**, generalizes maximum likelihood training by decomposing the loss over latent subspaces. This results in adjustable regularizers that steer the model towards disentangled and compressed representations.
- We propose a tractable stochastic estimator for a particular regularization term using Jacobian-vector products, which scales to high dimensions.
- Training on image data produces latent factors that represent distinct semantics and can be sorted by importance. This amounts to a non-linear generalization of principal component analysis in terms of a nearly-orthogonal curvilinear coordinate transformation. This highlights the benefits of learning core and detail features jointly, rather than focusing exclusively on the core representation.

2. Related Work

Unsupervised disentanglement with β -VAEs. The quest for semantically meaningful, independent factors of variation has been largely dominated by the β -VAE framework and its derivatives ([Higgins et al., 2017](#); [Burgess et al., 2018](#); [Kim & Mnih, 2018](#); [Chen et al., 2018](#); [Zhao et al., 2018](#); [Dupont, 2018](#)). These models rely on a bottleneck to enforce the discovery of informative features, often resulting in an inherent trade-off between disentanglement and recon-

struction quality. Recent studies suggest that the success of β -VAEs in disentangling features is closely linked to Independent Mechanism Analysis (IMA), because training is implicitly biased towards decoders with orthogonal Jacobians ([Rolinek et al., 2019](#); [Reizinger et al., 2022](#)). EOFFlows go beyond this by using bijective rather than injective models and can identify core features without an explicit bottleneck.

Normalizing flows for manifold learning. Standard bijective Normalizing Flows (NFs) struggle with data residing on low-dimensional manifolds. This is addressed by injective NF variants like \mathcal{M} -flows ([Brehmer & Cranmer, 2020](#)) and Rectangular Flows ([Caterini et al., 2021](#)). However, they require the intrinsic dimensionality C to be fixed as a training hyperparameter. The GIN method ([Sorrenson et al., 2020](#)) can identify the data manifold with full-dimensional, volume-preserving flows, but needs an auxiliary class label for each instance. In contrast, EOFFlows utilize the Maximum Manifold-Likelihood (MML) framework, which allows for unsupervised partitioning into core and detail subspaces to be determined flexibly at inference time.

Independent mechanism analysis and principal component flows. The insight that statistically independent features correspond to orthogonal columns in the decoder Jacobian is a central result of IMA ([Gresele et al., 2021](#); [Ghosh et al., 2023](#)). This concept was applied to normalizing flows in the form of Principal Component Flows ([Cunningham et al., 2022](#), PCF). While PCF derived the IMA contrast in a principled manner, it faced limited empirical success in scaling to high-dimensional data. Our work advances this line of research by proposing a tractable stochastic loss estimate using Jacobian-vector products.

Importance ordering of the latent features. Inducing a preference to channel important information through specific latent dimensions has been explored through Nested Dropout in both autoencoders ([Rippel et al., 2014](#)) and flows ([Bekasov & Murray, 2020](#)). While these methods encourage importance ordering, they often lack a rigorous information-theoretic grounding for the resulting spectrum. EOFFlows build upon Manifold Entropic Metrics ([Galperin & Koethe, 2025](#)) to define a natural importance ordering.

Inflation-deflation and generative quality. TarFlows ([Zhai et al., 2025](#)), a recently introduced improvement of normalizing flows, have highlighted the importance of adding noise during training. Noise inflation-deflation was formally analyzed by [Horvat & Pfister \(2023; 2022\)](#) and later adopted as a way to mitigate manifold overfitting ([Loaiza-Ganem et al., 2022](#)) and improve generative quality ([Loaiza-Ganem et al., 2023](#)). Their Denoising Normalizing Flows (DNF) ([Horvat & Pfister, 2021](#)) use hard regularization to force noise insensitivity in pre-selected dimensions, whereas EOFFlows auto-adapt the regularization dynamically.

Identification of the true generative factors. Hyvärinen et al. (2023) reviewed under which conditions learned features will correspond to the true generative factors or a trivial transformation of them, and Gresele et al. (2021) showed that IMA rules out well-known counterexamples. Moreover, Buchholz et al. (2022) proved that IMA is locally identifiable and includes a rich class of functions. Since EOFs build upon IMA, these results may hold here as well, but we leave a detailed analysis for future work. We also remark that in many scientific applications the true generative model is already known, but scales poorly with problem size, e.g. the Schrödinger equation in chemistry. Then, generative models are rather tasked with finding a much more efficient *effective* theory, and we expect EOFs to become useful tools in this situation.

3. Method

We consider three goals of generative modeling: **Density Learning** ($Den\mathcal{L}$) aims to approximate the ground-truth PDF $p^*(\mathbf{X})$ by the model PDF $q(\mathbf{X})$, and we focus on normalizing flows (NFs) that achieve this via the *maximum likelihood* objective. **Manifold Learning** ($Man\mathcal{L}$) assumes that the data lie on a manifold and strives to compress the representation accordingly, such that a minimal core subset of the latent dimensions spans the manifold as well as possible. We address this by sorting NF features by importance, so that a dynamic bottleneck can be defined at inference time. **Disentangled Representation Learning** ($Dis\mathcal{L}$) assumes that the true data-generating process is controlled by independent factors of variation. The goal is therefore to enforce statistical independence (*disentanglement*) between the learned features. Here, we build on principal component flows, who first applied the IMA principle to NFs. Specifically, our method combines density learning with disentangled representation learning, and we show that this implicitly leads to manifold learning as well, thanks to our ability to order features according to their explained entropy.

3.1. Normalizing Flows

NFs learn encoder/decoder pairs that define a bijective mapping between data and latent space:

$$\mathbf{z} = \mathbf{f}(\mathbf{x}), \quad \mathbf{x} = \mathbf{g}(\mathbf{z}) := \mathbf{f}^{-1}(\mathbf{z}), \quad (\mathbf{x}, \mathbf{z} \in \mathbb{R}^D). \quad (1)$$

We use invertible neural networks where the decoder is realized by running the encoder backwards, so that \mathbf{f} and \mathbf{g} share the learnable parameters θ . As usual, the latent prior is a standard normal $p(\mathbf{Z} = \mathbf{z}) = \mathcal{N}(\mathbf{z} | 0, \mathbf{I}_D)$. The decoder induces a push-forward distribution $q(\mathbf{X})$ in the data space, whose PDF is given by the change-of-variables formula

$$q(\mathbf{X} = \mathbf{g}(\mathbf{z})) = p(\mathbf{Z} = \mathbf{z}) \cdot |\mathbf{J}(\mathbf{z})|^{-1} \quad \text{with } \mathbf{z} \sim p(\mathbf{Z}) \quad (2)$$

where $\mathbf{J}(\mathbf{z}) := \frac{\partial \mathbf{g}(\mathbf{z}')}{\partial \mathbf{z}'}|_{\mathbf{z}'=\mathbf{z}}$ is the decoder Jacobian at \mathbf{z} and $|\mathbf{A}| := \det(\mathbf{A}^T \mathbf{A})^{\frac{1}{2}}$ the volume of a squared or rectangular matrix. NFs are trained by the maximum likelihood objective, i.e. by minimizing the negative log-likelihood of $q(\mathbf{X})$. For a standard normal latent prior, the loss reads:

$$\begin{aligned} \mathcal{L}_{ML}(\mathbf{x}) &:= -\log(q(\mathbf{X} = \mathbf{x})) \\ &= \frac{1}{2} \|\mathbf{f}(\mathbf{x})\|_2^2 + \log |\mathbf{J}(\mathbf{z} = \mathbf{f}(\mathbf{x}))| + \text{const.} \end{aligned} \quad (3)$$

We use index sets $\mathbb{S} \subseteq \{1, \dots, D\}$, with complement $\bar{\mathbb{S}}$, to specify subsets of latent variables. A latent partition is thus written $[\mathbb{S}, \bar{\mathbb{S}}]$, and the corresponding split of the latent vectors \mathbf{z} is expressed as $\mathbf{z} = [\mathbf{z}_{\mathbb{S}}, \mathbf{z}_{\bar{\mathbb{S}}}]$. Specifically, $[\mathbb{C}, \mathbb{D}]$ refers to a core-detail split after sorting by explained entropy, i.e. $\mathbb{C} := \{1, \dots, C\}$ and $\mathbb{D} := \{C+1, \dots, D\}$. The union of two disjoint subsets \mathbb{S} and \mathbb{T} is denoted as $\mathbb{S}\mathbb{T}$. The submatrix $\mathbf{J}_{\mathbb{S}}(\mathbf{z})$ contains only the columns of the Jacobian $\mathbf{J}(\mathbf{z})$ with indices in \mathbb{S} . Likewise, $\mathbf{f}_{\mathbb{S}}(\mathbf{x})$ is the latent subvector with indices in \mathbb{S} .

3.2. Derivation of the MML training objective

A normalizing flow defines an infinite number of data-space manifolds by implicit equations of the form

$$\mathcal{M}_{\mathbb{S}}(\mathbf{z}_{\bar{\mathbb{S}}}) = \{\mathbf{x} : \mathbf{f}_{\bar{\mathbb{S}}}(\mathbf{x}) = \mathbf{z}_{\bar{\mathbb{S}}}\} \quad (4)$$

The size of \mathbb{S} determines the dimension of $\mathcal{M}_{\mathbb{S}}(\mathbf{z}_{\bar{\mathbb{S}}})$, and $\mathbf{z}_{\bar{\mathbb{S}}}$ its location. The variables in \mathbb{S} define a parameterization of the manifold via the constrained decoder mapping

$$\mathbf{u}_{\mathbb{S}} \in \mathcal{M}_{\mathbb{S}}(\mathbf{z}_{\bar{\mathbb{S}}}) \iff \mathbf{u}_{\mathbb{S}} = \mathbf{g}([\mathbf{z}_{\mathbb{S}}, \mathbf{z}_{\bar{\mathbb{S}}}]) =: \mathbf{g}_{\mathbf{z}_{\bar{\mathbb{S}}}}(\mathbf{z}_{\mathbb{S}}) \quad (5)$$

with $\mathbf{z}_{\mathbb{S}} \in \mathbf{Z}_{\mathbb{S}}$ chosen freely. Thus, the function $\mathbf{g}_{\mathbf{z}_{\bar{\mathbb{S}}}}(\mathbf{z}_{\mathbb{S}})$ maps a Cartesian coordinate system for $\mathbf{Z}_{\mathbb{S}}$ onto an affine or curvilinear coordinate system on $\mathcal{M}_{\mathbb{S}}(\mathbf{z}_{\bar{\mathbb{S}}})$, depending on whether \mathbf{g} is linear or non-linear (see fig. 1).

The latent prior for a subspace \mathbb{S} is also standard normal, $p_{\mathbb{S}}(\mathbf{Z}_{\mathbb{S}} = \mathbf{z}_{\mathbb{S}}) = \mathcal{N}(\mathbf{z}_{\mathbb{S}} | 0, \mathbf{I}_{|\mathbb{S}|})$. The induced **manifold PDF** $q_{\mathbb{S}}(\mathbf{U}_{\mathbb{S}})$ on $\mathcal{M}_{\mathbb{S}}(\mathbf{z}_{\bar{\mathbb{S}}})$ is given by the *injective* change-of-variables formula

$$q_{\mathbb{S}}(\mathbf{U}_{\mathbb{S}} = \mathbf{g}_{\mathbf{z}_{\bar{\mathbb{S}}}}(\mathbf{z}_{\mathbb{S}})) = p_{\mathbb{S}}(\mathbf{Z}_{\mathbb{S}} = \mathbf{z}_{\mathbb{S}}) \cdot |\mathbf{J}_{\mathbb{S}}([\mathbf{z}_{\mathbb{S}}, \mathbf{z}_{\bar{\mathbb{S}}}])|^{-1} \quad (6)$$

Consider an index set \mathbb{U} that is further partitioned into disjoint subsets \mathbb{S} and \mathbb{T} such that $\mathbb{U} = \mathbb{S}\mathbb{T}$. Then the manifold PDF on $\mathcal{M}_{\mathbb{U}}(\mathbf{z}_{\bar{\mathbb{U}}})$ factorizes according to

$$q_{\mathbb{S}\mathbb{T}}(\mathbf{U}_{\mathbb{S}\mathbb{T}} = \mathbf{x}) = q_{\mathbb{S}}(\mathbf{U}_{\mathbb{S}} = \mathbf{x}) \cdot q_{\mathbb{T}}(\mathbf{U}_{\mathbb{T}} = \mathbf{x}) \cdot q_{\mathbb{S}\perp\mathbb{T}}(\mathbf{x}) \quad (7)$$

where $\mathbf{x} = \mathbf{g}([\mathbf{z}_{\mathbb{S}}, \mathbf{z}_{\mathbb{T}}, \mathbf{z}_{\bar{\mathbb{U}}}]$). The mixture term $q_{\mathbb{S}\perp\mathbb{T}} := q_{\mathbb{S}\mathbb{T}}/(q_{\mathbb{S}} \cdot q_{\mathbb{T}}) \geq 1$ accounts for the entanglement of $\mathbf{U}_{\mathbb{S}}$ and $\mathbf{U}_{\mathbb{T}}$. It is bounded below due to Hadamard's inequality, and equality is achieved if and only if the two random variables

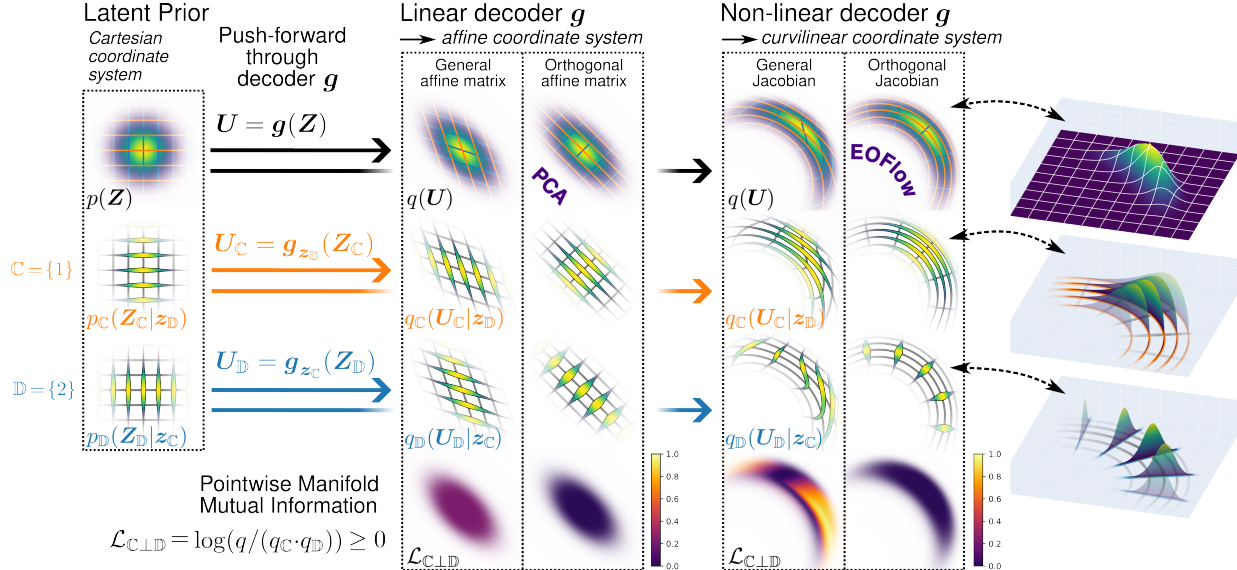


Figure 1. Depiction of different push-forwards of a latent standard normal (left) through linear (center) and non-linear (right) decoders, inducing affine and curvilinear coordinates in the data space respectively. Line width and color indicate the conditional densities along the coordinate lines in rows 2 and 3. Row 4 shows the pointwise manifold mutual information between U_C and U_D , defined as $\mathcal{L}_{C \perp D} = \log(q/(q_C \cdot q_D)) \geq 0$, which is a non-linear generalization of the classical correlation. Linear decoders can only generate Gaussian distributions, and the PCA-solution induces orthogonal coordinates such that q factorizes exactly into q_C and q_D . EOFows extend this to non-Gaussian distributions and non-linear mappings. When the decoder Jacobian has orthogonal columns everywhere, the resulting curvilinear coordinates become orthogonal, resembling polar coordinates in this example. Only in the orthogonal cases, $\mathcal{L}_{C \perp D}$ vanishes everywhere and the constituent densities factorize "cleanly" as $q = q_C \cdot q_D$ (purple in the bottom row).

are statistically independent. Since the standard normal prior factorizes and the corresponding contributions cancel, the entanglement term simplifies into a ratio of Jacobian determinants

$$q_{S \perp T} = |\mathbf{J}_S| \cdot |\mathbf{J}_T| / |\mathbf{J}_{ST}| \quad (8)$$

Although it does not correspond to a probability density, we write $q_{S \perp T}$ for notational convenience.

Using the preceding formulas, we now derive the Maximum Manifold Likelihood objective as a combination of density, manifold and disentanglement learning. We define the *pointwise manifold entropy*¹ of a point \mathbf{x} in its role as a member of a manifold over indices \mathbb{S} as the negative logarithm of $q_{\mathbb{S}}$ evaluated at \mathbf{x} :

$$\mathcal{L}_{\mathbb{S}}(\mathbf{x}) := -\log(q_{\mathbb{S}}(\mathbf{U}_{\mathbb{S}} = \mathbf{x})) \quad (9)$$

The manifold $\mathcal{M}_{\mathbb{S}}(z_{\bar{\mathbb{S}}})$ and the corresponding PDF $q_{\mathbb{S}}(\mathbf{U}_{\mathbb{S}})$ are uniquely defined by the decomposition $\mathbf{f}(\mathbf{x}) = [\mathbf{z}_{\mathbb{S}}, \mathbf{z}_{\bar{\mathbb{S}}}]$ of the encoder output induced by \mathbb{S} . Analogously, we define the *pointwise manifold mutual information*² between two disjoint subsets \mathbb{S} and \mathbb{T} as

$$\begin{aligned} \mathcal{L}_{S \perp T}(\mathbf{x}) &:= \mathcal{L}_{\mathbb{S}}(\mathbf{x}) + \mathcal{L}_{\mathbb{T}}(\mathbf{x}) - \mathcal{L}_{ST}(\mathbf{x}) \\ &\equiv \log(q_{S \perp T}(\mathbf{x})) \end{aligned} \quad (10)$$

¹Compare with manifold entropy $H_{\mathbb{S}}$ (Galperin & Koethe, 2025).

²Compare with manifold mutual information $I_{S,T}$ (Galperin & Koethe, 2025).

When $\mathbb{T} = \bar{\mathbb{S}}$, we have $\mathcal{L}_{ST} \equiv \mathcal{L}_{ML}$. Specifically, for the core/detail split $\mathbb{S} = \mathbb{C}$ and $\mathbb{T} = \mathbb{D}$, the ML objective decomposes as

$$\mathcal{L}_{ML} = \mathcal{L}_{\mathbb{C}} + \mathcal{L}_{\mathbb{D}} - \mathcal{L}_{C \perp D} \quad (11)$$

We finally define our **Maximum Manifold Likelihood** (MML) objective by weighting the terms in this expression with hyperparameters $\lambda_{\mathbb{C}}, \lambda_{\mathbb{D}}, \lambda_{C \perp D}$:

$$\begin{aligned} \mathcal{L}_{MML}(\mathbf{x}) &:= (1 + \lambda_{\mathbb{C}}) \mathcal{L}_{\mathbb{C}}(\mathbf{x}) + (1 + \lambda_{\mathbb{D}}) \mathcal{L}_{\mathbb{D}}(\mathbf{x}) \\ &\quad + (\lambda_{C \perp D} - 1) \mathcal{L}_{C \perp D}(\mathbf{x}) \end{aligned} \quad (12)$$

The regular ML objective is recovered when all weights are zero. Equivalently, one can view MML as ML with additional regularization:

$$\mathcal{L}_{MML} = \mathcal{L}_{ML} + \lambda_{\mathbb{C}} \cdot \mathcal{L}_{\mathbb{C}} + \lambda_{\mathbb{D}} \cdot \mathcal{L}_{\mathbb{D}} + \lambda_{C \perp D} \cdot \mathcal{L}_{C \perp D} \quad (13)$$

We refer to this joint goal by *ManDisDenL* as it combines *DenL* (\mathcal{L}_{ML}), *ManL* ($\mathcal{L}_{\mathbb{C}}/\mathcal{L}_{\mathbb{D}}$) and *DisL* ($\mathcal{L}_{C \perp D}$) into one objective, which will be clear soon. Using the properties of the standard normal prior and the injective change-of-variables formula, we can express the regularization terms explicitly

$$\begin{aligned} \mathcal{L}_{\mathbb{S}}(\mathbf{x}) &= \frac{1}{2} \|\mathbf{f}_{\mathbb{S}}(\mathbf{x})\|_2^2 + \log |\mathbf{J}_{\mathbb{S}}(\mathbf{f}(\mathbf{x}))| + \frac{|\mathbb{S}|}{2} \log(2\pi) \\ \mathcal{L}_{S \perp T}(\mathbf{x}) &= \log |\mathbf{J}_{\mathbb{S}}(\mathbf{f}(\mathbf{x}))| + \log |\mathbf{J}_{\mathbb{T}}(\mathbf{f}(\mathbf{x}))| \\ &\quad - \log |\mathbf{J}_{ST}(\mathbf{f}(\mathbf{x}))| \end{aligned} \quad (14)$$

When \mathbb{S} and \mathbb{T} are recursively subdivided further, we get a partition into M disjoint index sets $\mathcal{P} = [\mathbb{S}_1, \mathbb{S}_2, \dots, \mathbb{S}_M]$, whose MML loss becomes:

$$\mathcal{L}_{\text{MML}} = \mathcal{L}_{\text{ML}} + \lambda_{\perp} \cdot \mathcal{L}_{\mathbb{S}_1 \perp \dots \perp \mathbb{S}_M} + \sum_{\mathbb{S} \in \mathcal{P}} \lambda_{\mathbb{S}} \cdot \mathcal{L}_{\mathbb{S}} \quad (15)$$

Note that there is only a single disentanglement term with regularization parameter λ_{\perp} . Of particular interest will be the partition into singletons $\mathbb{S}_j = \{j\}$.

3.3. Entropy ordering and disentanglement

In order to sort latent features by importance, we must determine their explained entropy. More generally, we calculate the *manifold entropy* $H_{\mathbb{S}}$ of any subspace \mathbb{S} using the methodology from [Galperin & Kothe \(2025\)](#):

$$\begin{aligned} H_{\mathbb{S}} &:= H(\mathbf{U}_{\mathbb{S}}) = \mathbb{E}_{\mathbf{z} \sim p(\mathbf{Z})} [-\log(q_{\mathbb{S}}(\mathbf{U}_{\mathbb{S}} = \mathbf{g}(\mathbf{z})))] \\ &= \mathbb{E}_{\mathbf{x} \sim q(\mathbf{X})} [\mathcal{L}_{\mathbb{S}}(\mathbf{x})] \end{aligned} \quad (16)$$

The second form is just a reparametrization of the first in terms of the change-of-variables formula. The manifolds $\mathcal{M}_{\mathbb{S}}(\mathbf{z}_{\mathbb{S}})$ and corresponding PDFs $q_{\mathbb{S}}(\mathbf{U}_{\mathbb{S}})$ are again uniquely determined by the latent vector split $\mathbf{z} = [\mathbf{z}_{\mathbb{S}}, \mathbf{z}_{\mathbb{T}}]$. When $\mathbb{S} = \{j\}$ is a singleton, we get the explained entropy needed for sorting. However, comparison of two manifold entropies $H_{\mathbb{S}}$ and $H_{\mathbb{T}}$ is only meaningful if their sum is (approximately) equal to the total manifold entropy $H_{\mathbb{S}\mathbb{T}}$. Thus, we must also ensure that the *manifold mutual information* $\mathcal{I}_{\mathbb{S},\mathbb{T}} := \mathcal{I}(\mathbf{U}_{\mathbb{S}}, \mathbf{U}_{\mathbb{T}})$ is small:

$$\begin{aligned} \mathcal{I}_{\mathbb{S},\mathbb{T}} &= \mathbb{E}_{\mathbf{z} \sim p(\mathbf{Z})} \left[\log \left(\frac{q_{\mathbb{S}\mathbb{T}}(\mathbf{U}_{\mathbb{S}\mathbb{T}} = \mathbf{g}(\mathbf{z}))}{q_{\mathbb{S}}(\mathbf{U}_{\mathbb{S}} = \mathbf{g}(\mathbf{z}))q_{\mathbb{T}}(\mathbf{U}_{\mathbb{T}} = \mathbf{g}(\mathbf{z}))} \right) \right] \\ &= \mathbb{E}_{\mathbf{x} \sim q(\mathbf{X})} [\mathcal{L}_{\mathbb{S}\perp\mathbb{T}}(\mathbf{x})] \end{aligned} \quad (17)$$

3.4. Important special cases

When the dimension C of the core space is defined beforehand, the properties of the resulting core/detail split can be controlled explicitly by particular choices of the MML hyperparameters. One possibility is to emphasize **Core-Detail Disentanglement** by setting $\lambda_{\mathbb{C}} = \lambda_{\mathbb{D}} = 0$, resulting in the specialized MML loss

$$\mathcal{L}_{\text{MML}}(\mathbf{x}) = \mathcal{L}_{\text{ML}}(\mathbf{x}) + \lambda_{\mathbb{C}\perp\mathbb{D}} \cdot \mathcal{L}_{\mathbb{C}\perp\mathbb{D}}(\mathbf{x}), \quad \lambda_{\mathbb{C}\perp\mathbb{D}} > 0 \quad (18)$$

When the regularizer attains its lower bound $\mathcal{L}_{\mathbb{C}\perp\mathbb{D}} = 0$, the manifold mutual information vanishes, $\mathcal{I}_{\mathbb{C},\mathbb{D}} \rightarrow 0$, and \mathbb{C} and \mathbb{D} are perfectly disentangled. As $\mathcal{L}_{\mathbb{C}\perp\mathbb{D}}$ is a realization of DisDenL , eq.(18) jointly achieves DisDenL .

Alternatively, one can emphasize **Core-Detail Compression**, which means that one desires $H_{\mathbb{C}}/|\mathbb{C}| \gg H_{\mathbb{D}}/|\mathbb{D}|$. When the inequality holds, the information loss from disregarding the details $\mathbf{z}_{\mathbb{D}}$ is minimized. This is achieved by

setting $\lambda_{\mathbb{C}} = \lambda_{\mathbb{C}\perp\mathbb{D}} = 0$:

$$\mathcal{L}_{\text{MML}}(\mathbf{x}) = \mathcal{L}_{\text{ML}}(\mathbf{x}) + \lambda_{\mathbb{D}} \cdot \mathcal{L}_{\mathbb{D}}(\mathbf{x}), \quad \lambda_{\mathbb{D}} > 0 \quad (19)$$

This minimizes the information content in \mathbb{D} , since \mathcal{L}_{ML} is bounded from below by the true data entropy. Mathematically, we could also include $\lambda_{\mathbb{C}} \cdot \mathcal{L}_{\mathbb{C}}(\mathbf{x})$ with $\lambda_{\mathbb{C}} < 0$, but this lead to instable training in our experiments.

EOFlow compression is closely related to minimization of the L2 reconstruction error. Setting $\mathbf{z}_{\mathbb{D}} = 0$ before reconstruction means that all reconstructed data points $\hat{\mathbf{x}} = \mathbf{g}_{\mathbf{z}_{\mathbb{D}}=0}(\mathbf{f}_{\mathbb{C}}(\mathbf{x}))$ are located on the manifold $\mathcal{M}_{\mathbb{C}}(\mathbf{z}_{\mathbb{D}} = 0)$, analogously to the reconstruction manifold of an autoencoder. Conversely, all points in the complementary manifold, $\mathbf{x} \in \mathcal{M}_{\mathbb{D}}(\mathbf{z}_{\mathbb{C}} = \text{const})$ map to the *same* reconstruction $\hat{\mathbf{x}}$. When the $\mathcal{M}_{\mathbb{D}}(\mathbf{z}_{\mathbb{C}})$ are linear subspaces of the data domain and the conditional data distributions, given $\mathbf{z}_{\mathbb{C}}$, are isotropic Gaussian (a reasonable assumption when the off-manifold deviations are induced by additive noise), our compression loss minimizes the L2 error as well, see [Appendix B](#). From this we see that $\mathcal{L}_{\mathbb{D}}$ is a realization of ManL , thus eq.(19) jointly achieves ManDenL .

In order to select C *after* training (instead of fixing it beforehand), we need to ensure that the dimension-wise manifold entropies $H_j := H_{\mathbb{S}}$ with $\mathbb{S} = \{j\}$ are meaningfully comparable. That is, we must enforce disentanglement between all pairs j and j' . To this end, we define the *pointwise manifold total correlation*³ between the features as

$$\begin{aligned} \mathcal{L}_{\text{TC}}(\mathbf{x}) &:= \mathcal{L}_{1\perp 2 \perp \dots \perp D}(\mathbf{x}) = \sum_{j=1}^D \mathcal{L}_j(\mathbf{x}) - \mathcal{L}_{\text{ML}}(\mathbf{x}) \\ &= \sum_{j=1}^D \log |\mathbf{J}_j(\mathbf{f}(\mathbf{x}))| - \log |\mathbf{J}(\mathbf{f}(\mathbf{x}))| \end{aligned} \quad (20)$$

with \mathcal{L}_j a shorthand of the pointwise manifold entropy of a single feature. The **Total Disentanglement** objective also realizes DisDenL and specializes the MML loss:

$$\mathcal{L}_{\text{MML}}(\mathbf{x}) = \mathcal{L}_{\text{ML}}(\mathbf{x}) + \lambda_{\text{TC}} \cdot \mathcal{L}_{\text{TC}}(\mathbf{x}), \quad \lambda_{\text{TC}} > 0 \quad (21)$$

Since \mathcal{L}_{ML} is bounded from below, this loss induces vanishing total correlation between the features, $\mathcal{I}_{\text{TC}} \rightarrow 0$, upon perfect convergence. Our experiments exclusively use total disentanglement (21), since it allows for efficient approximation and gives very good results.

It was shown in [Cunningham et al. \(2022\)](#) that vanishing core-detail or total disentanglement are equivalent to the property that the respective Jacobian sub-matrices span orthogonal subspaces:

$$\mathcal{L}_{\mathbb{C}\perp\mathbb{D}}(\mathbf{x}) = 0 \Leftrightarrow \mathbf{J}_{\mathbb{C}}(\mathbf{f}(\mathbf{x})) \perp \mathbf{J}_{\mathbb{D}}(\mathbf{f}(\mathbf{x})) \quad (22)$$

$$\forall j' \neq j : \mathcal{L}_{\text{TC}}(\mathbf{x}) = 0 \Leftrightarrow \mathbf{J}_j(\mathbf{f}(\mathbf{x})) \perp \mathbf{J}_{j'}(\mathbf{f}(\mathbf{x})) \quad (23)$$

³Compare with manifold total correlation \mathcal{I}_{TC} ([Galperin & Kothe, 2025](#)).

Sorrenson et al. (2025) showed that the requirement of exact orthogonality is too restrictive, as it severely constrains the admissible function families for \mathbf{f} and \mathbf{g} . Our regularization treats orthogonality as a soft constraint regulated by λ_{TC} which avoids loss of model expressiveness and still arrives at nearly orthogonal solutions.

When the data distribution $p^*(\mathbf{X})$ is Gaussian, the optimal decoder is linear, $\mathbf{g}(\mathbf{z}) = \mathbf{A}\mathbf{z} + \mathbf{b}$. DenL alone fits \mathbf{b} to the data mean and \mathbf{A} to the square root of the data covariance matrix, still leaving $D(D-1)/2$ rotational degrees of freedom in \mathbf{A} . In this linear regime, we analytically verify that our objective of ManDisDenL converges to the optimal PCA-solution. We elaborate on this in Appendix D. In particular we proof that both ManDenL , implemented through recursive Core-Detail Compression, and DisDenL , implemented through Total Disentanglement, each independently lead to the PCA-solution and thus implicitly perform ManDisDenL . We hypothesize that DisDenL alone can induce ManL in the non-linear regime as well. Ultimately this means that the **Total Disentanglement**-goal may be sufficient to learn both disentangled and compressed representations.

4. Experiments

4.1. Inflation approach

Empirically we find that for successful DisDenL we rely training on inflated data samples, i.e. adding a large amount of isotropic gaussian noise as

$$\mathbf{x}_\epsilon := \mathbf{x} + \sigma_\epsilon \cdot \epsilon \quad \text{with } \mathbf{x} \sim p^*, \epsilon \sim \mathcal{N}(\mathbf{0}, \mathbf{I}_D) \quad (24)$$

While this "noise augmentation" visibly corrupts data samples and irreversibly destroys data structures below a threshold, EOFflows permit sampling noise-free samples via a dynamic bottleneck, effectively denoising/deflating the inflated distribution.

4.2. Numerical estimate of Total Disentanglement

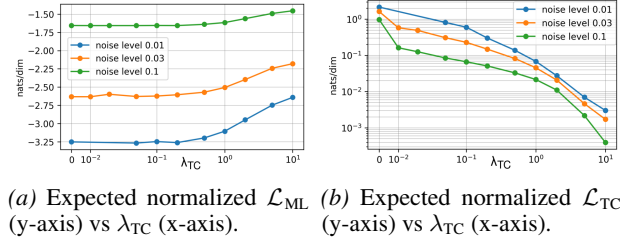
We introduce an unbiased stochastic estimate of the Total Disentanglement term \mathcal{L}_{TC} from eq.(21) which scales well to high-dimensional data. We first note that the determinant-term in each \mathcal{L}_i reduces to the L2-norm of the column vector \mathbf{J}_i . Thus only a single jacobian-vector-product (jvp) of a unit vector \mathbf{e}_i is needed to compute \mathcal{L}_i . As \mathcal{L}_{TC} requires a sum of \mathcal{L}_i over $i \in \{1, \dots, D\}$, it would make the computation scale linearly with D . However, we observe that for a batch of samples with batchsize $B \geq D$, the sum over \mathcal{L}_i can be well approximated by a stochastic estimate which only requires one jvp per batch, thus scaling to arbitrary dimensions. For this, we form a batch of unit vectors with B

randomly sampled indices⁴. Crucially, our estimate requires a batchsize greater or equal to D , which ensures that the "effective batchsize" for each \mathcal{L}_i -term in \mathcal{L}_{TC} remains ≥ 1 . Although this limitation requires sufficient GPU memory for large D , we believe it can be lifted, but leave this for future works. Finally, the training time wrt to ML-training increases by a factor of ≈ 2.5 , independent of D . More details and python code can be found in the Appendix C.

4.3. EMNIST

We train EOFflows on EMNIST digits ($D = 28 \times 28 = 784$) over three noise scales $\sigma_\epsilon \in [0.01, 0.03, 0.1]$ and Total Disentanglement strengths λ_{TC} ranging from 0.01 to 10, including vanilla ML Training at $\lambda_{\text{TC}} = 0$.

In figure fig.(2) we plot the expected Negative Log-Likelihood $\mathbb{E}_{\mathbf{x}} [\mathcal{L}_{\text{ML}}(\mathbf{x})]$ and Manifold Total Correlation $\mathbb{E}_{\mathbf{x}} [\mathcal{L}_{\text{TC}}(\mathbf{x})]$ for each run. The former is a measure of successful DenL and the latter of successful DisL , where lower is usually better. As expected, increasing λ_{TC} steadily improves DisL . We can also observe a tradeoff between DenL and DisL as training with a large λ_{TC} leads to an increase in \mathcal{L}_{ML} beyond some threshold. However, this tradeoff is favorable as it starts taking effect only at $\lambda_{\text{TC}} \approx 0.1 - 1.0$ and increases with increasing σ_ϵ . We also note that higher noise levels allow better DisL at constant λ_{TC} while weakening the tradeoff between DenL and DisL . This indicates that strongly inflated data is easier to learn under the joint goal of DisDenL and motivates us to set the noise level as large as possible.



(a) Expected normalized \mathcal{L}_{ML} (b) Expected normalized \mathcal{L}_{TC}
(y-axis) vs λ_{TC} (x-axis). (y-axis) vs λ_{TC} (x-axis).

Figure 2. Multiple EOFflows trained on EMNIST with varying noise level $\sigma_\epsilon \in \{0.01, 0.03, 0.1\}$ and varying Total Disentanglement strength $\lambda_{\text{TC}} \in [0, 10]$.

When analyzing the learned curvilinear coordinates, indirectly via Jacobian column vectors \mathbf{J}_i , we find recurring features resembling downsampling artifacts, as shown in fig. (3) for $\sigma_\epsilon = 0.01, \lambda_{\text{TC}} = 0.1$. As the noise level is sufficiently low, these features are unlikely to be "hallucinated" and must be present in the data itself. We hypothesize that they stem from the EMNIST-“conversion process” as outlined in Cohen et al. (2017). Noteworthy, these features are not present in MNIST, see Appendix E.3.

⁴We additionally ensure that each dimension is chosen at least once per batch.

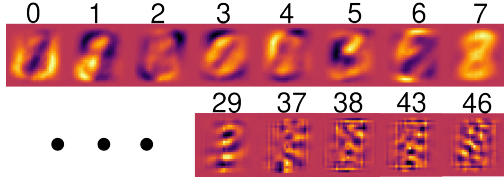


Figure 3. Average Jacobian column vectors $\mathbb{E} [J_i]$ of selected latent dimensions, where each image is normalized for increased contrast. High entropy dimensions (top row) are responsible for global factors such as slant, thickness, etc. Low entropy dimensions (bottom row) indicate preprocessing artifacts in EMNIST.

This result demonstrates the strength of our bijective approach: Although though most data features have low entropy - which injective models simply discard as noise - their application-dependent significance can only be assessed after training with all dimensions, as this could provide important insights into the data generation process.

4.4. Entangled Digits Dataset

To test the efficacy of our Total Disentanglement regularization, we train on a toy-dataset, coined "Entangled Digits". For this we construct *entangled* data samples which consist of sampling the digits 0, $\mathbf{x}^{\{0\}}$, and 1, $\mathbf{x}^{\{1\}}$, from EMNIST and superimposing their pixel values with a uniformly sampled weight $\alpha \sim \mathcal{U}_{[0,1]}$ s.t. $\mathbf{x}^{\{01\}} = \alpha \mathbf{x}^{\{0\}} + (1 - \alpha) \mathbf{x}^{\{1\}}$. We anticipate that a model trained by *DisDenL* on entangled samples, without access to α , will be able to distill or *disentangle* a given $\mathbf{x}^{\{01\}}$ back into its original constituents $\mathbf{x}^{\{0\}}$ and $\mathbf{x}^{\{1\}}$.

After training, we compute the manifold entropy of all latent dimensions H_i and reorder them in decreasing order s.t. $H_1 > H_2 > \dots > H_D$. Indeed we find that the first⁵ latent dimension is solely responsible for interpolating from one digit to the other. This can be observed in fig.(4) once for inflated samples and once additionally using a bottleneck with $C = 100$. We show that our EOFlow can successfully recover the corresponding digit 0 or 1 from entangled samples at $\alpha = 0.5$, simply by editing the latent code to ± 2 .⁶ Quantitatively we observe a strong absolute correlation of 0.92 between $z_1 = f_1(\mathbf{x}^{\{01\}})$ and α on the test set, see Appendix E.4.

4.5. CelebA

We chose CelebA as an easily interpretable high-dimensional dataset which was also studied by β -VAEs. Furthermore, we assume that CelebA essentially consists of

⁵We use 0-based indexing in the experiments as opposed to 1-based indexing in the formulas.

⁶We can not expect this procedure to reveal information which was not part of the entangled sample, e.g. for $\alpha = 0$, $\mathbf{x}^{\{01\}}$ only contains information of digit 1 as $\mathbf{x}^{\{0\}}$.

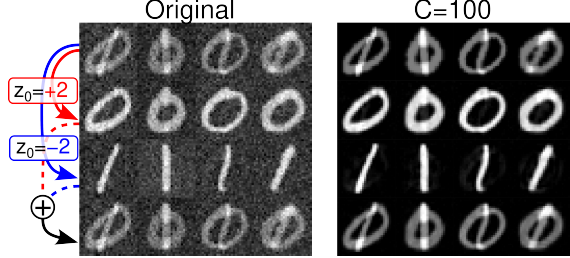


Figure 4. Disentangling entangled digits. Left block shows 4 random samples (left to right) of inflated data samples, right block mirrors the left block with a latent bottleneck of $C = 100$. Top row: Entangled data samples of $\alpha = 0.5$. Second/third row: The most important latent dimension is edited to the value $+2/-2$. Bottom row: Superposition of 2nd and 3rd row, which closely resembles the original 1st row.

one data cluster and thus closely resembles the topology of the latent prior.⁷ We train EOFows on samples from CelebA which are center cropped and downsampled to a resolution of $D = 28 \times 28 \times 3 = 2352$, and inflated strongly with a noise level of $\sigma_\epsilon = 0.1$. To this end we train multiple NFs with $\lambda_{TC} \in \{0, 0.01, 0.1, 1.0\}$ and perform PCA, which can be viewed as a linearized Normalizing Flow. See Appendix E for more details on the architecture, training and results.

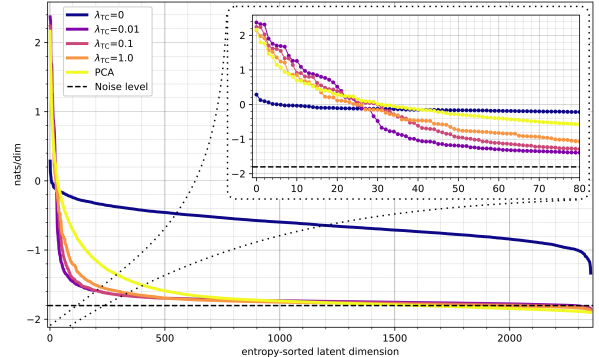


Figure 5. Manifold entropy spectra of multiple EOFows trained on CelebA with $\sigma_\epsilon = 0.1$ and varying $\lambda_{TC} \in \{0, 0.01, 0.1, 1.0\}$, where we additionally plot the PCA-solution as a linearized EOFow. The noise level becomes a lower bound on the manifold entropy and allows to specify a natural cutoff between core and detail dimensions.

The latent dimensions are re-ordered by decreasing manifold entropy. We depict the entropy spectra for all models in fig.(5), where we additionally show the entropy of the noise level $H_{\sigma_\epsilon} := 1/2 + \log(\sigma_\epsilon)$ ⁸ as a lower bound. Models

⁷One can see this intuitively by checking whether the data mean itself is in- or out-of-distribution. The average of all CelebA human faces roughly resembles a face, thus ID, whereas the average of all EMNIST digits does not resemble anything meaningful, thus OOD.

⁸For simplicity we drop the constant normalization factor of $1/2 \cdot \log(2\pi)$ in all entropy measures.

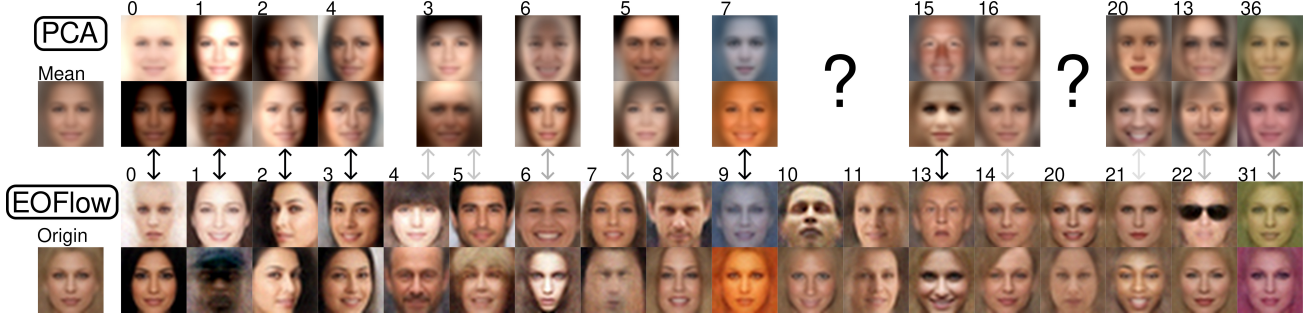


Figure 6. Archetypes of latent features in PCA (top) vs EOFFlow with $\lambda_{TC} = 1.0$ (bottom) on CelebA for selected dimensions, ordered from most important (left) to less important (right) by manifold entropy. Each archetype depicts the extreme deviations of the indicated latent dimensions after altering the latent codes ± 4 from the origin. Most PCA archetypes only vaguely resemble EOFFlow’s analogues.

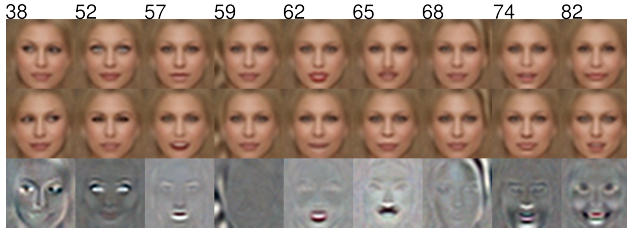


Figure 7. Archetypes of latent features learned by EOFFlow which depict local variations, not found in PCA. The two top rows show traversing ± 4 of a single latent dimension from the origin. The bottom row depicts a normalized contrast between both extremes.

succeeding at $\mathcal{M}an\mathcal{L}$ optimize the rate-distortion trade-off and should thus have an entropy spectrum which decays quickly to the noise level. Ultimately this allows one to set a small bottleneck dimension C without loosing much information.

We observe that the entropy spectrum of the unregularized model ($\lambda_{TC} = 0$) is flat, where each dimension induces a similar amount of information, and it fails at $\mathcal{M}an\mathcal{L}$. All models regularized with Total Disentanglement exhibit a sharp drop in entropy after the first few dimensions which saturates quickly at the noise level, while the spectrum of PCA decreases substantially slower.

Quantitatively we again note a slight negative impact of $\mathcal{Dis}\mathcal{L}$ on $\mathcal{Den}\mathcal{L}$ as shown in tab.(1). However this tradeoff appears favorable as it takes effect only at $\lambda_{TC} \gtrsim 0.01$.

Table 1. Expected Negative Log-Likelihood and Manifold Total Correlation for EOFflows of varying λ_{TC} trained on CelebA.

λ_{TC}	0	0.01	0.1	1.0
$\mathbb{E}_{\mathbf{x}} [\mathcal{L}_{ML}(\mathbf{x})]$	-1.729	-1.730	-1.717	-1.691
$\mathbb{E}_{\mathbf{x}} [\mathcal{L}_{TC}(\mathbf{x})]$	1.104	0.048	0.033	0.012

$\mathcal{Dis}\mathcal{L}$ encourages Archetype Learning: To demonstrate the rich and interpretable representation learned by EOFflows, fig. 6 shows ”archetypes” of selected latent dimensions (see Appendix E.5.4 for tentative semantic interpreta-

tions) and compares them with PCA. For this, we generate images from latent codes which deviate from the origin $\mathbf{z} = \mathbf{0}$ in a single dimension $z_i = \pm 4$. The corresponding PCA archetypes are formed by adding an eigenvector, rescaled with $\pm 4 \times$ the standard deviation, to the data mean.

We observe that EOFFlow archetypes are much less blurry than their PCA analogous while representing distinct, almost cartoonish, representatives of human faces. It is possible to match some EOFFlow archetypes with those of PCA, depicted by vertical arrows of varying opacity, although the similarity is mostly limited.

If we compare multiple trained EOFflows, we find strongly matching archetypes, see Appendix E.5.4. This hints at the fact that Total Disentanglement training is sufficient to form a *canonical* curvilinear coordinate system representing the intrinsic data structure, independent of architecture biases. However for the weak Total Disentanglement regularization $\lambda_{TC} = 0.01$, the archetypes become less clear and entangled, e.g. multiple latent features capture one semantic factor, indicating a lower threshold of required $\mathcal{Dis}\mathcal{L}$ for which meaningful representations can be learned.

$\mathcal{M}an\mathcal{L}$ through dynamic bottlenecks: EOFflows indirectly acquire the ability to strongly compress information via a dynamically adjustable bottleneck of C dimensions. In fig.(8) we show how EOFFlow’s dynamic bottleneck can reconstruct an original clean image \mathbf{x} from an inflated noisy one \mathbf{x}_ϵ with only $C = 50$ dimensions, while progressively removing finer details for even smaller C .

In fig.(9) we show that EOFflows attain high compression at low rates, demonstrating that a sufficiently small core representation deflates noisy data by only retaining high-entropy information, as seen in the manifold entropy spectra. For smaller λ_{TC} the distortion becomes even better, as it appears that less $\mathcal{Dis}\mathcal{L}$ can slightly improve $\mathcal{M}an\mathcal{L}$. For the model with $\lambda_{TC} = 0.01$ the PSNR can even surpass the denoising baseline, which is computed using Tweedie’s formula using the unregularized model.

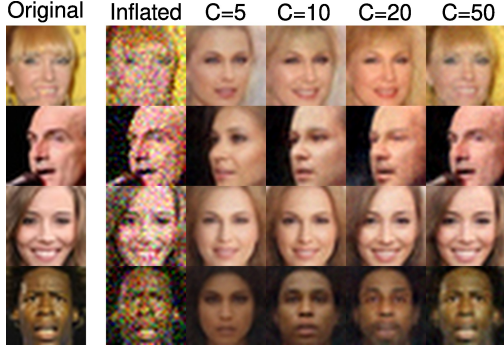


Figure 8. Reconstructions of noise-inflated training samples with bottleneck sizes $C \in \{5, 10, 20, 50\}$ at regularization $\lambda_{TC} = 0.1$.

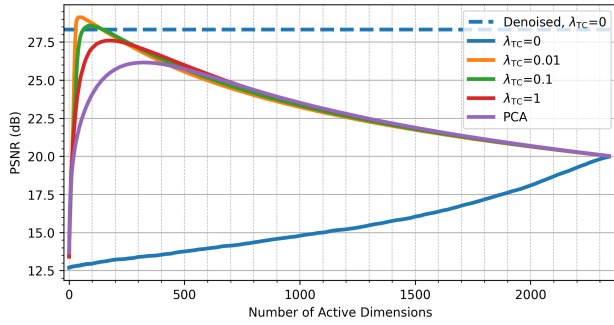


Figure 9. Rate-distortion curves of all trained EOFLOWS and PCA. The bottleneck size C (x-axis) varies from 0 to D where the distance metric is PSNR (y-axis), where higher is better. The distance is measured between clean samples \mathbf{x} and the bottleneck reconstructions of the associated noisy samples \mathbf{x}_ϵ by zeroing out the detail code. In dashed we plot the PSNR of classical denoising, given by Tweedies formula, using the unregularized model.

5. Conclusion

Our findings support our initial hypothesis that $DisDen\mathcal{L}$ induces $Man\mathcal{L}$ to a sufficient degree in the non-linear regime. Sole regularization by Total Disentanglement enables EOFLOWS to obtain interpretable and compressed data representations.

Acknowledgement

This work is supported by Deutsche Forschungsgemeinschaft (DFG, German Research Foundation) under Germany’s Excellence Strategy EXC-2181/1 - 390900948 (the Heidelberg STRUCTURES Cluster of Excellence). It is also supported by the Carl-Zeiss-Stiftung (Projekt P2021-02-001 “Model-based AI”). DG acknowledges support by the German Federal Ministry of Education and Research (BMBF) (project EMUNE/031L0293A). The authors acknowledge support by the state of Baden-Württemberg through bwHPC and the German Research Foundation (DFG) through grant INST 35/1597-1 FUGG. UK thanks the Klaus Tschira Stiftung for their support via the SIMPLAIX project.

Impact Statement

This paper presents work whose goal is to advance the field of Machine Learning. There are many potential societal consequences of our work, none which we feel must be specifically highlighted here.

References

Bekasov, A. and Murray, I. Ordering dimensions with nested dropout normalizing flows, 2020.

Blau, Y. and Michaeli, T. Rethinking lossy compression: The rate-distortion-perception tradeoff. In Chaudhuri, K. and Salakhutdinov, R. (eds.), *Proceedings of the 36th International Conference on Machine Learning*, volume 97 of *Proceedings of Machine Learning Research*, pp. 675–685. PMLR, 09–15 Jun 2019.

Brehmer, J. and Cranmer, K. Flows for simultaneous manifold learning and density estimation. In Larochelle, H., Ranzato, M., Hadsell, R., Balcan, M., and Lin, H. (eds.), *Advances in Neural Information Processing Systems*, volume 33, pp. 442–453. Curran Associates, Inc., 2020.

Buchholz, S., Besserve, M., and Schölkopf, B. Function classes for identifiable nonlinear independent component analysis. In Koyejo, S., Mohamed, S., Agarwal, A., Belgrave, D., Cho, K., and Oh, A. (eds.), *Advances in Neural Information Processing Systems*, volume 35, pp. 16946–16961. Curran Associates, Inc., 2022.

Burgess, C. P., Higgins, I., Pal, A., Matthey, L., Watters, N., Desjardins, G., and Lerchner, A. Understanding disentangling in β -vae, 2018.

Caterini, A. L., Loaiza-Ganem, G., Pleiss, G., and Cunningham, J. P. Rectangular flows for manifold learning. In Ranzato, M., Beygelzimer, A., Dauphin, Y., Liang, P., and Vaughan, J. W. (eds.), *Advances in Neural Information Processing Systems*, volume 34, pp. 30228–30241. Curran Associates, Inc., 2021.

Chen, R. T. Q., Li, X., Grosse, R. B., and Duvenaud, D. K. Isolating sources of disentanglement in variational autoencoders. In Bengio, S., Wallach, H., Larochelle, H., Grauman, K., Cesa-Bianchi, N., and Garnett, R. (eds.), *Advances in Neural Information Processing Systems*, volume 31. Curran Associates, Inc., 2018.

Cohen, G., Afshar, S., Tapson, J., and van Schaik, A. Emnist: an extension of mnist to handwritten letters, 2017.

Cunningham, E., Cobb, A. D., and Jha, S. Principal component flows. In Chaudhuri, K., Jegelka, S., Song, L., Szepesvari, C., Niu, G., and Sabato, S. (eds.), *Proceedings of the 39th International Conference on Machine*

Learning, volume 162 of *Proceedings of Machine Learning Research*, pp. 4492–4519. PMLR, 17–23 Jul 2022.

Defazio, A., Yang, X., Mehta, H., Mishchenko, K., Khaled, A., and Cutkosky, A. The road less scheduled. In Globerson, A., Mackey, L., Belgrave, D., Fan, A., Paquet, U., Tomczak, J., and Zhang, C. (eds.), *Advances in Neural Information Processing Systems*, volume 37, pp. 9974–10007. Curran Associates, Inc., 2024. doi: 10.52202/079017-0320.

Dinh, L., Sohl-Dickstein, J., and Bengio, S. Density estimation using real NVP. In *International Conference on Learning Representations*, 2017.

Dupont, E. Learning disentangled joint continuous and discrete representations. In Bengio, S., Wallach, H., Larochelle, H., Grauman, K., Cesa-Bianchi, N., and Garnett, R. (eds.), *Advances in Neural Information Processing Systems*, volume 31. Curran Associates, Inc., 2018.

Durkan, C., Bekasov, A., Murray, I., and Papamakarios, G. Neural spline flows. In Wallach, H., Larochelle, H., Beygelzimer, A., d'Alché-Buc, F., Fox, E., and Garnett, R. (eds.), *Advances in Neural Information Processing Systems*, volume 32. Curran Associates, Inc., 2019.

Galperin, D. and Kothe, U. Analyzing generative models by manifold entropic metrics. In *The 28th International Conference on Artificial Intelligence and Statistics*, 2025.

Ghosh, S., Gresele, L., von Kügelgen, J., Besserve, M., and Schölkopf, B. Independent mechanism analysis and the manifold hypothesis. In *Causal Representation Learning Workshop at NeurIPS 2023*, 2023.

Gresele, L., Kügelgen, J. V., Stimper, V., Schölkopf, B., and Besserve, M. Independent mechanism analysis, a new concept? In Beygelzimer, A., Dauphin, Y., Liang, P., and Vaughan, J. W. (eds.), *Advances in Neural Information Processing Systems*, 2021.

Gu, J., Chen, T., Berthelot, D., Zheng, H., Wang, Y., ZHANG, R., Dinh, L., Bautista, M. Á., Susskind, J. M., and Zhai, S. STARFlow: Scaling latent normalizing flows for high-resolution image synthesis. In *The Thirty-ninth Annual Conference on Neural Information Processing Systems*, 2025.

Higgins, I., Matthey, L., Pal, A., Burgess, C., Glorot, X., Botvinick, M., Mohamed, S., and Lerchner, A. beta-VAE: Learning basic visual concepts with a constrained variational framework. In *International Conference on Learning Representations*, 2017.

Horvat, C. and Pfister, J.-P. Denoising normalizing flow. In Ranzato, M., Beygelzimer, A., Dauphin, Y., Liang, P., and Vaughan, J. W. (eds.), *Advances in Neural Information Processing Systems*, volume 34, pp. 9099–9111. Curran Associates, Inc., 2021.

Horvat, C. and Pfister, J.-P. Intrinsic dimensionality estimation using normalizing flows. In Koyejo, S., Mohamed, S., Agarwal, A., Belgrave, D., Cho, K., and Oh, A. (eds.), *Advances in Neural Information Processing Systems*, volume 35, pp. 12225–12236. Curran Associates, Inc., 2022.

Horvat, C. and Pfister, J.-P. Density estimation on low-dimensional manifolds: an inflation-deflation approach. *Journal of Machine Learning Research*, 24(61):1–37, 2023.

Hyvärinen, A., Khemakhem, I., and Morioka, H. Nonlinear independent component analysis for principled disentanglement in unsupervised deep learning. *Patterns*, 4(10), 2023.

Kim, H. and Mnih, A. Disentangling by factorising. In Dy, J. and Krause, A. (eds.), *Proceedings of the 35th International Conference on Machine Learning*, volume 80 of *Proceedings of Machine Learning Research*, pp. 2649–2658. PMLR, 10–15 Jul 2018.

Kingma, D. P. and Dhariwal, P. Glow: Generative flow with invertible 1x1 convolutions. In Bengio, S., Wallach, H., Larochelle, H., Grauman, K., Cesa-Bianchi, N., and Garnett, R. (eds.), *Advances in Neural Information Processing Systems*, volume 31. Curran Associates, Inc., 2018.

Loaiza-Ganem, G., Ross, B. L., Cresswell, J. C., and Caterini, A. L. Diagnosing and fixing manifold overfitting in deep generative models. *Transactions on Machine Learning Research*, 2022. ISSN 2835-8856. Expert Certification.

Loaiza-Ganem, G., Ross, B. L., Wu, L., Cunningham, J. P., Cresswell, J. C., and Caterini, A. L. Denoising deep generative models. In Antorán, J., Blaas, A., Feng, F., Ghalebikesabi, S., Mason, I., Pradier, M. F., Rohde, D., Ruiz, F. J. R., and Schein, A. (eds.), *Proceedings on "I Can't Believe It's Not Better! - Understanding Deep Learning Through Empirical Falsification" at NeurIPS 2022 Workshops*, volume 187 of *Proceedings of Machine Learning Research*, pp. 41–50. PMLR, 03 Dec 2023.

Reizinger, P., Gresele, L., Brady, J., von Kügelgen, J., Zietlow, D., Schölkopf, B., Martius, G., Brendel, W., and Besserve, M. Embrace the gap: Vaes perform independent mechanism analysis. In Koyejo, S., Mohamed, S., Agarwal, A., Belgrave, D., Cho, K., and Oh, A. (eds.), *Advances in Neural Information Processing Systems*, volume 35, pp. 12040–12057. Curran Associates, Inc., 2022.

Rippel, O., Gelbart, M., and Adams, R. Learning ordered representations with nested dropout. In Xing, E. P. and Jebara, T. (eds.), *Proceedings of the 31st International Conference on Machine Learning*, volume 32 of *Proceedings of Machine Learning Research*, pp. 1746–1754, Beijing, China, 22–24 Jun 2014. PMLR.

Rolinek, M., Zietlow, D., and Martius, G. Variational autoencoders pursue pca directions (by accident). In *Proceedings of the IEEE/CVF Conference on Computer Vision and Pattern Recognition (CVPR)*, June 2019.

Sorrenson, P., Rother, C., and Köthe, U. Disentanglement by nonlinear ica with general incompressible-flow networks (gin). In *International Conference on Learning Representations*, 2020.

Sorrenson, P., Lührs, L., Olischläger, H., and Köthe, U. Beyond diagonal covariance: Flexible posterior vaes via free-form injective flows, 2025. URL <https://arxiv.org/abs/2506.01522>.

Zhai, S., ZHANG, R., Nakkiran, P., Berthelot, D., Gu, J., Zheng, H., Chen, T., Bautista, M. Á., Jaitly, N., and Susskind, J. M. Normalizing flows are capable generative models. In *Forty-second International Conference on Machine Learning*, 2025.

Zhao, S., Song, J., and Ermon, S. Infovae: Information maximizing variational autoencoders, 2018.

Appendix

A. Derivation

A.1. Normalizing Flows

Normalizing Flows (NF) transform data samples to the latent space via the encoder

$$\mathbf{z} = \mathbf{f}(\mathbf{x}) \quad (\text{A.1})$$

and latent samples back to data space via the decoder

$$\mathbf{x} = \mathbf{g}(\mathbf{z}) := \mathbf{f}^{-1}(\mathbf{z}) \quad (\text{A.2})$$

which is defined as the exact inverse of \mathbf{f} . Both encoder and decoder are parametrized by learnable and shared parameters θ . We omit writing out the dependence of \mathbf{f} and \mathbf{g} , and subsequent derived quantities, on θ .

The latent prior p is usually assumed to be a standard normal distribution. Its probability density function (PDF) is

$$p(\mathbf{Z} = \mathbf{z}) = \mathcal{N}(\mathbf{z} \mid 0, \mathbf{I}_D) \quad (\text{A.3})$$

To generate synthetic data points, one samples from the latent prior and pushes the instances to data space through the decoder.

NFs are an instance in the class of push-forward generative models (e.g. VAEs, GANs, Diffusion Models) as they induce a probability measure in the data space by the means of a push-forward of the latent PDF via the decoder. We denote the random variable induced in the data-space as $\mathbf{U} := \mathbf{g}(\mathbf{Z})$. The associated push-forward PDF q can be written explicitly via the change-of-variables formula:

$$q(\mathbf{U} = \mathbf{g}(\mathbf{z})) = p(\mathbf{Z} = \mathbf{z}) \cdot |\mathbf{J}(\mathbf{z})|^{-1} \quad (\text{A.4})$$

where we denote the Jacobian of the decoder at point \mathbf{z} as $\mathbf{J}(\mathbf{z}) := \frac{\partial \mathbf{g}(\mathbf{z}')}{\partial \mathbf{z}'} \Big|_{\mathbf{z}'=\mathbf{z}}$ and $|\cdot|$ denotes the volume of a squared or rectangular matrix $\mathbf{A} \in \mathbb{R}^{n \times m}$ with $n \geq m$ according to $|\mathbf{A}| := \det(\mathbf{A}^T \mathbf{A})^{\frac{1}{2}}$.

A.2. Maximum Likelihood

NFs are trained by the **Maximum Likelihood**-objective, that is, they maximize the likelihood of observing data samples sampled from the ground truth PDF $\mathbf{x} \sim p^*(\mathbf{x})$. This is equivalent to minimizing the Negative Log-Likelihood of the push-forward PDF evaluated at data points \mathbf{x} . Thus we write the point-wise estimate, i.e. the loss function, as:

$$\begin{aligned} \mathcal{L}_{\text{ML}}(\mathbf{x}) &:= -\log(q(\mathbf{U} = \mathbf{x})) \\ &= \frac{1}{2} |\mathbf{f}(\mathbf{x})|_2^2 + \log |\mathbf{J}(\mathbf{f}(\mathbf{x}))| + \text{const.} \end{aligned} \quad (\text{A.5})$$

where in the second step we used eq.(A.4, A.3) and $|\cdot|_2^2$ denotes the L2-norm of a vector.

A.3. Split

To specify subsets of individual latent variables, we use index sets $\mathbb{S} \subseteq \{1, \dots, D\}$, with complement $\bar{\mathbb{S}}$, such that we can write the split of all indices into a partition \mathcal{P} of two index sets as $\mathcal{P} = [\mathbb{S}, \bar{\mathbb{S}}]$. A corresponding split of the latent vector \mathbf{z} is expressed as $\mathbf{z} = [\mathbf{z}_{\mathbb{S}}, \mathbf{z}_{\bar{\mathbb{S}}}]$.

Furthermore, we usually denote \mathbb{S} and \mathbb{T} as the disjoint split of an arbitrary joint index set $\mathbb{S}\mathbb{T}$. We also denote the specific partition $\mathcal{P} = [\mathbb{C}, \mathbb{D}]$ as the core-detail split where the indices in \mathbb{C} and \mathbb{D} go from smallest to largest, i.e. $\mathbb{C} := \{1, \dots, C\}$ and $\mathbb{D} := \{C+1, \dots, D\}$. Finally, the submatrix $\mathbf{J}_{\mathbb{S}}(\mathbf{z})$ contains only the columns of $\mathbf{J}(\mathbf{z})$ with indices in \mathbb{S} .

Finally, using eq.(A.3), we can factorize the latent PDF into its constituents by the core-detail split

$$p(\mathbf{Z} = [\mathbf{z}_{\mathbb{C}}, \mathbf{z}_{\mathbb{D}}]) = p_{\mathbb{C}}(\mathbf{Z}_{\mathbb{C}} = \mathbf{z}_{\mathbb{C}}) \cdot p_{\mathbb{D}}(\mathbf{Z}_{\mathbb{D}} = \mathbf{z}_{\mathbb{D}}) \quad (\text{A.6})$$

where $p_{\mathbb{C}}(\mathbf{Z}_{\mathbb{C}} = \mathbf{z}_{\mathbb{C}}) = \mathcal{N}(\mathbf{z}_{\mathbb{C}} | 0, \mathbf{I}_{|\mathbb{C}|})$ and $p_{\mathbb{D}}(\mathbf{Z}_{\mathbb{D}} = \mathbf{z}_{\mathbb{D}}) = \mathcal{N}(\mathbf{z}_{\mathbb{D}} | 0, \mathbf{I}_{|\mathbb{D}|})$ are the marginal PDFs.

A.4. Derivation recipe

We adapt to definitions given in Galperin & Koethe (2025) and Cunningham et al. (2022):

Definition A.1 (Curvilinear coordinates). We define the set of **curvilinear coordinates** $\mathbf{u}_{\mathbb{S}}$ by varying a subset of latent dimensions $\mathbf{z}_{\mathbb{S}}$, while the remaining ones $\mathbf{z}_{\bar{\mathbb{S}}}$ are kept fixed, mapped through the decoder:

$$\mathbf{u}_{\mathbb{S}} := \mathbf{g}_{\mathbf{z}_{\bar{\mathbb{S}}}}(\mathbf{z}_{\mathbb{S}}) \equiv \mathbf{g}(\mathbf{z} = [\mathbf{z}_{\mathbb{S}}, \mathbf{z}_{\bar{\mathbb{S}}}] \text{ with } \mathbf{z}_{\bar{\mathbb{S}}} \text{ fixed}) \quad (\text{A.7})$$

Definition A.2 (Curvilinear manifold). We define the **curvilinear manifold** $\mathcal{M}_{\mathbb{S}}(\mathbf{z}_{\bar{\mathbb{S}}})$ as the set of all $\mathbf{u}_{\mathbb{S}}$ at constant $\mathbf{z}_{\bar{\mathbb{S}}}$:

$$\mathcal{M}_{\mathbb{S}}(\mathbf{z}_{\bar{\mathbb{S}}}) = \{ \mathbf{x} = \mathbf{g}_{\mathbf{z}_{\bar{\mathbb{S}}}}(\mathbf{z}_{\mathbb{S}}) : \mathbf{z}_{\mathbb{S}} \in \mathbb{R}^{|\mathbb{S}|} \} \quad (\text{A.8})$$

This allows us to denote the associated random variable $\mathbf{U}_{\mathbb{S}}$, which lives on the curvilinear manifold $\mathcal{M}_{\mathbb{S}}(\mathbf{z}_{\bar{\mathbb{S}}})$ as:

$$\mathbf{U}_{\mathbb{S}} = \mathbf{g}_{\mathbf{z}_{\bar{\mathbb{S}}}}(\mathbf{Z}_{\mathbb{S}}) \quad (\text{A.9})$$

Definition A.3 (Manifold PDF). We define the **manifold PDF** $q_{\mathbb{S}}$ as the push-forward of the marginal PDF $p_{\mathbb{S}}(\mathbf{Z}_{\mathbb{S}})$ through the decoder \mathbf{g} . It is induced via the injective change-of-variables formula on the curvilinear manifold as

$$q_{\mathbb{S}}(\mathbf{U}_{\mathbb{S}}) = p_{\mathbb{S}}(\mathbf{Z}_{\mathbb{S}} = \mathbf{z}_{\mathbb{S}}) \cdot |\mathbf{J}_{\mathbb{S}}([\mathbf{z}_{\mathbb{S}}, \mathbf{z}_{\bar{\mathbb{S}}}]])|^{-1} \quad (\text{A.10})$$

Even though $q_{\mathbb{S}}$ is only defined on one particular curvilinear manifold, one can always find the correct curvilinear manifold $\mathcal{M}_{\mathbb{S}}(\mathbf{z}_{\bar{\mathbb{S}}})$, which goes through any \mathbf{x} by specifying $\mathbf{z}_{\bar{\mathbb{S}}} = \mathbf{f}_{\bar{\mathbb{S}}}(\mathbf{x})$. Put simply, there is an infinite set of curvilinear manifolds and there always exists one at each data point \mathbf{x} .

It is easy to see that eq.(A.10) reduces to the usual change-of-variables formula by setting $\mathbb{S} = \{1, \dots, D\}$ s.t. $q_{\mathbb{S}} \equiv q$.

A.5. Factorization of manifold PDF

For a general $[\mathbb{S}, \mathbb{T}]$ -split we observe that the manifold PDF of the joint index set can always be rewritten to

$$q_{\mathbb{S}\mathbb{T}}(\mathbf{U} = \mathbf{x}) = q_{\mathbb{S}}(\mathbf{U}_{\mathbb{S}} = \mathbf{x}) \cdot q_{\mathbb{T}}(\mathbf{U}_{\mathbb{T}} = \mathbf{x}) \cdot q_{\mathbb{S}\perp\mathbb{T}}(\mathbf{x}) \quad (\text{A.11})$$

where we define the mixture term $q_{\mathbb{S}\perp\mathbb{T}} := q_{\mathbb{S}\mathbb{T}} / (q_{\mathbb{S}} \cdot q_{\mathbb{T}})$. This equation can be interpreted as a point-wise factorization, although "clean" factorization would imply that the mixture term drops everywhere, i.e. $q_{\mathbb{S}\perp\mathbb{T}}(\mathbf{x}) = 1 \forall \mathbf{x}$.

Using eq.(A.10) and the factorization of the prior, the mixture term simplifies to $q_{\mathbb{S}\perp\mathbb{T}} \equiv |\mathbf{J}_{\mathbb{S}}| \cdot |\mathbf{J}_{\mathbb{T}}| / |\mathbf{J}_{\mathbb{S}\mathbb{T}}|$. It is bounded, due to Hadamard's inequality, $q_{\mathbb{S}\perp\mathbb{T}} \geq 1$. This was noted in

Thus equality represents a "clean" factorization of $q_{\mathbb{S}\mathbb{T}}$ into $q_{\mathbb{S}}$ and $q_{\mathbb{T}}$. Importantly, as $q_{\mathbb{S}\perp\mathbb{T}}(\mathbf{x})$ solely depends on change-of-volume terms, it does not represent a proper push-forward density. Nonetheless we denote it by q for notational convenience.

A.6. Maximum Manifold-Likelihood Training

Definition A.4 (Pointwise Manifold Entropy). We define the **pointwise manifold entropy** (\mathbf{x} -ME) $\mathcal{L}_{\mathbb{S}}(\mathbf{x})$ as the negative logarithm of $q_{\mathbb{S}}$ evaluated at a point \mathbf{x} :

$$\begin{aligned} \mathcal{L}_{\mathbb{S}}(\mathbf{x}) &:= -\log(q_{\mathbb{S}}(\mathbf{U}_{\mathbb{S}} = \mathbf{x})) \\ &= \frac{1}{2} |\mathbf{f}_{\mathbb{S}}(\mathbf{x})|_2^2 + \log |\mathbf{J}_{\mathbb{S}}(\mathbf{f}(\mathbf{x}))| + \frac{|\mathbb{S}|}{2} \log(2\pi) \end{aligned} \quad (\text{A.12})$$

where we used eq.(A.10,A.3).

This term was derived in Principal Component Flows (PCF) (Cunningham et al., 2022) under the name "log likelihood of a contour".

Definition A.5 (Pointwise Manifold Mutual Information). We define the **pointwise manifold mutual information** (\mathbf{x} -MMI) $\mathcal{L}_{\mathbb{S} \perp \mathbb{T}}(\mathbf{x})$ as the logarithm of $q_{\mathbb{S} \perp \mathbb{T}}$ evaluated at a point \mathbf{x} :

$$\begin{aligned}\mathcal{L}_{\mathbb{S} \perp \mathbb{T}}(\mathbf{x}) &:= \log(q_{\mathbb{S} \perp \mathbb{T}}(\mathbf{x})) \equiv \mathcal{L}_{\mathbb{S}}(\mathbf{x}) + \mathcal{L}_{\mathbb{T}}(\mathbf{x}) - \mathcal{L}_{\mathbb{S} \mathbb{T}}(\mathbf{x}) \\ &= \log|\mathbf{J}_{\mathbb{S}}(\mathbf{f}(\mathbf{x}))| + \log|\mathbf{J}_{\mathbb{T}}(\mathbf{f}(\mathbf{x}))| - \log|\mathbf{J}_{\mathbb{S} \mathbb{T}}(\mathbf{f}(\mathbf{x}))|\end{aligned}\quad (\text{A.13})$$

where we used eq.(A.10,A.3).

This term was derived in PCF under the name "Pointwise mutual information between disjoint contours". It is easy to see that \mathbf{x} -MMI is non-negative $\mathcal{L}_{\mathbb{S} \perp \mathbb{D}} \geq 0$, as $q_{\mathbb{S} \perp \mathbb{D}} \geq 1$.

Using the core-detail split with $\mathbb{S} = \mathbb{C}$, $\mathbb{T} = \mathbb{D}$ we observe that $\mathcal{L}_{\mathbb{C} \mathbb{D}} \equiv \mathcal{L}_{\text{ML}}$. Using eq.(A.13), we note that the Maximum Likelihood objective eq.(A.5) can be rewritten

$$\mathcal{L}_{\text{ML}}(\mathbf{x}) = \mathcal{L}_{\mathbb{C}}(\mathbf{x}) + \mathcal{L}_{\mathbb{D}}(\mathbf{x}) - \mathcal{L}_{\mathbb{C} \perp \mathbb{D}}(\mathbf{x}) \quad (\text{A.14})$$

where $\mathcal{L}_{\mathbb{C}}$ is the core \mathbf{x} -ME, $\mathcal{L}_{\mathbb{D}}$ is the detail \mathbf{x} -ME and $\mathcal{L}_{\mathbb{C} \perp \mathbb{D}}$ is the core-detail \mathbf{x} -MMI. From here one can see, that Maximum Likelihood is optimized in three ways: a) minimizing $\mathcal{L}_{\mathbb{C}}$, b) minimizing $\mathcal{L}_{\mathbb{C}}$ and c) maximizing $\mathcal{L}_{\mathbb{C} \perp \mathbb{D}}$.

From this decomposition we finally derive the generalization of the Maximum Likelihood (ML)-objective for the core-detail split

Definition A.6 (Maximum Manifold Likelihood objective). We define the general **Maximum Manifold Likelihood** (MML)-objective of the core-detail split as a re-weighting of constituent terms in the Maximum Likelihood objective

$$\begin{aligned}\mathcal{L}_{\text{MML}}(\mathbf{x}) &:= (1 + \lambda_{\mathbb{C}}) \mathcal{L}_{\mathbb{C}}(\mathbf{x}) + (1 + \lambda_{\mathbb{D}}) \mathcal{L}_{\mathbb{D}}(\mathbf{x}) \\ &\quad + (\lambda_{\mathbb{C} \perp \mathbb{D}} - 1) \mathcal{L}_{\mathbb{C} \perp \mathbb{D}}(\mathbf{x})\end{aligned}\quad (\text{A.15})$$

where $\lambda_{\mathbb{C}}, \lambda_{\mathbb{D}}, \lambda_{\mathbb{C} \perp \mathbb{D}}$ are hyperparameter. Setting all of them to zero, we obtain the regular Maximum Likelihood-objective as in eq.(A.14).

Equivalently, we can view MML training simply as ML training with additional regularization:

$$\mathcal{L}_{\text{MML}}(\mathbf{x}) = \mathcal{L}_{\text{ML}}(\mathbf{x}) + \lambda_{\mathbb{C}} \cdot \mathcal{L}_{\mathbb{C}}(\mathbf{x}) + \lambda_{\mathbb{D}} \cdot \mathcal{L}_{\mathbb{D}}(\mathbf{x}) + \lambda_{\mathbb{C} \perp \mathbb{D}} \cdot \mathcal{L}_{\mathbb{C} \perp \mathbb{D}}(\mathbf{x}) \quad (\text{A.16})$$

We argue that the Maximum Manifold-Likelihood Objective can achieve the goals of $\mathcal{M}an\mathcal{D}is\mathcal{D}en\mathcal{L}$ by an appropriate weighting of hyperparameters.

A.7. Dimension-wise split

One can also derive analogous terms to eq.(A.12, A.13) for different latent splits and rewrite the ML objective as in eq.(A.15). Here, however, we will only focus on the natural **dimension-wise split** $\mathcal{P} = [\{1\}, \{2\}, \dots, \{D\}]$. For notational convenience, we will denote quantities corresponding to a single dimension $\{i\}$ by sub-scripting the relevant index e.g. \mathbf{U}_i , q_i , \mathcal{L}_i .

1. We write the curvilinear coordinate of a single dimension as \mathbf{u}_i .
2. We write the manifold PDF of a single dimension as $q_i(\mathbf{U}_i)$.
3. We rewrite the full push-forward PDF $q(\mathbf{U})$ in terms of $q_i \forall i \in \{1, \dots, D\}$:

$$q(\mathbf{U} = \mathbf{x}) = \prod_{i=1}^D q_i(\mathbf{U}_i = \mathbf{x}) \cdot q_{1 \perp 2 \perp \dots \perp D}(\mathbf{x}) \quad (\text{A.17})$$

where $q_{1 \perp 2 \perp \dots \perp D}$ denotes the mixture term between all dimensions simultaneously.

4. We define the \mathbf{x} -MMI of $q_{1 \perp 2 \perp \dots \perp D}$ analogously

Definition A.7 (Pointwise Manifold Total Correlation). We define the **Pointwise Manifold Total Correlation** (\mathbf{x} -MTC) $\mathcal{L}_{\text{TC}}(\mathbf{x})$ as the logarithm of $q_{1 \perp 2 \perp \dots \perp D}$ evaluated at a point \mathbf{x} :

$$\begin{aligned}\mathcal{L}_{\text{TC}}(\mathbf{x}) &:= \log(q_{1 \perp 2 \perp \dots \perp D}(\mathbf{x})) \equiv \sum_{i=1}^D \mathcal{L}_i(\mathbf{x}) - \mathcal{L}_{\text{ML}}(\mathbf{x}) \\ &= \sum_{i=1}^D \log |\mathbf{J}_i(\mathbf{f}(\mathbf{x}))| - \log |\mathbf{J}(\mathbf{f}(\mathbf{x}))|\end{aligned}\quad (\text{A.18})$$

where we used eq.(A.10,A.3).

A.8. Connection between Manifold Entropic Metrics and Pointwise estimates

There is a direct relation between the Manifold Entropic Metrics introduced in [Galperin & Koethe \(2025\)](#) and the pointwise estimates \mathbf{x} -ME and \mathbf{x} -MMI. Recall that the manifold entropy of a index set \mathbb{S} is defined as:

$$H(\mathbf{U}_{\mathbb{S}}) := \mathbb{E}_{\mathbf{z}} [-\log(q_{\mathbb{S}}(\mathbf{U}_{\mathbb{S}} = \mathbf{g}(\mathbf{z})))] \equiv \mathbb{E}_{\mathbf{z}} [\mathcal{L}_{\mathbb{S}}(\mathbf{g}(\mathbf{z}))] \quad (\text{A.19})$$

and the manifold mutual information between \mathbb{S} and \mathbb{T} as

$$\mathcal{I}(\mathbf{U}_{\mathbb{S}}, \mathbf{U}_{\mathbb{T}}) := \mathbb{E}_{\mathbf{z}} \left[\log \left(\frac{q_{\mathbb{S}\mathbb{T}}(\mathbf{U}_{\mathbb{S}\mathbb{T}} = \mathbf{g}(\mathbf{z}))}{q_{\mathbb{S}}(\mathbf{U}_{\mathbb{S}} = \mathbf{g}(\mathbf{z}))q_{\mathbb{T}}(\mathbf{U}_{\mathbb{T}} = \mathbf{g}(\mathbf{z}))} \right) \right] \equiv \mathbb{E}_{\mathbf{z}} [\mathcal{L}_{\mathbb{S}\perp\mathbb{T}}(\mathbf{g}(\mathbf{z}))] \quad (\text{A.20})$$

If one succeeds at $\mathcal{D}\text{en}\mathcal{L}$ the push-forward PDF equals the data PDF $q(\mathbf{U} = \mathbf{x}) \approx p^*(\mathbf{X} = \mathbf{x})$, i.e the KL-divergence goes to zero. Then the expectation over $\mathbf{z} \sim p(\mathbf{Z})$ becomes identical to the expectation over $\mathbf{x} \sim p^*(\mathbf{x})$, as per change-of-variables. Thus the manifold entropy will equal the expected pointwise manifold entropy:

$$H_{\mathbb{S}} := H(\mathbf{U}_{\mathbb{S}}) \equiv \mathbb{E}_{\mathbf{x}} [\mathcal{L}_{\mathbb{S}}(\mathbf{x})] \quad (\text{A.21})$$

This holds similarly for the manifold mutual information and the expected pointwise manifold mutual information:

$$\mathcal{I}_{\mathbb{S},\mathbb{T}} := \mathcal{I}(\mathbf{U}_{\mathbb{S}}, \mathbf{U}_{\mathbb{T}}) \equiv \mathbb{E}_{\mathbf{x}} [\mathcal{L}_{\mathbb{S}\perp\mathbb{T}}(\mathbf{x})] \quad (\text{A.22})$$

We note that manifold entropic metrics measure the intrinsic properties of a trained model independent of any data, whereas the point-wise estimates are usually evaluated at given data samples $\mathbf{x} \sim p^*$.

A.9. Core-Detail split

Here we assume a Core-Detail split of the latent random variables and correspondingly of the manifold random variables:

$$\mathbf{Z} = [\mathbf{Z}_{\mathbb{C}}, \mathbf{Z}_{\mathbb{D}}] \iff \mathbf{U} = [\mathbf{U}_{\mathbb{C}}, \mathbf{U}_{\mathbb{D}}] \quad (\text{A.23})$$

This split is (particularly) useful if we expect the training data to approximately lie on a manifold of dimensionality $|\mathbb{C}|$ and we wish to model the "Core"-information via $\mathbf{U}_{\mathbb{C}}$ and the "Detail"-information (possibly only noise) via $\mathbf{U}_{\mathbb{D}}$. We do not make any assumptions about the data structure within a subset by only regularizing the joint set of latent dimensions.

In this setting, we can enforce the following goals:

Core-Detail Disentanglement: Regularizing the pointwise manifold mutual information between core and detail $\downarrow \mathcal{L}_{\mathbb{C}\perp\mathbb{D}}$ jointly with Maximum Likelihood forces the corresponding manifold mutual information to go to zero $\mathcal{I}(\mathbf{U}_{\mathbb{C}}, \mathbf{U}_{\mathbb{D}}) \rightarrow 0$.

This can be easily seen as $\mathcal{L}_{\mathbb{C}\perp\mathbb{D}}$ is bounded from below and becomes $\mathcal{I}(\mathbf{U}_{\mathbb{C}}, \mathbf{U}_{\mathbb{D}})$ for successful $\mathcal{D}\text{en}\mathcal{L}$.

Definition A.8. We introduce **Core-Detail Disentanglement** as a $\mathcal{D}\text{is}\mathcal{D}\text{en}\mathcal{L}$ -goal inducing $\mathcal{I}(\mathbf{U}_{\mathbb{C}}, \mathbf{U}_{\mathbb{D}}) \rightarrow 0$ by the following Maximum Manifold Likelihood objective

$$\mathcal{L}_{\text{MML}}(\mathbf{x}) = \mathcal{L}_{\text{ML}}(\mathbf{x}) + \lambda_{\mathbb{C}\perp\mathbb{D}} \cdot \mathcal{L}_{\mathbb{C}\perp\mathbb{D}}(\mathbf{x}), \quad \lambda_{\mathbb{C}\perp\mathbb{D}} > 0 \quad (\text{A.24})$$

Core-Detail Compression: Regularizing the detail pointwise manifold entropy $\downarrow \mathcal{L}_{\mathbb{D}}$ jointly with Maximum Likelihood induces an ordering between the (normalized) Manifold Entropies of core and detail $H(\mathbf{U}_{\mathbb{C}})/|\mathbb{C}| > H(\mathbf{U}_{\mathbb{D}})/|\mathbb{D}|$.

This can be seen by first noting that \mathcal{L}_{ML} is bounded from below by the data entropy.⁹ Thus, given the decomposition eq.(A.14), minimizing $\mathcal{L}_{\mathbb{D}}$ at constant $\mathcal{L}_{\mathbb{C} \perp \mathbb{D}}$ will indirectly force $\mathcal{L}_{\mathbb{C}}$ to increase. As $\mathcal{L}_{\mathbb{S}}$ scales linearly with the length of the index set $|\mathbb{S}|$, we can only hope to induce an ordering in the normalized Pointwise quantities i.e. $\mathcal{L}_{\mathbb{C}}/|\mathbb{C}| > \mathcal{L}_{\mathbb{D}}/|\mathbb{D}|$. In the limit of successful $\mathcal{D}\text{en}\mathcal{L}$ this induces an ordering in the manifold entropies.

Definition A.9. We introduce **Core-Detail Compression**¹⁰ as a $\mathcal{M}\text{an}\mathcal{D}\text{en}\mathcal{L}$ -goal which induces the ordering $H(\mathbf{U}_{\mathbb{C}})/|\mathbb{C}| > H(\mathbf{U}_{\mathbb{D}})/|\mathbb{D}|$ by the following Maximum Manifold-Likelihood objective

$$\mathcal{L}_{\text{MML}}(\mathbf{x}) = \mathcal{L}_{\text{ML}}(\mathbf{x}) + \lambda_{\mathbb{D}} \cdot \mathcal{L}_{\mathbb{D}}(\mathbf{x}), \lambda_{\mathbb{D}} > 0 \quad (\text{A.25})$$

A.10. Dimension-wise split

Here we assume a Dimension-wise split of the latent space:

$$\mathbf{Z} = [\mathbf{Z}_1, \dots, \mathbf{Z}_D] \iff \mathbf{U} = [\mathbf{U}_1, \dots, \mathbf{U}_D] \quad (\text{A.26})$$

This split is useful if we don't want to make any assumptions about the data and thus allow each \mathbf{U}_i to be regularized independently.

Total Disentanglement: Regularizing $\downarrow \mathcal{L}_{\text{TC}}$ jointly with Maximum Likelihood forces the Manifold Total Correlation to go to zero $\mathcal{I}_{\text{TC}} \rightarrow 0$.

This can easily seen as \mathcal{L}_{TC} is bounded by 0 from below and becomes \mathcal{I}_{TC} for successful $\mathcal{D}\text{en}\mathcal{L}$.

Definition A.10. We introduce **Total Disentanglement** as a $\mathcal{D}\text{is}\mathcal{D}\text{en}\mathcal{L}$ -goal inducing $\mathcal{I}_{\text{TC}} \rightarrow 0$ by the following Maximum Manifold Likelihood objective

$$\mathcal{L}_{\text{MML}}(\mathbf{x}) = \mathcal{L}_{\text{ML}}(\mathbf{x}) + \lambda_{\text{TC}} \cdot \mathcal{L}_{\text{TC}}(\mathbf{x}), \lambda_{\text{TC}} > 0 \quad (\text{A.27})$$

A.11. Disentanglement as geometric regularization

The loss objective of Core-Detail Disentanglement and that of Total Disentanglement are bounded by zero from below, which occurs iff the respective Jacobian sub-matrices are orthogonal to each other:

$$\mathcal{L}_{\mathbb{C} \perp \mathbb{D}}(\mathbf{x}) = 0 \Leftrightarrow \mathbf{J}_{\mathbb{C}}(\mathbf{f}(\mathbf{x})) \perp \mathbf{J}_{\mathbb{D}}(\mathbf{f}(\mathbf{x})) \quad (\text{A.28})$$

$$\mathcal{L}_{\text{TC}}(\mathbf{x}) = 0 \Leftrightarrow \mathbf{J}_i(\mathbf{f}(\mathbf{x})) \perp \mathbf{J}_j(\mathbf{f}(\mathbf{x})) \forall i \neq j \quad (\text{A.29})$$

A full derivation can be found in Cunningham et al. (2022). The proof builds on Hadamard's inequality, which states that the determinant of a matrix is bounded from above by the product of the lengths of its column vectors. This can be generalized to the fact that the matrix is also bounded by the volume of any submatrix of itself. In this case, equality occurs iff the subspaces, which are spanned by the respective submatrices, intersect orthogonal. Only in this case, the volume of the full matrix factorizes into the volumes of its submatrices.

Thus we can generally think of **Disentanglement** as a regularization on the curvilinear manifolds to become more orthogonal to each other at any point \mathbf{x} .

Moreover, if we assume that a Normalizing Flow has $\mathcal{L}_{\text{TC}}(\mathbf{x}) = 0 \forall \mathbf{x}$, the decoder formally describes an **Orthogonal Coordinate Transform** (OCT)-map, or simply an orthogonal transform. Buchholz et al. (2022) studied the class of functions covered by OCT-maps and found that they still "constitutes a rich class of functions". Independent Mechanism Analysis (IMA) restricts itself to decoders which are exact OCT-maps. In this work, we lift the strict requirement of $\mathcal{L}_{\text{TC}}(\mathbf{x}) = 0 \forall \mathbf{x}$ and aim at "weakly" regularizing Total Disentanglement such that $\mathcal{L}_{\text{TC}}(\mathbf{x}) = \epsilon \forall \mathbf{x}$ for a small positive ϵ . Thus, the decoders formed by EOFs only represent **near-orthogonal** transforms.

⁹This is because the KL-divergence is strictly non-negative.

¹⁰In (Galperin & Kothe, 2025) this was known as Alignment.

B. Core-Detail Compression Loss generalizes the Reconstruction Loss

Theorem B.1. Assume a core-detail split of the latent space $\mathbf{z} = [\mathbf{z}_{\mathbb{C}}, \mathbf{z}_{\mathbb{D}}]$ and the following decoder

$$\mathbf{x} = \mathbf{g}(\mathbf{z}) := \hat{\mathbf{g}}(\mathbf{z}_{\mathbb{C}}) + \sigma \cdot \mathbf{U}_{\mathbb{D}}(\mathbf{z}_{\mathbb{C}})\mathbf{z}_{\mathbb{D}} \quad (\text{B.1})$$

where $\hat{\mathbf{g}} : \mathbb{R}^{|\mathbb{C}|} \rightarrow \mathbb{R}^D$ is a (unrestricted) injective mapping, $\mathbf{U}_{\mathbb{D}} \in \mathbb{R}^{D \times (D-C)}$ a semi-orthonormal (projection) matrix, which can depend on $\mathbf{z}_{\mathbb{C}}$ and $\sigma > 0$ a non-negative scalar. Importantly, $\hat{\mathbf{g}}$, $\mathbf{U}_{\mathbb{D}}$ and σ are learnable. For simplicity we assume that \mathbf{g} is invertible everywhere with the inverse given by the encoder \mathbf{f} . Moreover $\mathbf{f}_{\mathbb{C}} : \mathbb{R}^D \rightarrow \mathbb{R}^{|\mathbb{C}|}$ is the pseudo/left-inverse of $\hat{\mathbf{g}}$ at $\mathbf{z}_{\mathbb{D}} = \mathbf{0}$:

$$\mathbf{z}_{\mathbb{C}} = \mathbf{f}_{\mathbb{C}}(\mathbf{x}) \quad (\text{B.2})$$

Then we can show that

$$\mathcal{L}_{\mathbb{D}}(\mathbf{x}) \equiv \alpha \mathcal{L}_{\text{rec}}(\mathbf{x}) + \text{const.} \quad (\text{B.3})$$

where the reconstruction loss is defined as

$$\frac{1}{2} |\mathbf{x} - \mathbf{g}([\mathbf{z}_{\mathbb{C}} = \mathbf{f}_{\mathbb{C}}(\mathbf{x}), \mathbf{z}_{\mathbb{D}} = \mathbf{0}])|^2 \quad (\text{B.4})$$

i.e. both losses are equal up to a constant rescaling factor and additive constant.

Proof. Let us assume that there is bijective map $\mathbf{g} : \mathbb{R}^D \rightarrow \mathbb{R}^D$, the *decoder*, which maps from $Z \in \mathbb{R}^D$ to $X \in \mathbb{R}^D$. Its inverse $\mathbf{f} := \mathbf{g}^{-1}$, the *encoder*, maps from $X \in \mathbb{R}^D$ to $Z \in \mathbb{R}^D$. We split the latent space into core \mathbb{C} and detail \mathbb{D} as $\mathbf{z} = [\mathbf{z}_{\mathbb{C}}, \mathbf{z}_{\mathbb{D}}]$ s.t.:

$$\mathbf{x} = \mathbf{g}(\mathbf{z} = [\mathbf{z}_{\mathbb{C}}, \mathbf{z}_{\mathbb{D}}]), \quad \mathbf{z} = \begin{pmatrix} \mathbf{z}_{\mathbb{C}} \\ \mathbf{z}_{\mathbb{D}} \end{pmatrix} = \begin{pmatrix} \mathbf{f}_{\mathbb{C}}(\mathbf{x}) \\ \mathbf{f}_{\mathbb{D}}(\mathbf{x}) \end{pmatrix} \quad (\text{B.5})$$

We will now force restrictions on the decoder, which are equally applied on the encoder. Specifically, we assume that first a data sample is generated on the core-manifold and subsequently the detail-part is added in a linear fashion. Concretely, there is an injective map $\hat{\mathbf{g}} : \mathbb{R}^{|\mathbb{C}|} \rightarrow \mathbb{R}^D$ which takes in a core-latent $\mathbf{z}_{\mathbb{C}}$ and maps it to X :

$$\hat{\mathbf{x}} := \hat{\mathbf{g}}(\mathbf{z}_{\mathbb{C}}) \quad (\text{B.6})$$

The decoder \mathbf{g} now adds the detail latent $\mathbf{z}_{\mathbb{D}}$ linearly on to $\hat{\mathbf{x}}$:

$$\mathbf{g}(\mathbf{z} = [\mathbf{z}_{\mathbb{C}}, \mathbf{z}_{\mathbb{D}}]) := \hat{\mathbf{g}}(\mathbf{z}_{\mathbb{C}}) + \sigma \cdot \mathbf{U}_{\mathbb{D}}(\mathbf{z}_{\mathbb{C}})\mathbf{z}_{\mathbb{D}} \quad \forall \mathbf{z}_{\mathbb{C}}, \mathbf{z}_{\mathbb{D}} \quad (\text{B.7})$$

$\mathbf{U}_{\mathbb{D}} \in \mathbb{R}^{|\mathbb{C}|} \rightarrow \mathbb{R}^{D \times |\mathbb{D}|}$ is semi-orthonormal everywhere s.t. $\mathbf{U}_{\mathbb{D}}^T \mathbf{U}_{\mathbb{D}} = I_{|\mathbb{D}|}$.

Intuitively, it can be seen that $\mathbf{U}_{\mathbb{D}}$ determines the relative orientation of detail latents $\mathbf{z}_{\mathbb{D}}$ and σ scales them locally. As \mathbf{g} is bijective, we can reformulate eq.(B.7) in terms of a data-point \mathbf{x} :

$$\mathbf{x} = \hat{\mathbf{g}}(\mathbf{z}_{\mathbb{C}} = \mathbf{f}_{\mathbb{C}}(\mathbf{x})) + \sigma \cdot \mathbf{U}_{\mathbb{D}}(\mathbf{z}_{\mathbb{C}} = \mathbf{f}_{\mathbb{C}}(\mathbf{x}))\mathbf{f}_{\mathbb{D}}(\mathbf{x}) \quad \forall \mathbf{x} \quad (\text{B.8})$$

Lastly, we define the projection $\Phi_{\text{rec}} : \mathbb{R}^D \rightarrow \mathbb{R}^D$, which maps a data-point \mathbf{x} onto the image of $\hat{\mathbf{g}}$, as

$$\Phi_{\text{rec}}(\mathbf{x}) := \mathbf{g}([\mathbf{z}_{\mathbb{C}} = \mathbf{f}_{\mathbb{C}}(\mathbf{x}), \mathbf{z}_{\mathbb{D}} = \mathbf{0}]) = \hat{\mathbf{g}}(\mathbf{z}_{\mathbb{C}} = \mathbf{f}_{\mathbb{C}}(\mathbf{x})) \quad (\text{B.9})$$

This is the *reconstruction* of a data-point as in Autoencoders but generalized to bijective maps. Furthermore, we define the *reconstruction manifold* \mathcal{M}_{rec} as the set of all reconstructed points

$$\mathcal{M}_{\text{rec}} := \{\hat{\mathbf{g}}(\mathbf{z}_{\mathbb{C}} = \mathbf{f}_{\mathbb{C}}(\mathbf{x})) \mid \mathbf{x} \in \mathbb{R}^D\} \quad (\text{B.10})$$

Using eq.(B.8, B.9) we can write:

$$\mathbf{x} - \Phi_{\text{rec}}(\mathbf{x}) = \sigma \cdot \mathbf{U}_{\mathbb{D}}(\mathbf{z}_{\mathbb{C}} = \mathbf{f}_{\mathbb{C}}(\mathbf{x}))\mathbf{f}_{\mathbb{D}}(\mathbf{x}) \quad \forall \mathbf{x} \quad (\text{B.11})$$

Omitting the argument in $\mathbf{U}_{\mathbb{D}}$, we can calculate

$$\begin{aligned} (\mathbf{x} - \Phi_{\text{rec}}(\mathbf{x}))^T (\mathbf{x} - \Phi_{\text{rec}}(\mathbf{x})) &= (\sigma \cdot \mathbf{U}_{\mathbb{D}} \mathbf{f}_{\mathbb{D}}(\mathbf{x}))^T (\sigma \mathbf{U}_{\mathbb{D}} \mathbf{f}_{\mathbb{D}}(\mathbf{x})) \\ |\mathbf{x} - \Phi_{\text{rec}}(\mathbf{x})|^2 &= \sigma^2 \cdot \mathbf{f}_{\mathbb{D}}(\mathbf{x})^T (\mathbf{U}_{\mathbb{D}}^T \mathbf{U}_{\mathbb{D}}) \mathbf{f}_{\mathbb{D}}(\mathbf{x}) \\ |\mathbf{x} - \Phi_{\text{rec}}(\mathbf{x})|^2 &= \sigma^2 \cdot |\mathbf{f}_{\mathbb{D}}(\mathbf{x})|^2 \end{aligned} \quad (\text{B.12})$$

This equality relates the L2-distance of a reconstruction to the data-point with the norm of the detail latent. Rearranging, we obtain

$$\frac{1}{2} |\mathbf{f}_{\mathbb{D}}(\mathbf{x})|^2 = \frac{1}{2\sigma^2} \cdot |\mathbf{x} - \Phi_{\text{rec}}(\mathbf{x})|^2 \quad (\text{B.13})$$

Let us now compute the detail decoder Jacobian $\mathbf{J}_{\mathbb{D}}(\mathbf{z})$, or equivalently the derivative of $\mathbf{g}(\mathbf{z})$ towards $\mathbf{z}_{\mathbb{D}}$, given a constant $\mathbf{z}_{\mathbb{C}}$:

$$\mathbf{J}_{\mathbb{D}} := \frac{\partial \mathbf{g}([\mathbf{z}_{\mathbb{C}}, \mathbf{z}_{\mathbb{D}}])}{\partial \mathbf{z}_{\mathbb{D}}} \Bigg|_{\mathbf{z}_{\mathbb{C}} \text{ const.}} = \frac{\partial [\hat{\mathbf{g}}(\mathbf{z}_{\mathbb{C}}) + \sigma \cdot \mathbf{U}_{\mathbb{D}}(\mathbf{z}_{\mathbb{C}}) \mathbf{z}_{\mathbb{D}}]}{\partial \mathbf{z}_{\mathbb{D}}} \Bigg|_{\mathbf{z}_{\mathbb{C}}} = \sigma(\mathbf{z}_{\mathbb{C}}) \cdot \mathbf{U}_{\mathbb{D}} \quad (\text{B.14})$$

The matrix volume can be determined to

$$|\mathbf{J}_{\mathbb{D}}| = \sqrt{\det(\mathbf{J}_{\mathbb{D}}^T \mathbf{J}_{\mathbb{D}})} = \sigma^{|\mathbb{D}|} \cdot \sqrt{\det(\mathbf{U}_{\mathbb{D}}^T \mathbf{U}_{\mathbb{D}})} = \sigma^{|\mathbb{D}|} \quad (\text{B.15})$$

where we again used that $\mathbf{U}_{\mathbb{D}}$ is a semi-orthogonal matrix. Finally, replacing \mathbf{z} by $\mathbf{f}(\mathbf{x})$, we can write the log-determinant of $\mathbf{J}_{\mathbb{D}}$ as

$$\log |\mathbf{J}_{\mathbb{D}}(\mathbf{f}(\mathbf{x}))| = |\mathbb{D}| \cdot \log |\sigma| \quad (\text{B.16})$$

We remind ourselves the definition of the reconstruction loss

$$\mathcal{L}_{\text{rec}}(\mathbf{x}) = \frac{1}{2} |\mathbf{x} - \Phi_{\text{rec}}(\mathbf{x})|^2 \quad (\text{B.17})$$

Now that we have all the necessary quantities, we can formulate the core-detail compression loss as

$$\mathcal{L}_{\mathbb{D}}(\mathbf{x}) = \frac{1}{2} |\mathbf{f}_{\mathbb{D}}(\mathbf{x})|^2 + \log |\mathbf{J}_{\mathbb{D}}(\mathbf{f}(\mathbf{x}))| \stackrel{(\text{B.13}, \text{B.16})}{=} \frac{1}{2\sigma^2} \cdot |\mathbf{x} - \Phi_{\text{rec}}(\mathbf{x})|^2 + |\mathbb{D}| \cdot \log |\sigma| \quad (\text{B.18})$$

From here it can be seen that both losses are identical up to a learnable rescaling factor $1/\sigma^2$ plus a learnable additive constant. The additional dependence on σ implies that $\mathcal{L}_{\mathbb{D}}$ adapts to the "thickness" of the manifold, whereas \mathcal{L}_{rec} does not. If we furthermore restrict σ to be a non-learnable constant, we obtain the stated equivalence. \square

C. Numerical estimation of Pointwise Manifold Total Correlation

NF architectures are typically designed to output the log-determinant of the Jacobian along a forward pass which makes Maximum Likelihood Training tractable.

On first sight, implementing $\mathcal{L}_{\mathbb{S}}(\mathbf{x})$ requires access to the full Jacobian-matrix \mathbf{J} at a point $\mathbf{z} = \mathbf{f}(\mathbf{x})$ in order to compute sub-matrices thereof, $\mathbf{J}_{\mathbb{S}}$. Although common autodiff-libraries allow computing (Jacobian) primitives with minimal performance overhead, this procedure would still scale with the dimensionality of the data (plus the costly computation of $|\mathbf{J}_{\mathbb{S}}| \equiv \det(\mathbf{J}_{\mathbb{S}}^T \mathbf{J}_{\mathbb{S}})^{\frac{1}{2}}$).

This is the case for the estimates e.g. for a core-detail split, which is intractable for high-dimensional problems. For the element-wise split however we propose a tractable unbiased batched estimate which scales favorably with increasing D . The Maximum Manifold Likelihood objective with Total Disentanglement regularizatin can be written as

$$\mathcal{L}_{\text{MML}}(\mathbf{x}) = (1 - \lambda_{\text{TC}}) \cdot \mathcal{L}_{\text{ML}}(\mathbf{x}) + \sum_{i=1}^D \lambda_{\text{TC}} \cdot \mathcal{L}_i(\mathbf{x}) \quad (\text{C.1})$$

with

$$\mathcal{L}_i(\mathbf{x}) = \frac{1}{2} |\mathbf{f}_i(\mathbf{x})|^2 + \frac{1}{2} \log \left(\sum_{k=1}^D \mathbf{J}_{ik}(\mathbf{f}(\mathbf{x}))^2 \right) \quad (\text{C.2})$$

where the change-of-volume-term simplifies to the L2-norm of the column vector \mathbf{J}_i .

As \mathcal{L}_{ML} and the vector $\mathbf{f}(\mathbf{x})$ are readily available, the bottleneck is the computation of the change-of-volume-term as the indices go over i, k , which we aim to estimate more efficiently.

For a random batch of indices \mathbb{B} in the dataset we denote the data batch as $\mathbf{x}^{\mathbb{B}} = \{\mathbf{x}^k\}_{k \in \mathbb{B}}$. We assume that it contains the same or more number of samples than the dimensionality $|\mathbb{B}| \geq D$.

The batched MML objective $\mathcal{L}_{\text{MML}}(\mathbf{x}^{\mathbb{B}})$ contains the change-of-volume-term

$$\dots + \frac{1}{|\mathbb{B}|} \sum_{j \in \mathbb{B}} \sum_{i=1}^D \cdot \frac{\lambda_{\text{TC}}}{2} \log \left(\sum_{k=1}^D \mathbf{J}_{ik}(\mathbf{f}(\mathbf{x}^j))^2 \right) \quad (\text{C.3})$$

This requires the following computation:

For $j \in \mathbb{B}$ do:

For $i \in \{1, \dots, D\}$ do:

$\mathbf{g}(\mathbf{z}^j), \mathbf{J}_i(\mathbf{z}^j) = \text{jvp}(\mathbf{g}, \mathbf{z}^j, \mathbf{e}_i)$ where \mathbf{e}_i denotes the unit vector with index i .

Now, instead of computing a jvp for each dimension i per sample j , we only compute the jvp of one randomly chosen basis vector \mathbf{e}_i per sample j , thus only requiring one (batched) jvp step. For this we randomly sample a batch of indices i to obtain the batch $\mathbf{e}^{\mathbb{B}} = \{i\}_{j \in \mathbb{B}} \in \mathbb{R}^{|\mathbb{B}|}$. i is sampled uniformly with the restriction that every dimension is chosen at least once per batch.

Finally, this requires the computation:

For $j \in \mathbb{B}$ do:

$\mathbf{g}(\mathbf{z}^j), \mathbf{J}_{i=\mathbf{e}^j}(\mathbf{z}^j) = \text{jvp}(\mathbf{g}, \mathbf{z}^j, \mathbf{e}_{i=\mathbf{e}^j})$

Our method effectively uses a batchsize of 1, estimating the change-of-volume for a sampled point $\mathbf{z}^j = \mathbf{f}(\mathbf{x}^j)$ by a randomly chosen axis-aligned direction $\mathbf{e}_{i=\mathbf{e}^j}$.

In short, we absorb the sum over the latent dimensions into the sum over batch samples with $i = \mathbf{e}^j$ and rescale the estimate for each dimension to account for the missing samples. Thus, the stochastic batched MML objective $\tilde{\mathcal{L}}_{\text{MML}}(\mathbf{x}^{\mathbb{B}})$ contains

$$\dots + \frac{1}{|\mathbb{B}|} \sum_{j \in \mathbb{B}, i=\mathbf{e}^j} \frac{D}{m_i} \cdot \frac{\lambda_{\text{TC}}}{2} \log \left(\sum_{k=1}^D \mathbf{J}_{ik}(\mathbf{f}(\mathbf{x}^j))^2 \right) \quad (\text{C.4})$$

where \mathbf{e}^j denotes the latent dimension for which a sample j computes the jvp, and $m_i := \sum_{j \in \mathbb{B}} \mathbb{1}(i = \mathbf{e}^j)$ counts the number of samples per dimension i .

For completeness, we write out the full batch-wise expectation of the MML objective

$$\mathbb{E}_{\mathbf{x}^{\mathbb{B}}} [\mathcal{L}_{\text{MML}}(\mathbf{x}^{\mathbb{B}})] = \mathbb{E}_{\mathbf{x}^{\mathbb{B}}} \left[(1 - \lambda_{\text{TC}}) \cdot \mathcal{L}_{\text{ML}}(\mathbf{x}^{\mathbb{B}}) + \sum_{i=1}^D \lambda_{\text{TC}} \cdot \mathcal{L}_i(\mathbf{x}^{\mathbb{B}}) \right] \quad (\text{C.5})$$

$$= (1 - \lambda_{\text{TC}}) \mathbb{E}_{\mathbf{x}^{\mathbb{B}}} [\mathcal{L}_{\text{ML}}(\mathbf{x}^{\mathbb{B}})] + \lambda_{\text{TC}} \sum_{i=1}^D \mathbb{E}_{\mathbf{x}^{\mathbb{B}}} [\mathcal{L}_i(\mathbf{x}^{\mathbb{B}})] \quad (\text{C.6})$$

$$= (1 - \lambda_{\text{TC}}) \mathbb{E}_{\mathbf{x}^{\mathbb{B}}} [\mathcal{L}_{\text{ML}}(\mathbf{x}^{\mathbb{B}})] + \lambda_{\text{TC}} \sum_{i=1}^D \mathbb{E}_{\mathbf{x}^{\mathbb{B}}} \left[\frac{1}{2} |\mathbf{f}_i(\mathbf{x}^{\mathbb{B}})|^2 + \frac{1}{2} \log \left(\sum_{k=1}^D \mathbf{J}_{ik}(\mathbf{f}(\mathbf{x}^{\mathbb{B}}))^2 \right) \right] \quad (\text{C.7})$$

$$= (1 - \lambda_{\text{TC}}) \mathbb{E}_{\mathbf{x}^{\mathbb{B}}} [\mathcal{L}_{\text{ML}}(\mathbf{x}^{\mathbb{B}})] + \lambda_{\text{TC}} \sum_{i=1}^D \left(\mathbb{E}_{\mathbf{x}^{\mathbb{B}}} \left[\frac{1}{2} |\mathbf{f}_i(\mathbf{x}^{\mathbb{B}})|^2 \right] + \mathbb{E}_{\mathbf{x}^{\mathbb{B}}} \left[\frac{1}{2} \log \left(\sum_{k=1}^D \mathbf{J}_{ik}(\mathbf{f}(\mathbf{x}^{\mathbb{B}}))^2 \right) \right] \right) \quad (\text{C.8})$$

(C.9)

Our estimate replaces the expectation of the change-of-volume term over all samples in the batch $\mathbf{x}^{\mathbb{B}}$ by an expectation over a random subset $\mathbf{x}^{\tilde{\mathbb{B}}} \subset \mathbf{x}^{\mathbb{B}}$, where each $|\tilde{\mathbb{B}}| \geq 1$. Thus the stochastic loss is

$$\mathbb{E}_{\mathbf{x}^{\mathbb{B}}} [\tilde{\mathcal{L}}_{\text{MML}}(\mathbf{x}^{\mathbb{B}})] = (1 - \lambda_{\text{TC}}) \mathbb{E}_{\mathbf{x}^{\mathbb{B}}} [\mathcal{L}_{\text{ML}}(\mathbf{x}^{\mathbb{B}})] + \lambda_{\text{TC}} \sum_{i=1}^D \left(\mathbb{E}_{\mathbf{x}^{\mathbb{B}}} \left[\frac{1}{2} |\mathbf{f}_i(\mathbf{x}^{\mathbb{B}})|^2 \right] + \mathbb{E}_{\mathbf{x}^{\tilde{\mathbb{B}}}} \left[\frac{1}{2} \log \left(\sum_{k=1}^D \mathbf{J}_{ik}(\mathbf{f}(\mathbf{x}^{\tilde{\mathbb{B}}}))^2 \right) \right] \right) \quad (\text{C.10})$$

(C.11)

C.1. Python Implementation

Listing C.1. Minimal implementation examples of the Jacobian computation using reverse and forward auto-differentiation in pytorch

```

import torch
from torch.autograd import grad
from torch.autograd.forward_ad import dual_level, make_dual, unpack_dual

def get_NLL_z(z):
    return 1/2*(z**2) + torch.tensor(1/2*np.log(2*np.pi))

def get_loss(model, x, **kwargs):
    use_MML = kwargs['use_MER'] #use Maximum Manifold Likelihood training -> add
        regularization terms
    mode_MML = kwargs['mode_MML'] #computation mode, either full or stochastic
    assert mode_MML in ['full', 'stochastic'], "mode_MML not recognized!"
    device = x.device
    batchsize = x.shape[0]
    N_dim = x.shape[1]
    if mode_MML == 'stochastic':
        assert batchsize >= N_dim, "For mode_MML = stochastic, the number of samples per
            batch must be equal to or larger than the number of latent dimensions!"
    lam_TC = kwargs['lam_TC'] #weight of Pointwise Manifold Total Correlation i.e. Total
        Disentanglement

    z, ljd_enc = model(x, rev=False) # pass through encoder
    NLL_z_i = get_NLL_z(z) #Negative Log-likelihood of prior, per sample x dimension
    # note that ljd_dec = - ljd_enc
    L_ML = NLL_z_i.sum(-1) - ljd_enc #Negative Log-likelihood term, per sample

    if use_MML:
        if mode_MER == 'full':
            jac_dec = []
            x_rec, ljd_dec = model(z, rev=True) # pass through decoder
            # For full Jacobian computation, using backward-autodiff is usually faster than
                forward-autodiff
            for j in range(N_dim): #iterate over data dimension
                jac_dec.append(grad(x_rec[:, j].sum(), z, create_graph=True)[0])
            jac_dec = torch.stack(jac_dec, axis=2) #decoder Jacobian, per sample x latent
                dimension x data dimension
            ljd_dec_i = 1/2*torch.log(torch.sum(jac_dec**2, axis=-1)) #log-det of sub-
                Jacobian, per sample x latent dimension
            L_i = NLL_z_i + ljd_dec_i #Negative Manifold-Log-Likelihood term, per sample x
                dimension
        elif mode_MER == 'stochastic':
            p = [1/N_dim]*N_dim #sample random indices
            e = torch.multinomial(torch.tensor(p), batchsize, replacement=True).to(device)
            rand_perm = torch.randperm(N_dim) #first shuffle to not prefer the [0:N] samples
            e[rand_perm[0:N_dim]] = torch.arange(0, N_dim).to(device) #ensure that each
                dimension is sampled at least once
            e = nn.functional.one_hot(e, num_classes=N_dim).to(x.dtype) #one-hot-vector
            with dual_level(): #compute one jvp via forward-autodiff
                dual_z = make_dual(z, e)
                dual_x, _ = model(dual_z, rev=True)
                _, x_jvp = unpack_dual(dual_x)
                ljd_dec_i = 1/2*torch.log(torch.sum(x_jvp.reshape(batchsize, N_dim)**2, axis=-1))
                    #log-det of sub-Jacobian, per sample
                M = torch.sum(e, dim=0) #[D]
                m = e * batchsize/M[None,:] #[B x D]
                M = M.to(torch.bool) #[D]
                L_i = M[None,:]*NLL_z_i + m[:,M]*ljd_dec_i[:,None] #[B x D]
                L_MML = torch.sum((1 - lam_MTC) * L_ML, dim=(0)) + lam_MTC * torch.sum(L_i, dim
                    =(0,1)) / (batchsize * N_dim)
            return L_MML
        else:
            L_ML = L_ML.sum() / (batchsize * N_dim)
            return L_ML
    else:
        L_ML = L_ML.sum() / (batchsize * N_dim)
        return L_ML

```

D. Linearized Normalizing Flows and PCA

D.1. Setup

We assume a Linearized Normalizing Flow where we instantiate the decoder as an affine transformation

$$\mathbf{g}(\mathbf{z}) = A\mathbf{z} + b \quad (\text{D.1})$$

$A \in \mathbb{R}^{D \times D}$ is an invertible "mixing" matrix and has per convention (without loss of generality) only positive eigenvalues. $b \in \mathbb{R}^D$ is the "bias" term. The decoder Jacobian \mathbf{J} is simply A .

For completeness, the encoder becomes the inverse of the affine transformation:

$$\mathbf{f}(\mathbf{x}) = A^{-1}(\mathbf{x} - b) \quad (\text{D.2})$$

Assume that the data distribution has mean μ and covariance matrix Σ (of finite second moment). We assume that Σ has the following eigendecomposition

$$\Sigma = Q\Lambda Q^T \quad (\text{D.3})$$

where $Q = [Q_1, \dots, Q_D]$ is an orthogonal matrix and the columns are orthonormal eigenvectors of Σ . The diagonal matrix $\Lambda = \text{diag}(\lambda_1, \dots, \lambda_D)$ collects the eigenvalues, which we assume are ordered as

$$\lambda_1 > \lambda_2 > \dots > \lambda_D > 0 \quad (\text{D.4})$$

D.2. PCA

PCA can be viewed as a linear normalizing flow that matches the first two moments of the data. In particular, PCA first centers the data by choosing the bias to match the data mean

$$b \equiv \mu \quad (\text{D.5})$$

It then aligns the latent coordinates with the principal directions Q_i and scales them according to the data variance λ_i . In our affine decoder setting, this corresponds to choosing

$$A \equiv Q\Lambda^{\frac{1}{2}} \quad (\text{D.6})$$

With this choice, $AA^T = Q\Lambda Q^T = \Sigma$, i.e. the decoder maps a standard normal latent $\mathbf{z} \sim \mathcal{N}(\mathbf{0}, \mathbf{I})$ to a Gaussian in data space with the same covariance as the data distribution. Equivalently, the encoder

$$\mathbf{f}(\mathbf{x}) = A^{-1}(\mathbf{x} - b) = \Lambda^{-\frac{1}{2}}Q^T(\mathbf{x} - \mu) \quad (\text{D.7})$$

is the usual PCA whitening transform: it rotates into the orthonormal eigenbasis and rescales each component by the inverse standard deviation $\lambda_i^{-1/2}$.

D.3. Maximum-Likelihood objective

Let us write out the expectation of the ML objective

$$\mathbb{E}_{\mathbf{x} \sim p^*} [\mathcal{L}_{\text{ML}}(\mathbf{x})] = \mathbb{E}_{\mathbf{x} \sim p^*} [-\log(q(\mathbf{X} = \mathbf{x}))] = \mathbb{E}_{\mathbf{x} \sim p^*} \left[\frac{1}{2} |\mathbf{f}(\mathbf{x})|_2^2 + \log |\mathbf{J}(\mathbf{f}(\mathbf{x}))| + \frac{D}{2} \log(2\pi) \right] \quad (\text{D.8})$$

Inserting the linear encoder/decoder definition, we abbreviate $\mathcal{L}_{\text{ML}}(A, b) := \mathbb{E}_{\mathbf{x} \sim p^*} [\mathcal{L}_{\text{ML}}(\mathbf{x})]$ as a minimization objective under A and b :

$$\mathcal{L}_{\text{ML}}(A, b) = \mathbb{E}_{\mathbf{x} \sim p^*} \left[\frac{1}{2} (A^{-1}(\mathbf{x} - b))^T (A^{-1}(\mathbf{x} - b)) + \log |A| + \frac{D}{2} \log(2\pi) \right] \quad (\text{D.9})$$

$$= \mathbb{E}_{\mathbf{x} \sim p^*} \left[\frac{1}{2} (\mathbf{x} - b)^T (AA^T)^{-1} (\mathbf{x} - b) \right] + \log |A| + \frac{D}{2} \log(2\pi) \quad (\text{D.10})$$

$$= \mathbb{E}_{\mathbf{x} \sim p^*} \left[\frac{1}{2} \text{tr}((AA^T)^{-1} (\mathbf{x} - b)(\mathbf{x} - b)^T) \right] + \log |A| + \frac{D}{2} \log(2\pi) \quad (\text{D.11})$$

$$= \frac{1}{2} \text{tr} \left((AA^T)^{-1} \mathbb{E}_{\mathbf{x} \sim p^*} [(\mathbf{x} - b)(\mathbf{x} - b)^T] \right) + \log |A| + \frac{D}{2} \log(2\pi) \quad (\text{D.12})$$

where

$$\mathbb{E}_{\mathbf{x} \sim p^*} [(\mathbf{x} - b)(\mathbf{x} - b)^T] = \mathbb{E}_{\mathbf{x} \sim p^*} [\mathbf{x}\mathbf{x}^T - \mathbf{x}\mathbf{b}^T - \mathbf{b}\mathbf{x}^T + \mathbf{b}\mathbf{b}^T] = \Sigma + \mu\mu^T - \mu\mathbf{b}^T - \mathbf{b}\mu^T + \mathbf{b}\mathbf{b}^T \quad (\text{D.13})$$

$$= \Sigma + (\mu - b)(\mu - b)^T \quad (\text{D.14})$$

such that

$$\mathcal{L}_{\text{ML}}(A, b) = \frac{1}{2} \text{tr}((AA^T)^{-1}(\Sigma + (\mu - b)(\mu - b)^T)) + \log|A| + \frac{D}{2} \log(2\pi) \quad (\text{D.15})$$

$$= \frac{1}{2} \text{tr}((AA^T)^{-1}\Sigma) + \frac{1}{2} \text{tr}((\mu - b)^T(AA^T)^{-1}(\mu - b)) + \log|A| + \frac{D}{2} \log(2\pi) \quad (\text{D.16})$$

$$= \frac{1}{2} [\text{tr}((AA^T)^{-1}\Sigma) + (\mu - b)^T(AA^T)^{-1}(\mu - b) + 2\log|A| + D\log(2\pi)] \quad (\text{D.17})$$

Theorem D.1. *The loss $\mathcal{L}_{\text{ML}}(A, b)$ obtains its global minimum for $b = \mu$ and $AA^T = \Sigma$.*

Proof. Let $C := AA^T \succ 0$ be a symmetric positive definite matrix. The loss is:

$$\mathcal{L}_{\text{ML}}(A, b) = \frac{1}{2} [\text{tr}(C^{-1}\Sigma) + (\mu - b)^T C^{-1}(\mu - b) + \log|C|] + \text{const.} \quad (\text{D.18})$$

Since $C^{-1} \succ 0$, the quadratic term $(\mu - b)^T C^{-1}(\mu - b)$ is non-negative and vanishes only at $b = \mu$.

Substituting into the loss,

$$\mathcal{L}_{\text{ML}}(A, b) = \frac{1}{2} [\text{tr}(C^{-1}\Sigma) + \log|C|] + \text{const.} \quad (\text{D.19})$$

Let $M := C^{-\frac{1}{2}}\Sigma C^{-\frac{1}{2}} \succ 0$. We can write $\text{tr}(M) = \text{tr}(C^{-1}\Sigma)$ and $\log|M| = \log|\Sigma| - \log|C|$ and substitute

$$\mathcal{L}_{\text{ML}}(A, b) = \frac{1}{2} [\text{tr}(M) - \log|M| + \log|\Sigma|] + \text{const.} \quad (\text{D.20})$$

By the inequality

$$\text{tr}(M) - \log|M| \geq D \quad (\text{D.21})$$

with equality iff $M = \mathbf{I}_D$, we obtain

$$\mathcal{L}_{\text{ML}}(A, b) \geq \frac{1}{2} [D + \log|\Sigma|] + \text{const.} \quad (\text{D.22})$$

Thus equality holds iff

$$M = \mathbf{I}_D \iff C^{-\frac{1}{2}}\Sigma C^{-\frac{1}{2}} = \mathbf{I}_D \iff C = \Sigma \iff AA^T = \Sigma \quad (\text{D.23})$$

□

D.4. Maximum Manifold-Likelihood objectives

Let us write the expectation of the pointwise manifold entropy of a single dimension i

$$\mathbb{E}_{\mathbf{x} \sim p^*} [\mathcal{L}_i(\mathbf{x})] = \mathbb{E}_{\mathbf{x} \sim p^*} [-\log(q_i(\mathbf{X}_i = \mathbf{x}))] = \mathbb{E}_{\mathbf{x} \sim p^*} \left[\frac{1}{2} |\mathbf{f}_i(\mathbf{x})|^2 + \log|\mathbf{J}_i(\mathbf{f}(\mathbf{x}))| + \frac{1}{2} \log(2\pi) \right] \quad (\text{D.24})$$

As a prerequisite we need to evaluate the i -th entry of the encoder output:

$$\mathbf{f}_i(\mathbf{x}) = (A^{-1}(\mathbf{x} - b))_i \quad (\text{D.25})$$

which can be explicitly written by the SVD decomposition of A

$$A = USV^T, \quad A^{-1} = VS^{-1}U^T \quad (\text{D.26})$$

The diagonal matrix S has only positive entries (convention without loss of generality). We denote the i -th row vector of V by $V_{i,*}$ such that

$$\mathbf{f}_i(\mathbf{x}) = V_{i,*} S^{-1} U^T (\mathbf{x} - b) \quad (\text{D.27})$$

The i -th column vector of the decoder Jacobian \mathbf{J}_i is the i -th column vector of A , which we denote as $(A)_{*,i} := A_i$:

$$A_i = (USV^T)_{*,i} = US(V_{i,*})^T \quad (\text{D.28})$$

For shorter notation we will abbreviate the i -th row vector $V_{i,*}$ simply as V_i

Inserting the linear encoder/decoder definition, we abbreviate $\mathcal{L}_i(A, b) := \mathbb{E}_{\mathbf{x} \sim p^*} [\mathcal{L}_i(\mathbf{x})]$ as a minimization objective under A and b :

$$\mathcal{L}_i(A, b) = \mathbb{E}_{\mathbf{x} \sim p^*} \left[\frac{1}{2} ((\mathbf{f}_i(\mathbf{x}))^T (\mathbf{f}_i(\mathbf{x}))) + \log |A_i| + \frac{1}{2} \log(2\pi) \right] \quad (\text{D.29})$$

$$= \mathbb{E}_{\mathbf{x} \sim p^*} \left[\frac{1}{2} (V_i S^{-1} U^T (\mathbf{x} - b))^T (V_i S^{-1} U^T (\mathbf{x} - b)) + \log |USV_i^T| + \frac{1}{2} \log(2\pi) \right] \quad (\text{D.30})$$

$$= \mathbb{E}_{\mathbf{x} \sim p^*} \left[\frac{1}{2} (\mathbf{x} - b)^T US^{-1} V_i^T V_i S^{-1} U^T (\mathbf{x} - b) \right] + \frac{1}{2} \log |\det((USV_i^T)^T (USV_i^T))| + \frac{1}{2} \log(2\pi) \quad (\text{D.31})$$

$$= \mathbb{E}_{\mathbf{x} \sim p^*} \left[\frac{1}{2} \text{tr}(US^{-1} V_i^T V_i S^{-1} U^T (\mathbf{x} - b)(\mathbf{x} - b)^T) \right] + \frac{1}{2} \log |\det(V_i S^2 V_i^T)| + \frac{1}{2} \log(2\pi) \quad (\text{D.32})$$

$$= \frac{1}{2} \text{tr} \left(US^{-1} V_i^T V_i S^{-1} U^T \mathbb{E}_{\mathbf{x} \sim p^*} [(\mathbf{x} - b)(\mathbf{x} - b)^T] \right) + \frac{1}{2} \log |\det(V_i S^2 V_i^T)| + \frac{1}{2} \log(2\pi) \quad (\text{D.33})$$

Inserting the solution eq.(D.13)

$$\mathcal{L}_i(A, b) = \frac{1}{2} [\text{tr}(US^{-1} V_i^T V_i S^{-1} U^T (\Sigma + (\mu - b)(\mu - b)^T)) + \log |\det(V_i S^2 V_i^T)| + \log(2\pi)] \quad (\text{D.34})$$

D.4.1. TOTAL DISENTANGLEMENT OBJECTIVE

The regularization objective of Total Disentanglement was shown to simplify to

$$\mathcal{L}_{\text{TC}}(A, b) := \sum_i \mathcal{L}_i(A, b) - \mathcal{L}_{\text{ML}}(A, b) \quad (\text{D.35})$$

Inserting the previous results

$$\mathcal{L}_{\text{TC}}(A, b) = \frac{1}{2} \sum_{i=1}^D [\text{tr}(US^{-1} V_i^T V_i S^{-1} U^T (\Sigma + (\mu - b)(\mu - b)^T)) + \log |\det(V_i S^2 V_i^T)| + \log(2\pi)] \quad (\text{D.36})$$

$$- \frac{1}{2} [\text{tr}((AA^T)^{-1} (\Sigma + (\mu - b)(\mu - b)^T)) + 2 \log |A| + D \log(2\pi)] \quad (\text{D.37})$$

Inserting the SVD decomposition of A , we can simplify the determinant of A

$$\det(A) = \det(S) = \prod_i s_i \quad (\text{D.38})$$

where s_i are the, strictly positive, singular values. We can also simplify the second determinant expression by observing that $V_i S^2 V_i^T$ is a scalar and strictly positive.

$$\mathcal{L}_{\text{TC}}(A, b) = \frac{1}{2} \sum_{i=1}^D [\text{tr}(US^{-1}V_i^T V_i S^{-1}U^T (\Sigma + (\mu - b)(\mu - b)^T)) + \log(V_i S^2 V_i^T) + \log(2\pi)] \quad (\text{D.39})$$

$$- \frac{1}{2} \left[\text{tr}(US^{-2}U^T (\Sigma + (\mu - b)(\mu - b)^T)) + 2 \log \left(\prod_{i=1}^D s_i \right) + D \log(2\pi) \right] \quad (\text{D.40})$$

$$= \frac{1}{2} \text{tr} \left(\sum_{i=1}^D [US^{-1}V_i^T V_i S^{-1}U^T - US^{-2}U^T] (\Sigma + (\mu - b)(\mu - b)^T) \right) \quad (\text{D.41})$$

$$+ \left[\frac{1}{2} \sum_{i=1}^D \log(V_i S^2 V_i^T) - \log \left(\prod_{i=1}^D s_i \right) \right] \quad (\text{D.42})$$

$$= \frac{1}{2} \text{tr} \left(US^{-1} \underbrace{\left[\sum_{i=1}^D V_i^T V_i - \mathbf{I}_D \right]}_{\equiv 0} S^{-1}U^T (\Sigma + (\mu - b)(\mu - b)^T) \right) \quad (\text{D.43})$$

$$+ \sum_{i=1}^D \left[\frac{1}{2} \log(V_i S^2 V_i^T) - \log(s_i) \right] \quad (\text{D.44})$$

$$= \frac{1}{2} \sum_{i=1}^D \log \left(\frac{V_i S^2 V_i^T}{s_i^2} \right) \quad (\text{D.45})$$

Since V is orthonormal, the trace term vanished fully.

Theorem D.2. *The loss $\mathcal{L}_{\text{TC}}(A, b)$ obtains its global minimum if V equals any permutation matrix P .*

Proof. The loss is:

$$\mathcal{L}_{\text{TC}}(A, b) = \frac{1}{2} \sum_{i=1}^D \log \left(\frac{V_i S^2 V_i^T}{s_i^2} \right) \quad (\text{D.46})$$

Since V is orthonormal, the coefficients V_{ij}^2 form a probability distribution for each i . By Jensen's inequality applied to the concave function \log :

$$\log(V_i S^2 V_i^T) = \log \left(\sum_j V_{ij}^2 s_j^2 \right) \geq \sum_j V_{ij}^2 \log s_j^2 \quad (\text{D.47})$$

Summing over i and using $\sum_i V_{ij}^2 = 1$ yields

$$\sum_i \log(V_i S^2 V_i^T) \geq \sum_i \log s_i^2 \quad (\text{D.48})$$

Equality holds iff V_{ij}^2 is a delta mass, i.e each row has exactly one entry. Thus V is a permutation matrix (and sign flip). \square

We see that the global minimum of $\mathbb{E}[\mathcal{L}_{\text{TC}}]$ is attained if the decoder Jacobian A has orthogonal column vectors A_i as

$$A_i = US(P_{i,*})^T = U_j s_j \text{ where } P_{ij} = 1 \quad (\text{D.49})$$

Thus we can only hope to obtain a permuted PCA solution as the loss is blind to permutations of the latent dimensions.

D.4.2. CORE-DETAIL COMPRESSION

Let us now write the expectation of the pointwise manifold entropy of a index set \mathbb{S}

$$\mathbb{E}_{\mathbf{x} \sim p^*} [\mathcal{L}_{\mathbb{S}}(\mathbf{x})] = \mathbb{E}_{\mathbf{x} \sim p^*} [-\log(q_{\mathbb{S}}(\mathbf{X}_{\mathbb{S}} = \mathbf{x}))] = \mathbb{E}_{\mathbf{x} \sim p^*} \left[\frac{1}{2} |f_{\mathbb{S}}(\mathbf{x})|^2 + \log |J_{\mathbb{S}}(f(\mathbf{x}))| + \frac{|\mathbb{S}|}{2} \log(2\pi) \right] \quad (\text{D.50})$$

We will use the core-detail split where the core index set is defined as $\mathbb{C} := \{1, \dots, C\}$ and the detail index set as $\mathbb{D} := \{C+1, \dots, D\}$.

Inserting the linear encoder/decoder definition (where we can simply substitute $V_i \rightarrow V_{\mathbb{S}}$ in eq.(D.29,D.34)) we abbreviate $\mathcal{L}_{\mathbb{S}}(A, b) := \mathbb{E}_{\mathbf{x} \sim p^*} [\mathcal{L}_{\mathbb{S}}(\mathbf{x})]$ for $\mathbb{S} \in \{\mathbb{C}, \mathbb{D}\}$ as a minimization objective under A and b . Thus the core loss reads

$$\mathcal{L}_{\mathbb{C}}(A, b) = \frac{1}{2} [\text{tr}(US^{-1}V_{\mathbb{C}}^T V_{\mathbb{C}} S^{-1}U^T (\Sigma + (\mu - b)(\mu - b)^T)) + \log |\det(V_{\mathbb{C}} S^2 V_{\mathbb{C}}^T)| + C \log(2\pi)] \quad (\text{D.51})$$

and analogously for the detail loss

$$\mathcal{L}_{\mathbb{D}}(A, b) = \frac{1}{2} [\text{tr}(US^{-1}V_{\mathbb{D}}^T V_{\mathbb{D}} S^{-1}U^T (\Sigma + (\mu - b)(\mu - b)^T)) + \log |\det(V_{\mathbb{D}} S^2 V_{\mathbb{D}}^T)| + (D - C) \log(2\pi)] \quad (\text{D.52})$$

We will now show that, given the Maximum Likelihood minimizer $\mathcal{L}_{\text{ML}}(A, b)$, the loss $\mathcal{L}_{\mathbb{D}}(A, b)$ attains its global minimum if $V_{\mathbb{D}}$ aligns with the $(D - C)$ smallest eigenvalues in Λ and the loss $\mathcal{L}_{\mathbb{C}}(A, b)$ attains its global maximum if $V_{\mathbb{C}}$ aligns with the C largest eigenvalues in Λ .

We restrict our attention to the "covariance-matching" solution which is the set of global minimizers of $\mathcal{L}_{\text{ML}}(A, b)$

$$b = \mu, \quad AA^T = \Sigma. \quad (\text{D.53})$$

Hence, from now on, we write all loss objectives as a minimization objective under A , as b is fixed. On this solution set, \mathcal{L}_{ML} is constant, hence minimizing the combined objectives

$$\mathcal{L}_{\text{ML}} + \lambda_{\mathbb{D}} \mathcal{L}_{\mathbb{D}} \quad \text{or} \quad \mathcal{L}_{\text{ML}} - \lambda_{\mathbb{C}} \mathcal{L}_{\mathbb{C}} \quad (\lambda_{\mathbb{D}}, \lambda_{\mathbb{C}} > 0)$$

over eq.(D.53) is equivalent to minimizing $\mathcal{L}_{\mathbb{D}}$ or maximizing $\mathcal{L}_{\mathbb{C}}$ over eq.(D.53), respectively.

Lemma D.3. $AA^T = \Sigma$ if and only if there exists an orthogonal matrix $R \in O(D)$ such that

$$A = Q\Lambda^{1/2}R.$$

Proof. If $A = Q\Lambda^{1/2}R$ with $R^T R = \mathbf{I}$, then $AA^T = Q\Lambda^{1/2}RR^T\Lambda^{1/2}Q^T = Q\Lambda Q^T = \Sigma$. Conversely, if $AA^T = \Sigma$, set $B := \Lambda^{-1/2}Q^T A$. Then $BB^T = \Lambda^{-1/2}Q^T AA^T Q\Lambda^{-1/2} = \Lambda^{-1/2}\Lambda\Lambda^{-1/2} = \mathbf{I}$, so B is orthogonal; take $R = B$. \square

Hence within eq.(D.53) the only remaining freedom is the orthogonal "mixing" R .

Assume eq.(D.53) and write $A = Q\Lambda^{1/2}R$. For an index set \mathbb{S} of size k , define $U := R_{*,\mathbb{S}} \in \mathbb{R}^{D \times k}$ (the columns of R indexed by \mathbb{S}). Then $U^T U = \mathbf{I}_k$. Moreover

$$J_{\mathbb{S}} = A_{*,\mathbb{S}} = Q\Lambda^{1/2}U \implies J_{\mathbb{S}}^T J_{\mathbb{S}} = U^T \Lambda U.$$

Also, with $b = \mu$ we have $f(x) = A^{-1}(x - \mu)$ and $x - \mu \sim \mathcal{N}(0, \Sigma)$, hence

$$\mathbb{E} [|f_{\mathbb{S}}(x)|^2] = \mathbb{E} [|f(A^{-1}(x - \mu))_{\mathbb{S}}|^2] = \text{tr}((A^{-1}\Sigma A^{-T})_{\mathbb{S}\mathbb{S}}) = \text{tr}(\mathbf{I}_k) = k,$$

because $A^{-1}\Sigma A^{-T} = A^{-1}AA^TA^{-T} = \mathbf{I}$ under $AA^T = \Sigma$. Therefore, up to an additive constant independent of R ,

$$\mathcal{L}_{\mathbb{S}}(A) \equiv \frac{1}{2} \log \det(U^T \Lambda U). \quad (\text{D.54})$$

We now optimize eq.(D.54) over orthonormal frames U of the appropriate dimension.

Lemma D.4 (Extrema of $\det(U^\top \Lambda U)$). *Let $\Lambda = \text{diag}(\lambda_1 \geq \dots \geq \lambda_D > 0)$. Among all $U \in \mathbb{R}^{D \times k}$ with $U^\top U = \mathbf{I}_k$,*

$$\min_{U^\top U = \mathbf{I}_k} \det(U^\top \Lambda U) = \prod_{i=D-k+1}^D \lambda_i, \quad \max_{U^\top U = \mathbf{I}_k} \det(U^\top \Lambda U) = \prod_{i=1}^k \lambda_i.$$

Both extrema are attained by choosing U to span the eigenvectors of Λ corresponding to the selected eigenvalues (i.e. $U = [e_{i_1}, \dots, e_{i_k}]$).

Proof. This is a standard eigen-subspace selection result and can be found under Poincaré separation / Courant–Fischer theory for compressions of Hermitian matrices and the fact that the eigenvalues of $U^\top \Lambda U$ lie between those of Λ (interlacing). Since $\log \det$ is the sum of logs of the eigenvalues of the compression, the minimum is achieved by selecting the k smallest eigenvalues and the maximum by selecting the k largest. \square

Combining eq.(D.54) with Lemma D.4 yields the desired statement.

Theorem D.5 (Core–detail extrema within eq.(D.53)). *Restrict to the covariance-matching solution in eq.(D.53). Then:*

1. **(Detail minimum)** $\mathcal{L}_{\mathbb{D}}(A)$ is minimized when the detail columns of A span the eigenspace of Σ corresponding to its $(D - C)$ smallest eigenvalues, i.e. $\{\lambda_{C+1}, \dots, \lambda_D\}$.
2. **(Core maximum)** $\mathcal{L}_{\mathbb{C}}(A)$ is maximized when the core columns of A span the eigenspace of Σ corresponding to its C largest eigenvalues, i.e. $\{\lambda_1, \dots, \lambda_C\}$.

Equivalently, in the parameterization $A = Q\Lambda^{1/2}R$, the optimum is attained by an orthogonal R that (up to permutation/sign within blocks) assigns \mathbb{D} to the smallest-eigenvalue directions and \mathbb{C} to the largest-eigenvalue directions.

Proof. By Lemma D.3 we write $A = Q\Lambda^{1/2}R$. For $\mathbb{S} \in \{\mathbb{C}, \mathbb{D}\}$, eq.(D.54) shows that (up to constants) $\mathcal{L}_{\mathbb{S}}$ equals $\frac{1}{2} \log \det(U^\top \Lambda U)$ with $U = R_{*,\mathbb{S}}$ an orthonormal frame of dimension $|\mathbb{S}|$. Thus minimizing/maximizing $\mathcal{L}_{\mathbb{S}}$ is equivalent to minimizing/maximizing $\det(U^\top \Lambda U)$. Lemma D.4 yields the claimed eigenvalue selection. \square

Remark on the combined objectives. On the solution set eq.(D.53), \mathcal{L}_{ML} is constant. Hence, for any $\lambda_{\mathbb{D}}, \lambda_{\mathbb{C}} > 0$, minimizing $\mathcal{L}_{\text{ML}} + \lambda_{\mathbb{D}}\mathcal{L}_{\mathbb{D}}$ over eq.(D.53) is equivalent to minimizing $\mathcal{L}_{\mathbb{D}}$ over eq.(D.53); and minimizing $\mathcal{L}_{\text{ML}} - \lambda_{\mathbb{C}}\mathcal{L}_{\mathbb{C}}$ over eq.(D.53) is equivalent to maximizing $\mathcal{L}_{\mathbb{C}}$ over eq.(D.53). Therefore Theorem D.5 applies directly to the combined objectives.

D.4.3. NESTED COMPRESSION

For each $C \in \{1, \dots, D - 1\}$ we define the tail index set $\mathbb{D}_C := \{C + 1, \dots, D\}$ of size $k_C = D - C$. Then we can define the goal of Nested Compression as the sum over Core-detail Compression terms as

$$\mathcal{L}_{\text{NestComp}} := \sum_{C=1}^{D-1} \lambda_{\mathbb{D}_C} \cdot \mathbb{E}_{\mathbf{x} \sim p^*} [\mathcal{L}_{\mathbb{D}_C}(\mathbf{x})], \quad \lambda_{\mathbb{D}_C} > 0 \quad (\text{D.55})$$

Again, by inserting the linear encoder/decoder definition we obtain

$$\mathcal{L}_{\text{NestComp}}(A, b) := \sum_{C=1}^{D-1} \lambda_{\mathbb{D}_C} \cdot \mathcal{L}_{\mathbb{D}_C}(A, b), \quad \lambda_{\mathbb{D}_C} > 0 \quad (\text{D.56})$$

We will now show that, under the Maximum Likelihood minimizer $\mathcal{L}_{\text{ML}}(A, b)$, the loss $\mathcal{L}_{\text{NestComp}}(A)$ attains its global minimum if V aligns with each eigenvalue separately or simply $V = \mathbf{I}$, which is precisely the PCA solution.

Setup (Option A). Again, we restrict our attention to the "covariance-matching" solution

$$b = \mu, \quad AA^T = \Sigma,$$

and let $\Sigma = Q\Lambda Q^T$ with $\Lambda = \text{diag}(\lambda_1, \dots, \lambda_D)$ and

$$\lambda_1 \geq \lambda_2 \geq \dots \geq \lambda_D > 0.$$

As before, all such decoders can be written as

$$A = Q\Lambda^{1/2}R, \quad R \in O(D).$$

Reduction. Under $AA^T = \Sigma$ and $b = \mu$, each tail term reduces (up to an additive constant independent of R) to

$$\mathcal{L}_{\mathbb{D}_C}(A) \equiv \frac{1}{2} \log \det(U_C^T \Lambda U_C), \quad U_C := R_{*,\mathbb{D}_C} \in \mathbb{R}^{D \times k_C}, \quad U_C^T U_C = \mathbf{I}.$$

In particular, if R is a permutation/sign-flip matrix, then U_C selects a subset of k_C coordinate axes, and

$$\det(U_C^T \Lambda U_C) = \prod_{j \in S_C(R)} \lambda_j,$$

where $S_C(R)$ is the set of eigenvalue indices chosen by the tail \mathbb{D}_C .

Since the tails are nested, for a permutation R the selected sets are nested:

$$S_1(R) \supset S_2(R) \supset \dots \supset S_{D-1}(R), \quad |S_C(R)| = D - C.$$

Equivalently, choosing such a nested family is the same as choosing an ordering (a permutation) π of $\{1, \dots, D\}$ and letting

$$S_C(R) = \{\pi(C+1), \dots, \pi(D)\}.$$

Thus, up to constants, minimizing $\mathcal{L}_{\text{NestComp}}$ over permutation/sign-flip R is equivalent to minimizing

$$F(\pi) := \sum_{C=1}^{D-1} \lambda_{\mathbb{D}_C} \sum_{t=C+1}^D \log \lambda_{\pi(t)}. \quad (\text{D.57})$$

Rearranging the double sum, each position t contributes to all $C < t$, hence

$$F(\pi) = \sum_{t=2}^D w_t \log \lambda_{\pi(t)}, \quad w_t := \sum_{C=1}^{t-1} \lambda_{\mathbb{D}_C}. \quad (\text{D.58})$$

Since all $\lambda_{\mathbb{D}_C} > 0$, the weights satisfy

$$0 < w_2 < w_3 < \dots < w_D.$$

Lemma D.6 (Rearrangement step). *Let $a_2 \leq a_3 \leq \dots \leq a_D$ and $w_2 < \dots < w_D$ with $w_t > 0$. Then $\sum_{t=2}^D w_t a_{\pi(t)}$ is minimized by taking π such that $a_{\pi(2)} \geq a_{\pi(3)} \geq \dots \geq a_{\pi(D)}$ (largest a paired with smallest weight).*

Proof. This is the standard rearrangement inequality; it also follows by a pairwise swap argument: if $w_i < w_j$ but $a_{\pi(i)} < a_{\pi(j)}$, swapping $\pi(i)$ and $\pi(j)$ changes the sum by

$$\Delta = (w_i - w_j)(a_{\pi(j)} - a_{\pi(i)}) < 0,$$

so the value decreases. Repeating eliminates all inversions. \square

Theorem D.7 (Nested compression forces sorted eigenvalue alignment). *Restrict to the covariance-matching solution in eq.(D.53) and assume $\lambda_{\mathbb{D}_C} > 0$ for all C . Then $\mathcal{L}_{\text{NestComp}}(A)$ is minimized when R orders the eigen-directions so that*

$$\pi(2), \dots, \pi(D) \text{ list eigenvalues in nonincreasing order, i.e. } \lambda_{\pi(2)} \geq \lambda_{\pi(3)} \geq \dots \geq \lambda_{\pi(D)}.$$

Equivalently, each tail \mathbb{D}_C selects the $D - C$ smallest eigenvalues. If $\lambda_1 > \lambda_2 > \dots > \lambda_D$ are strictly ordered, the minimizer is unique up to sign flips. In the eigenbasis of Σ , this corresponds to $V = I$ as, per convention, the eigenvalues are already sorted.

Proof. Let $a_i := \log \lambda_i$. Since $\lambda_1 \geq \dots \geq \lambda_D$, we have $a_1 \geq \dots \geq a_D$. By equation D.58, minimizing $F(\pi)$ is minimizing $\sum_{t=2}^D w_t a_{\pi(t)}$ with strictly increasing weights w_t . By Lemma D.6, the minimum is achieved by pairing the smallest weights with the largest a 's, i.e.

$$a_{\pi(2)} \geq a_{\pi(3)} \geq \dots \geq a_{\pi(D)} \iff \lambda_{\pi(2)} \geq \dots \geq \lambda_{\pi(D)}.$$

Thus the positions $t = 2, \dots, D$ must follow the global decreasing eigenvalue order, which means the tails $\{\pi(C+1), \dots, \pi(D)\}$ are exactly the sets of smallest eigenvalues. \square

E. Experiments

E.1. Normalizing Flow architecture

Although our training objective can be applied to any invertible Normalizing Flow architecture, there are some important considerations to take into account and motivates the use of a particular architecture, which ensures that training converges to a global optimum. In particular, one has to strike a balance between expressivity, unbiased-ness and training speed.

More recent NF designs, termed Autoregressive Flows (AF) (Gu et al., 2025), have shown to be highly expressive NF models with comparable training time. The expressivity of this auto-regressive approach comes at the cost of very slow decoder throughput-time. As our training scheme depends on the fast evaluation of the decoder, AF are not tractable as an architecture for EOFLOWS. We thus opt for a symmetric encoder-decoder design, in particular coupling layers.

As we are aiming to find features which are stemming from the data-generating process, we opt out of using convolutional layers as this would introduce a bias towards local-pixel correlations. Nonetheless we believe that a convolution approach as in Kingma & Dhariwal (2018) is possible, but leave it for future work to explore.

Finally, Neural Spline Flows (NSF) (Durkan et al., 2019) is a family of highly expressive NF architectures, which allow learning highly complex low-dimensional distributions. This, however, comes at the cost of throughput time and makes training very slow. We thus opt for the less expressive, yet still effective, affine coupling layers introduced in Dinh et al. (2017).

The final architecture of EOFLOWS trained on image data is a stack of 8 (EMNIST) or 12 (CelebA) blocks, each consisting of a fixed $D \times D$ rotation/permuation and an affine coupling layer with fully-connected MLPs as parameter networks. The MLP constitutes 3 hidden layers of size 1024 (EMNIST) or 3072 (CelebA). After the final block we add one learnable $D \times D$ rotation matrix to ensure thorough mixing between all (latent) dimensions. Most importantly, Maximum Likelihood is invariant to such a rotation of the latent space whereas Maximum Manifold-Likelihood is not.

To summarize, we employ a heavily over-parametrized architecture with fast encoder and decoder throughput times. We believe that in practice, the parameter-count can be reduced by an order of magnitude, either by using less blocks with smaller MLP hidden layers, which showed comparable performance in early tests, or by using biased subnetworks such as convolutions or Transformers.

E.2. Training setup

EMNIST/Entangled Digits The data is normalized to $[0, 1]$. We use the AdamWScheduleFree (Defazio et al., 2024) optimizer with a learning rate of $1e - 3$. We use a batchsize of 1024 and train each run for 23400 steps.

CelebA The data is normalized to $[0, 1]$, center cropped and downsampled, using Lanczos, to a resolution of $D = 28 \times 28 \times 3 = 2352$, as outlined in the following pseudocode

Listing E.1. CelebA data preparation

```
from torchvision import transforms
from torchvision.transforms.v2 import functional as F, InterpolationMode, Transform

class CenterCrop(Transform):
    _v1_transform_cls = _transforms.CenterCrop

    def __init__(self, size: Union[int, Sequence[int]]):
        super().__init__()
        self.size = _setup_size(size, error_msg="Please provide only two dimensions (h, w)
            for size.")

    def _transform(self, inpt: Any, params: Dict[str, Any]) -> Any:
        return self._call_kernel(F.center_crop, inpt, output_size=self.size)

class Crop(Transform):
    _v1_transform_cls = _transforms.CenterCrop

    def __init__(self, top: int, left: int, height: int, width: int):
        super().__init__()
```

```

        self.top = top
        self.left = left
        self.height = height
        self.width = width

    def __transform(self, inpt: Any, params: Dict[str, Any]) -> Any:
        return self.__call_kernel(F.crop, inpt, top=self.top, left=self.left, height=self.
        height, width=self.width)

CelebA_transform = transforms.Compose([
    CenterCrop(178),
    Crop(43, 33, 112, 112),
    transforms.Resize((28, 28), interpolation=InterpolationMode.LANCZOS),
    transforms.ToTensor(),
])
    
```

We use a batchsize of 2352, i.e. the dimensionality of the data, which requires substantial GPU memory. We use the AdamWScheduleFree (Defazio et al., 2024) optimizer with 100 warm-up steps and a base learning rate of $3e-4$. After training for 100k steps, we decrease lr to $3e-5$ and finetune for another 50k steps. A single run finishes in $\approx 45h$ on a single NVIDIA RTX 4090 (24GB).

E.3. EMNIST vs MNIST Results

We trained once on EMNIST and once on MNIST, for 232k steps each with noise level $\sigma_\epsilon = 0.01$ and $\lambda_{TC} = 0.1$.

In fig.(E.1) we plot the Jacobian column vectors averaged over a batch of data samples $\mathbb{E}_x [J_i(f(x))]$ for the 100 most important dimensions. A similar technique was employed in Galperin & Koethe (2025). One can find multiple latents depicting horizontally/vertically aligned artifacts in EMNIST which are not found in MNIST.

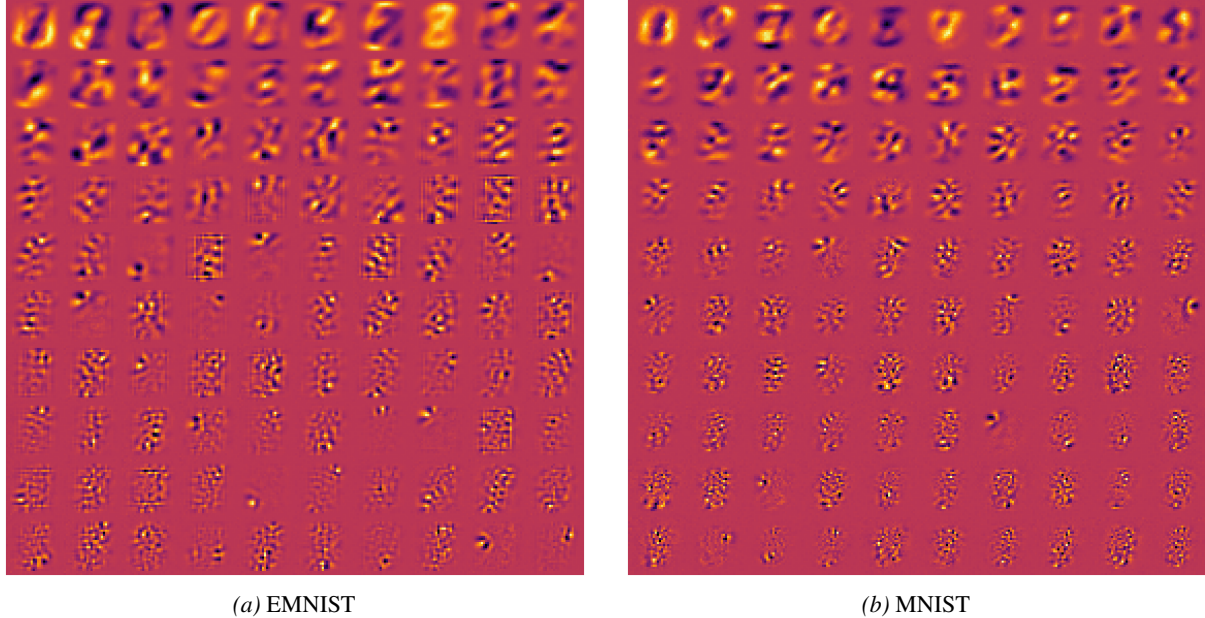


Figure E.1. Depiction of curvilinear coordinates \mathbf{u}_i by plotting averaged Jacobian column vectors $\mathbb{E}_x [J_i(f(x))]$. Plots show the 100 most important dimension, from top left to bottom right, learned by EOFlow models trained once on EMNIST (left) and once on MNIST (right). Each individual image is normalized to $[0, 1]$ for increased contrast.

E.4. Entangled Digits Results

We create the Entangled Digits dataset by sampling a digit "0" $\mathbf{x}^{\{0\}}$ and a digit "1" $\mathbf{x}^{\{1\}}$ from the EMNIST digits dataset and mixing them as

$$\mathbf{x}^{\{01\}} = \alpha \mathbf{x}^{\{0\}} + (1 - \alpha) \mathbf{x}^{\{1\}} \text{ with } \alpha \sim \mathcal{U}_{[0,1]} \quad (\text{E.1})$$

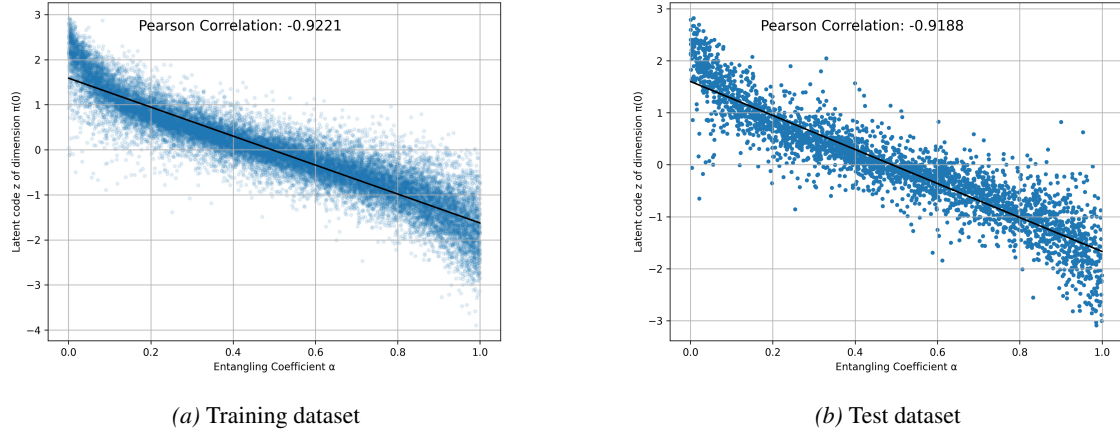


Figure E.2. Correlation plot of z_0 (y-axis) vs α (x-axis) for "clean" entangled data samples.

At training time we additionally inflate each sample with noise:

$$\mathbf{x}_\epsilon^{\{01\}} = \mathbf{x}^{\{01\}} + \sigma_\epsilon \cdot \boldsymbol{\epsilon} \quad \text{with } \boldsymbol{\epsilon} \sim \mathcal{N}(\mathbf{0}, \mathbf{I}_D) \quad (\text{E.2})$$

In fig.(E.2) we plot the correlation plots of the 0-th latent code $z_0 = \mathbf{f}_0(\mathbf{x}^{\{01\}})$ vs α for "clean" samples $\mathbf{x}^{\{01\}}$ once for the training dataset and once for the test set.

E.5. CelebA Results

E.5.1. SMOOTHED VISUALIZATION

As we work with relatively low resolution images, we upscale all CelebA images using Lanczos interpolation before plotting which greatly improves visibility and interpretation.

E.5.2. TRAINING DATA

In fig.(E.3) we show a random batch of training samples, both original i.e. clean and inflated. The models are exclusively trained on inflated samples whereas clean ones are only used to asses the models performance at inference time.



(a) Original/clean data

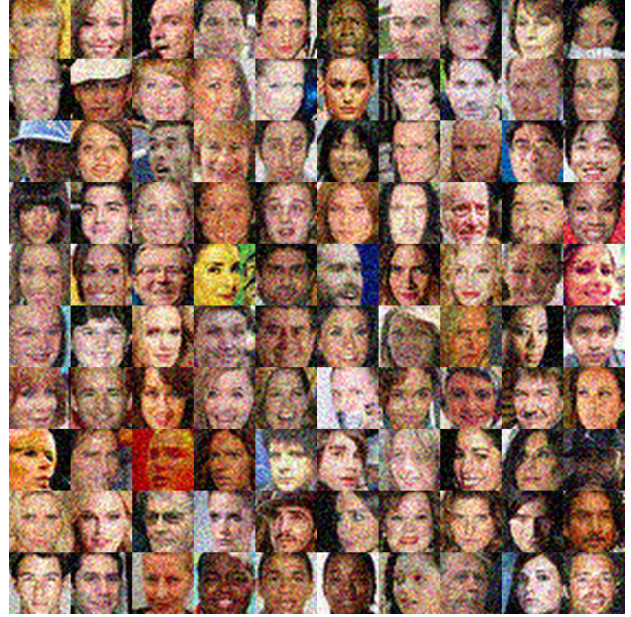

 (b) Inflated/noisy data with $\sigma_\epsilon = 0.1$ used to train EOFFlows

Figure E.3. CelebA samples

E.5.3. GENERATING SAMPLES THROUGH A BOTTLENECK

As EOFFlows learn a meaningful ordering of the inflated data from core to detail, it is possible to sample from the core prior and set the detail latents to their mean, i.e. to zero. This artificial bottleneck resembles an injective model, which should only generate "clean" samples i.e. with little to no noise:

$$\mathbf{x} = \mathbf{g}(\mathbf{z} = [\mathbf{z}_{\mathbb{C}}, \mathbf{z}_{\mathbb{D}}]), \quad \mathbf{z}_{\mathbb{C}} \sim p_{\mathbb{C}}(\mathbf{Z}_{\mathbb{C}}), \mathbf{z}_{\mathbb{D}} = \mathbf{0} \quad (\text{E.3})$$

In fig.(E.4) we show a random batch of generated "clean" samples from EOFFlows with a bottleneck of $C = 50$.

As the model without regularization, i.e. $\lambda_{\text{TC}} = 0$, did not learn to properly differentiate between core and detail information, a bottleneck of \mathbb{C} does not have any meaningful effect. Thus, in practice, one can only hope to generate samples from the full data distribution, i.e. strongly noised data samples resembling fig.(E.3b).


 (a) $\lambda_{TC} = 0.01$

 (b) $\lambda_{TC} = 0.1$

 (c) $\lambda_{TC} = 1.0$


(d) PCA

 Figure E.4. Generated samples using a bottleneck of $C = 50$ of EOFflows and PCA.

Unsupervised Disentanglement with Entropy-Ordered Flows

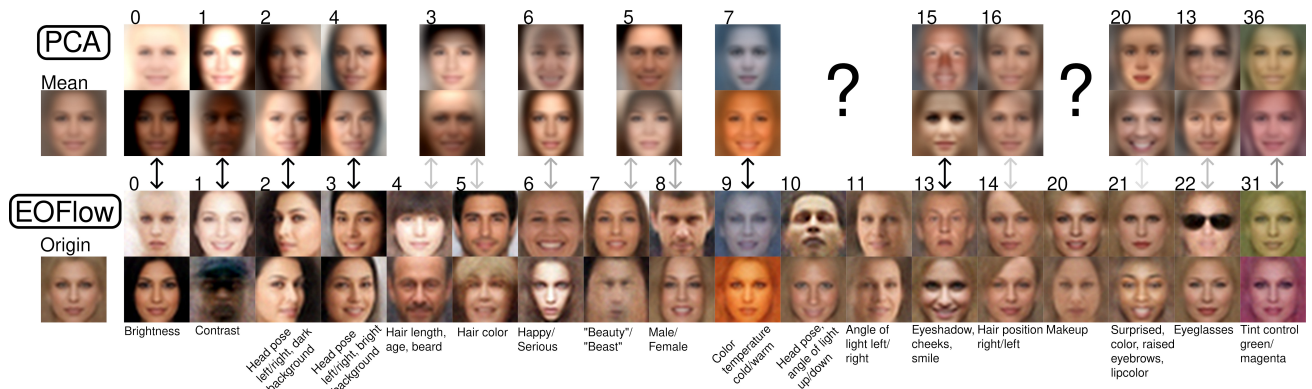


Figure E.5. Archetypes of latent features in PCA (top) vs EOFFlow with $\lambda_{TC} = 1.0$ (bottom) on CelebA for selected dimensions, ordered from most important (left) to less important (right) by manifold entropy. Each archetype depicts the extreme deviations of the indicated latent dimensions after altering the latent codes ± 4 from the origin. Most PCA archetypes only vaguely resemble EOFFlow’s analogues. We annotate each archetype by a short semantic description.

E.5.4. ARCHETYPES

In fig.(E.5) we show the archetypes learned by EOFlow with $\lambda_{TC} = 1.0$ where we add a short semantic description to each latent dimension.

For completeness, we show contrast images of archetypes of the 200 most important dimension learned by EOFflows trained on $\lambda_{TC} \in \{0.01, 0.1, 1.0\}$ and that of PCA, which are plotted in fig.(E.6, E.7, E.8, E.9).

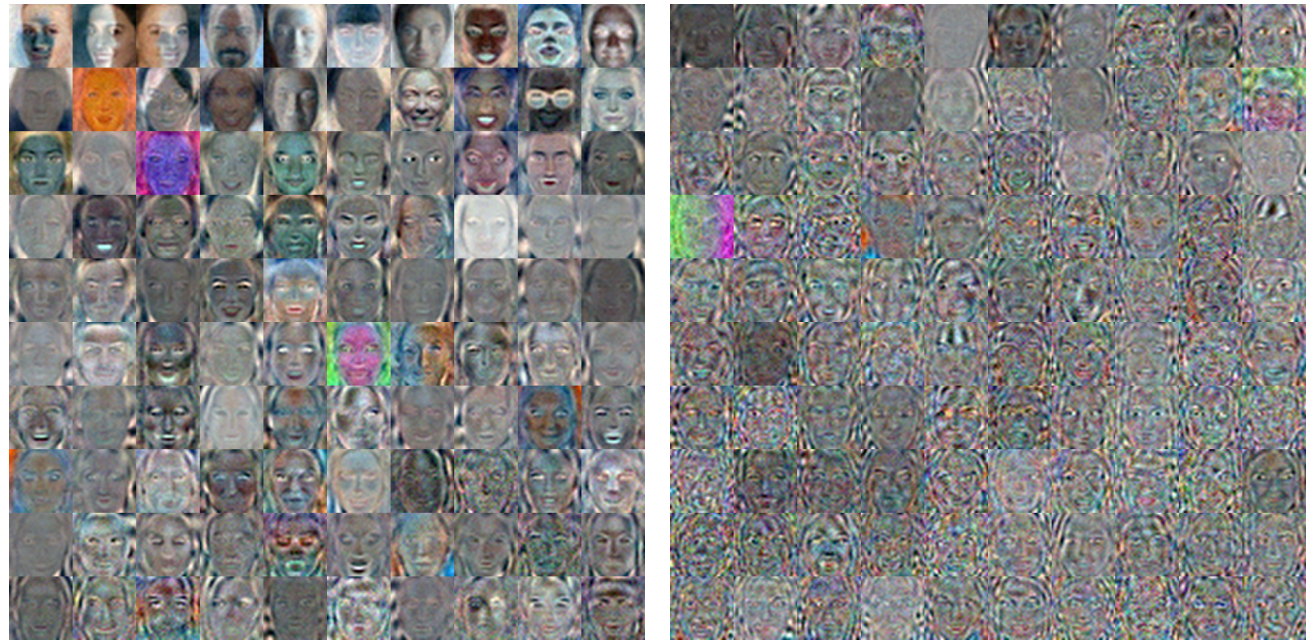


Figure E.6. Archetypes of the 200 most important dimension learned by EOFlow trained on $\lambda_{TC} = 0.01$. Each individual archetype image shows the difference image between the latent extremes ± 4 and is normalized individually to be in $[0, 1]$ for increased contrast. Left: 0-99 from top left to bottom right. Right: 100-199 from top left to bottom right.

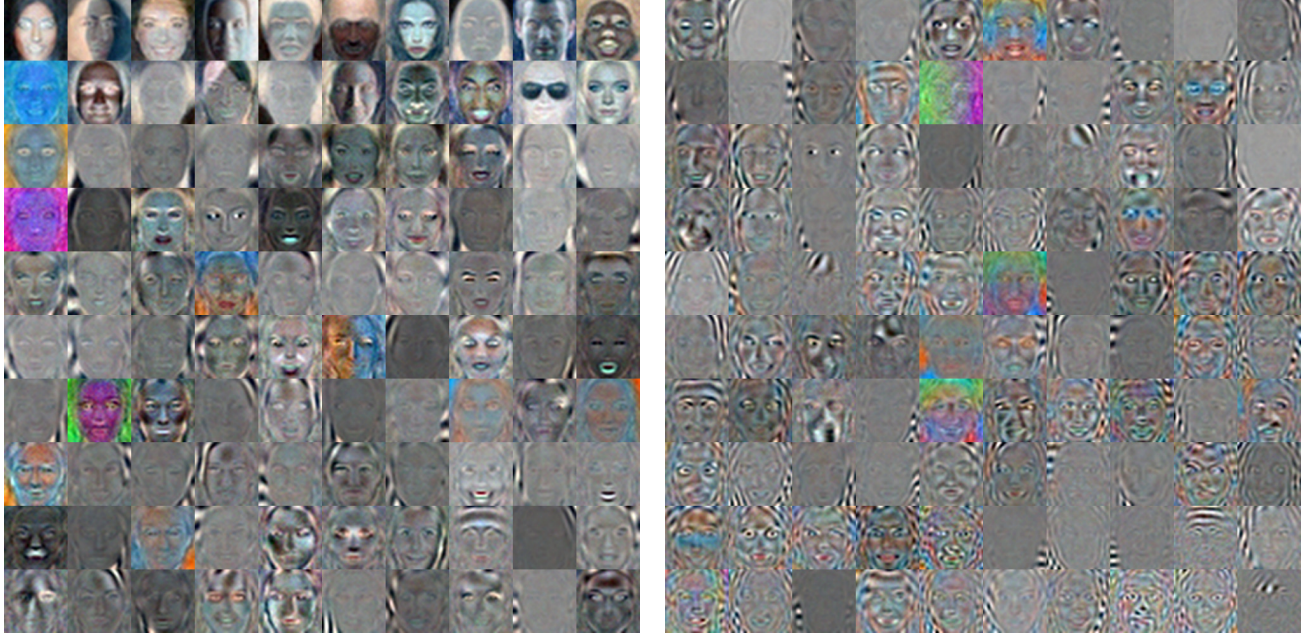


Figure E.7. Archetypes of the 200 most important dimension learned by EOFlow trained on $\lambda_{TC} = 0.1$. Each individual archetype image shows the difference image between the latent extremes ± 4 and is normalized individually to be in $[0, 1]$ for increased contrast. Left: 0-99 from top left to bottom right. Right: 100-199 from top left to bottom right.

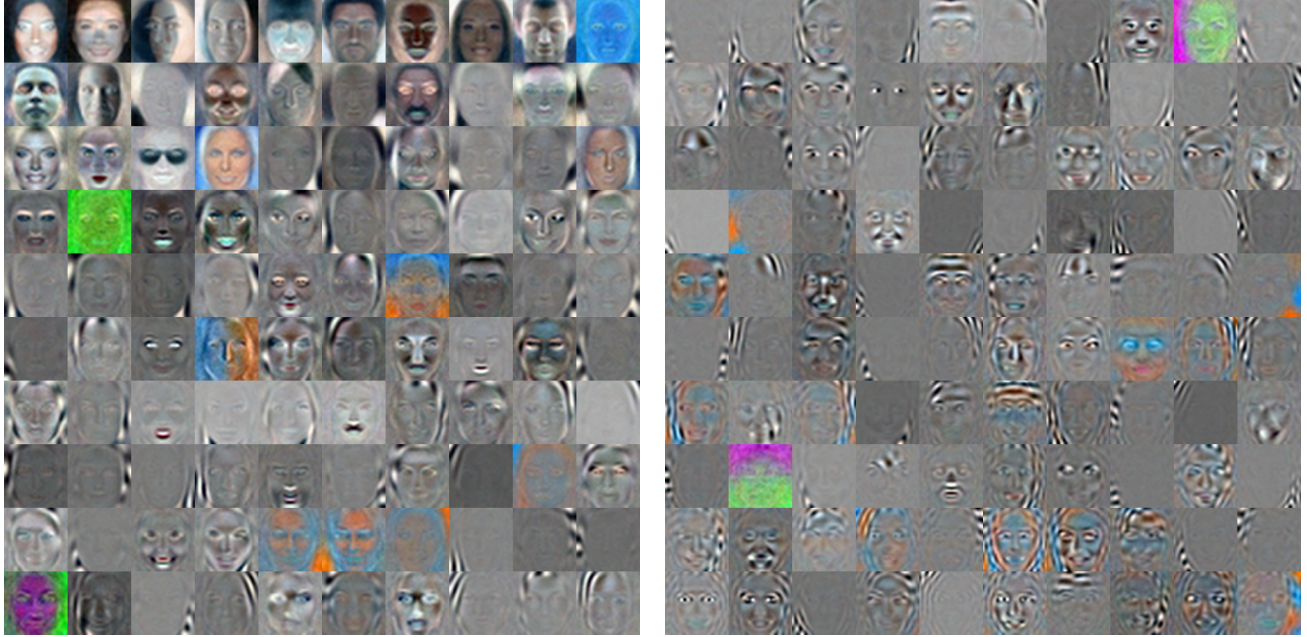


Figure E.8. Archetypes of the 200 most important dimension learned by EOFlow trained on $\lambda_{TC} = 1$. Each individual archetype image shows the difference image between the latent extremes ± 4 and is normalized individually to be in $[0, 1]$ for increased contrast. Left: 0-99 from top left to bottom right. Right: 100-199 from top left to bottom right.

E.5.5. RECONSTRUCTIONS

Here we show the ability of EOFlows to reconstruct inflated training data from a dynamic bottleneck, determined by a bottleneck size of $C \in \{5, 10, 20, 50, 100, 500\}$. The model deflates inflated data samples back onto a learned core manifold \mathcal{M}_C by removing the detail code z_D , i.e. setting it to zero.

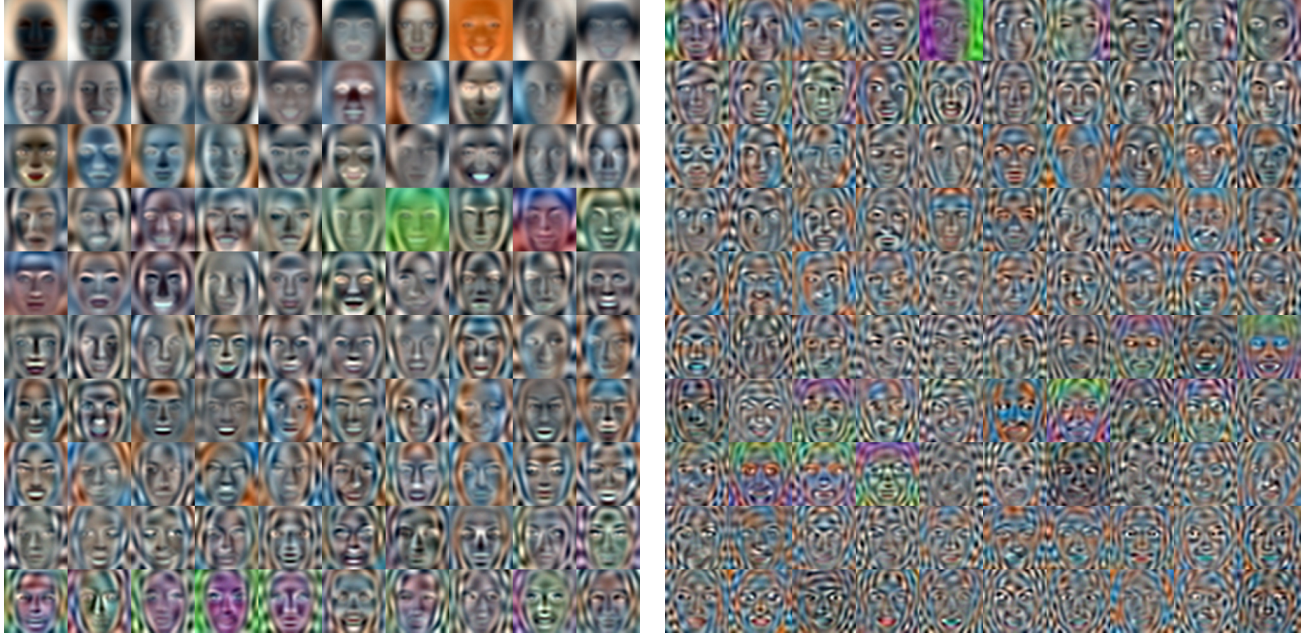


Figure E.9. Archetypes of the 200 most important dimension found by PCA. Each individual archetype image shows the normalized eigenvector, normalized individually to $[0, 1]$ for increased contrast. Left: 0-99 from top left to bottom right. Right: 100-199 from top left to bottom right.

In fig.(E.10a) we see that the model trained without regularization is not able to faithfully reconstruct the input data through a bottleneck as the information is encoded uniformly over its 2352 latent dimensions.

In fig.(E.10b, E.11a, E.11b) we see that EOFFlows regularized with Total Disentanglement learn to reconstruct the input data with a small number of core dimensions C , while denoising the data at the same time. Usually a bottleneck of $C = 50$ is sufficient to obtain a good reconstruction, resembling most of the information present in the clean, i.e not inflated, sample. Reconstructions with too large of a bottleneck, e.g. $C = 500$, become noisier. This is because latent dimensions after some threshold model mostly noise. Thus one picks up too much information from the noisy input.

Finally, we wish to stress, that the models never "sees" clean images during training, as we do not use a reconstruction loss.

E.5.6. EDITING

Here we wish to show how a trained EOFFlow can be used to edit meaningful semantic features of a given image. For this we compute the latent code of a clean (i.e. not noised) data point (sampled from the training set) $\mathbf{z} = \mathbf{f}(\mathbf{x})$ and change a single latent dimension \mathbf{z}_i while fixing all others. This shows the traversal along a single curvilinear coordinate. We choose the EOFFlow trained with $\lambda_{TC} = 0.1$. We do not need to fix a bottleneck dimension and simply pass the altered latent code through the decoder to obtain the edited image. The figures (E.13, E.14) show the edits of 8 random training samples over 5 selected latent dimensions, which have shown to be semantically interpretable.

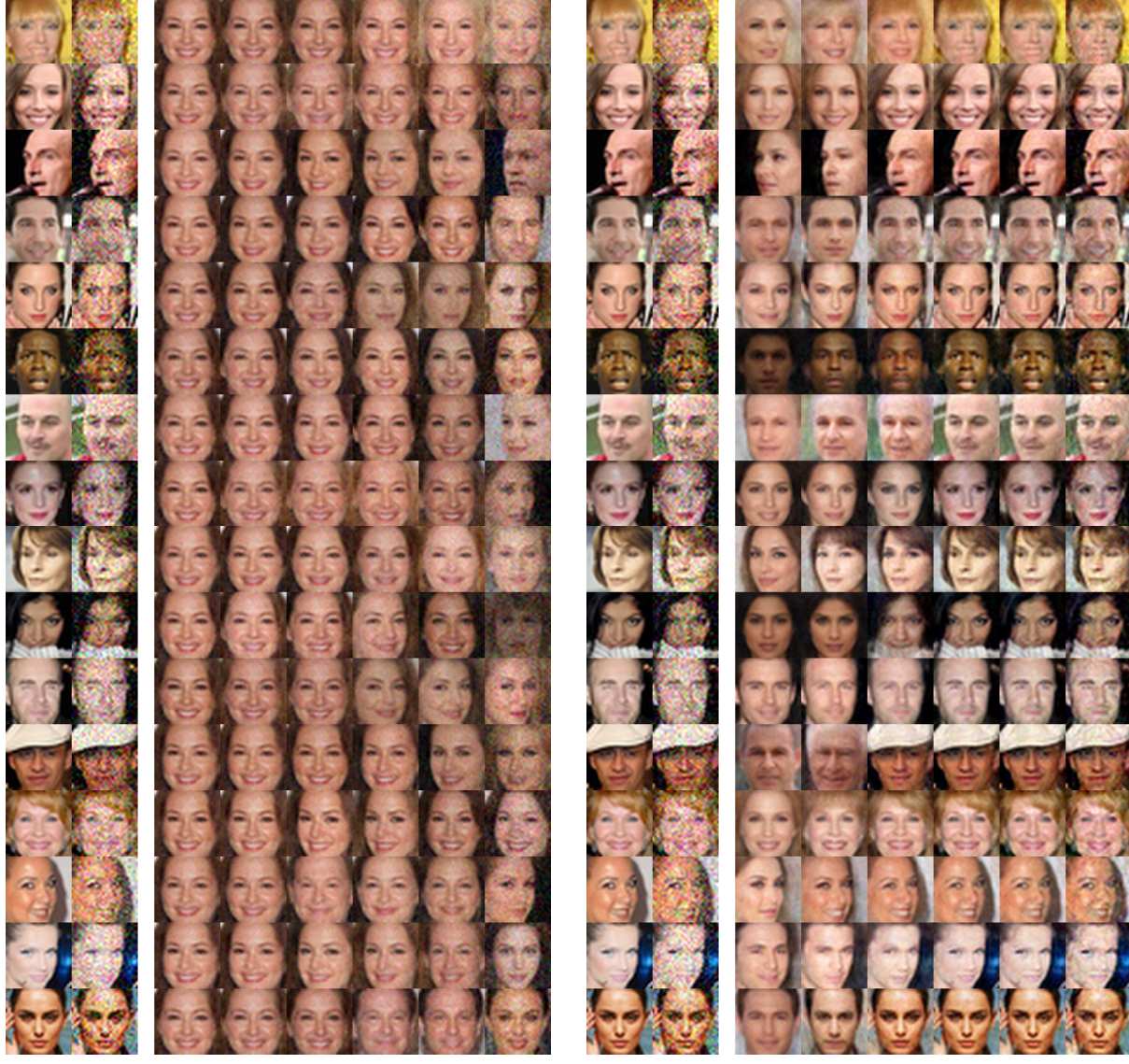
E.5.7. SCORE-BASED DENOISING BY TWEEDIE'S FORMULA

In Loaiza-Ganem et al. (2023) and Zhai et al. (2025) the authors denoise using the score of the NF's density prediction. A "noisy" sample \mathbf{x}_ϵ is denoised by applying the following formula once

$$\mathbf{x} = \mathbf{x}_\epsilon + \sigma_\epsilon^2 \cdot \nabla_{\mathbf{x}_\epsilon} \log(q(\mathbf{x}_\epsilon)) \quad (\text{E.4})$$

E.5.8. RATE-DISTORTION PLOTS

We show rate-distortion curves for all four trained EOFFlows with $\lambda_{TC} \in \{0, 0.01, 0.1, 1.0\}$ and optionally PCA. For this we take 1024 (clean) samples from the training set, inflate them with noise $\sigma_\epsilon = 0.1$ and compute the associated latent codes $\mathbf{z} = \mathbf{f}(\mathbf{x})$. Then, we either zero out the detail part $\mathbf{z}_D = 0$ or resample it from the prior $\mathbf{z}_D \sim p_D(\mathbf{Z}_D)$ and generate the


 (a) Normalizing Flow with $\lambda_{TC} = 0$

 (b) EOFFlow with $\lambda_{TC} = 0.01$

Figure E.10. Reconstructions of training data for model a) (left block) and model b) (right block). The two leftmost rows show original and inflated data samples respectively. The subsequent rows show the reconstruction of the inflated data with a bottleneck of $C = \{5, 10, 20, 50, 100, 500\}$ from left to right.

associated reconstructions \mathbf{x}_{rec} . Finally, we compute the Peak signal-to-noise ratio (PSNR) from sample to the reconstruction and perform this for bottleneck sizes $C \in \{1, \dots, D\}$. Results can be observed in fig.(E.15). If we shift the rate-distortion curve of the zeroed $\mathbf{z}_{\mathbb{D}}$ reconstructions down by 3db (more precisely if we half the reconstruction error), we obtain a lower bound on the curve with resampled $\mathbf{z}_{\mathbb{D}}$. Ultimately this verifies the bound in Theorem 2 in [Blau & Michaeli \(2019\)](#). It states that one can attain perfect perceptual quality without increasing the rate, i.e. if we sample the details $\mathbf{z}_{\mathbb{D}}$ from the full prior distribution $p_{\mathbb{D}}$, by sacrificing no more than a 2-fold increase in the MSE.

Additionally to PSNR, we also compute the structural similarity index measure (SSIM), which is a better distance metric for comparing images. Here we only zero out the detail part, thus we denote the bottleneck reconstruction by $\phi(\cdot)$ s.t.

$$\phi(\mathbf{x}) = \mathbf{g}(\mathbf{z} = [\mathbf{z}_C = \mathbf{f}_C(\mathbf{x}), \mathbf{z}_{\mathbb{D}} = 0]) \quad (\text{E.5})$$

We compute the SSIM between inflated data samples and their reconstruction which we denote by $SSIM(\mathbf{x}_{\text{infl}}, \phi(\mathbf{x}_{\text{infl}}))$, the SSIM between original data samples and their reconstructions which we denote by $SSIM(\mathbf{x}_{\text{clean}}, \phi(\mathbf{x}_{\text{clean}}))$ and the SSIM

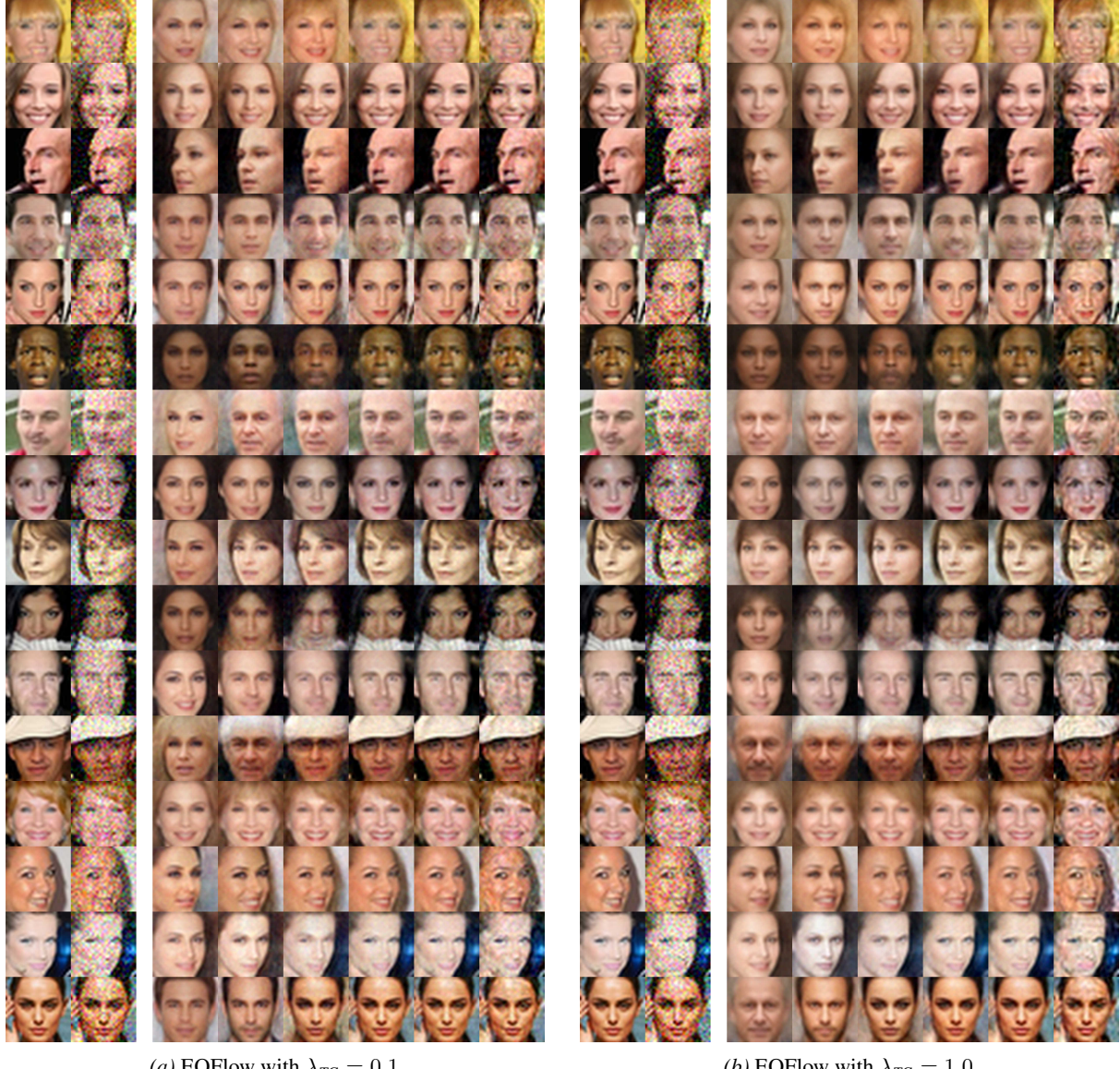


Figure E.11. Reconstructions of training data for model a (left block) and model b (right block). The two leftmost rows show original and inflated data samples respectively. The subsequent rows show the reconstruction of the inflated data with a bottleneck of $C = \{5, 10, 20, 50, 100, 500\}$ from left to right.

between original data samples and the reconstructions of the inflated counterpart which we denote by $SSIM(\mathbf{x}_{\text{clean}}, \phi(\mathbf{x}_{\text{infl}}))$. Results can be observed in fig.(E.16).

E.5.9. MANIFOLD PAIRWISE MUTUAL INFORMATION PLOTS

As shown in Galperin & Koethe (2025), one can asses the "residual entanglement" of latent dimensions in a trained generative model by computing the Manifold Pairwise Mutual Information (MPMI) \mathcal{I}_{ij} , which is the manifold mutual information between individual latent dimensions $\mathcal{I}(\mathbf{U}_i, \mathbf{U}_j)$:

$$\mathcal{I}_{ij} := \mathcal{I}(\mathbf{U}_i, \mathbf{U}_j) = \mathbb{E}_{\mathbf{z}} [\log(q_{i \perp j}(\mathbf{x} = \mathbf{g}(\mathbf{z})))] = \mathbb{E}_{\mathbf{z}} [\log |\mathbf{J}_i(\mathbf{z})| + \log |\mathbf{J}_j(\mathbf{z})| - \log |\mathbf{J}_{\{i,j\}}(\mathbf{z})|] \quad (\text{E.6})$$

where $\mathbf{J}_{\{i,j\}}$ denotes the submatrix of \mathbf{J} with column vectors of indices i and j . Moreover, \mathcal{I}_{ij} is symmetric and undefined for $i = j$.

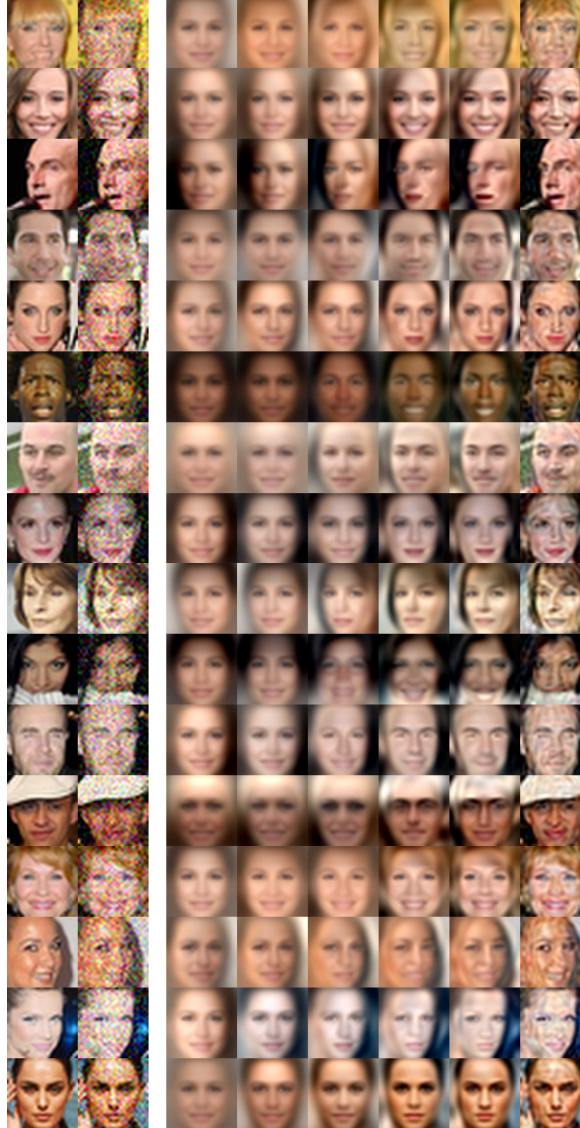


Figure E.12. Reconstructions of training data on PCA. The two leftmost rows show original and inflated data samples respectively. The subsequent rows show the reconstruction of the inflated data with a bottleneck of $C = \{5, 10, 20, 50, 100, 500\}$ from left to right.

As was shown in Galperin & Kothe (2025) it can be related to the Cosine Similarity between Jacobian column vectors. Thus it is a measure of how orthogonal individual curvilinear coordinates are to each other. By regularizing with Total Disentanglement we aim to decrease \mathcal{I}_{TC} , and thus indirectly regularize $\mathcal{I}(\mathbf{U}_i, \mathbf{U}_j)$ as well. In the limit, a flow with a perfectly orthogonal curvilinear coordinate system has $\mathcal{I}_{ij} = 0 \forall i \neq j$. It is thus easy to see that PCA, which constructs a orthogonal affine coordinate system, has a MPMI of exactly zero everywhere.

In fig.(E.17) we plot the MPMI matrices of EOFflows trained with different $\lambda_{\text{TC}} \in \{0, 0.01, 0.1, 1.0\}$ for the first 200 latent dimensions. We observe that the matrix entries decrease overall with increasing λ_{TC} regularization, which is expected. Interestingly, the largest contribution of "activations" \mathcal{I}_{ij} is dominated at the most important dimensions i, j and decreases quickly for larger dimensions. This means that curvilinear coordinates \mathbf{u}_i with a manifold entropy greatly above the noise level $H_i >> H_{\sigma_\epsilon}$ can not be made perfectly orthogonal to others. On the other hand, curvilinear coordinates which encode mostly noise $H_i \approx H_{\sigma_\epsilon}$ can be made perfectly orthogonal to each other. This peculiarity could hint at the origin of the tradeoff between DenL and DisL more generally. Some "residual entanglement" might be necessary such that the model retains some flexibility to approximate the ground truth pdf by its push-forward density. A perfectly disentangled model on the other hand is too expressive and can not represent the data well. In the extreme case a linear model, i.e. PCA,

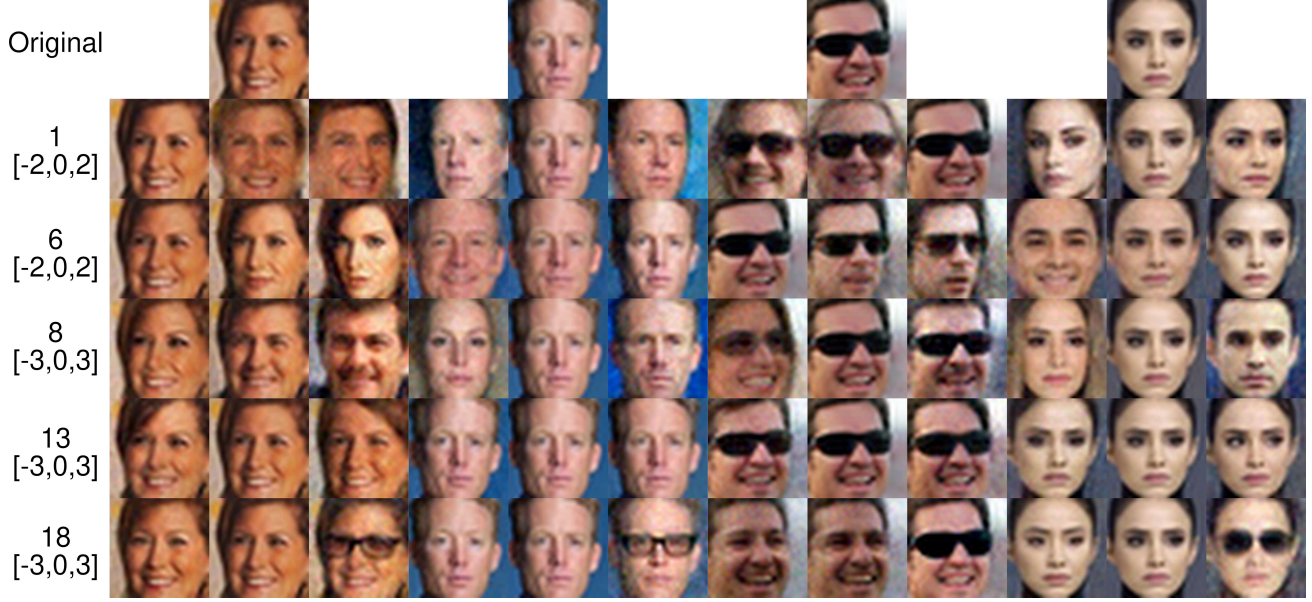


Figure E.13. Latent edits of a single latent dimension z_i create meaningful interpolations for a given original input image (top). We show edits of the dimensions $\{1, 6, 8, 13, 18\}$ (top to bottom) where the respective latent variable is set to either one of three values (noted in brackets) sweeping left to right (per column).

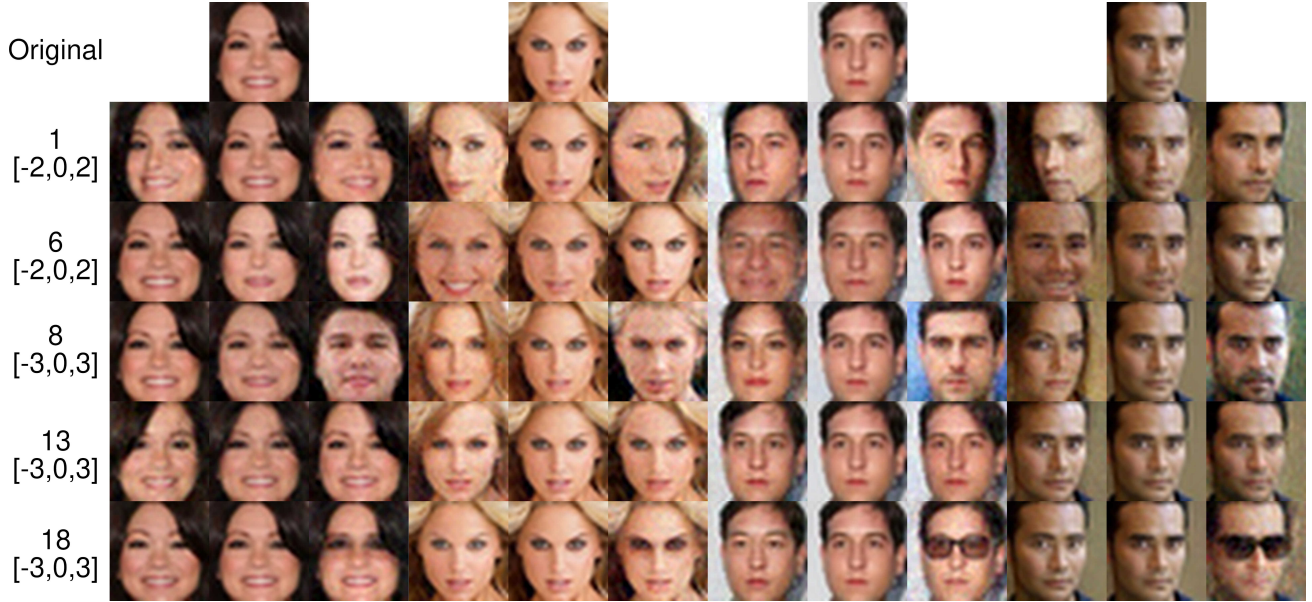


Figure E.14. Latent edits of a single latent dimension z_i create meaningful interpolations for a given original input image (top). We show edits of the dimensions $\{1, 6, 8, 13, 18\}$ (top to bottom) where the respective latent variable is set to either one of three values (noted in brackets) sweeping left to right (per column).

can not adapt to non-linear data manifolds. Interestingly, these higher-order correlations can be mostly concentrated in the core representation as shown in the MPMI plots, thus a well compressed representation is not necessarily at odds with a disentangled one.

E.5.10. CORRELATION WITH CELEBA ATTRIBUTES AND LANDMARKS

We show how each learned feature of EOFows matches the biases of the CelebA dataset. For this we compute the correlations between latent activations, i.e. $f_i(x)$, and CelebA features, given by 40 binary attributes and 10 float landmarks.

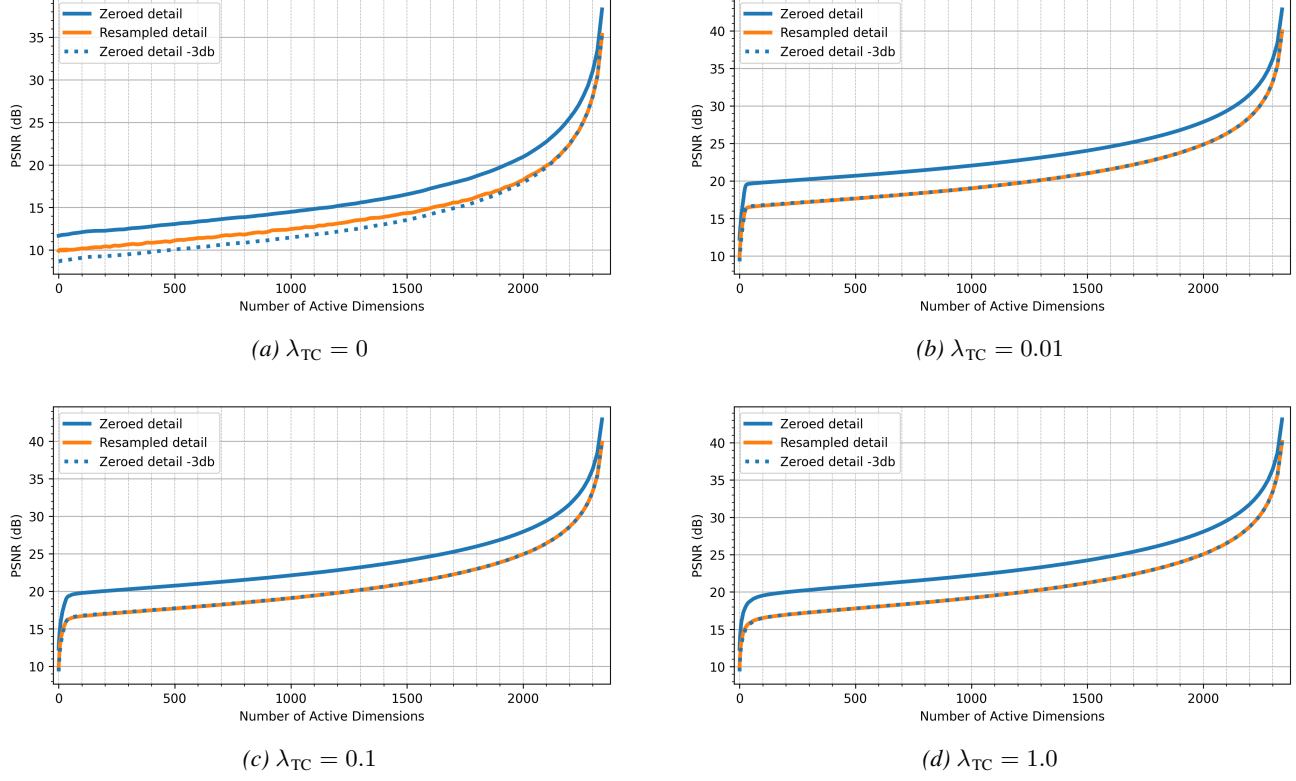


Figure E.15. Rate-distortion plots using PSNR as distortion metric.

In fig.(E.18) we plot the correlation matrix between all CelebA features and the latent activations of the 50 most important latent dimensions of EOFlow trained on $\lambda_{TC} = 0.1$ as a representative example. Some latents correlate highly with distinct features, such as $i = 1$ and $i = 9$, which rotate the pose of the head horizontally and vertically. Other latents do not appear to correlate at all with CelebA features, such as $i = 3$ or $i = 10$. Comparing to fig.(E.7) we can see that the 3th dimension resembles how the angle of light changes from left to right and the 10th dimension only regulates the color temperature, which are both not described by any CelebA features.

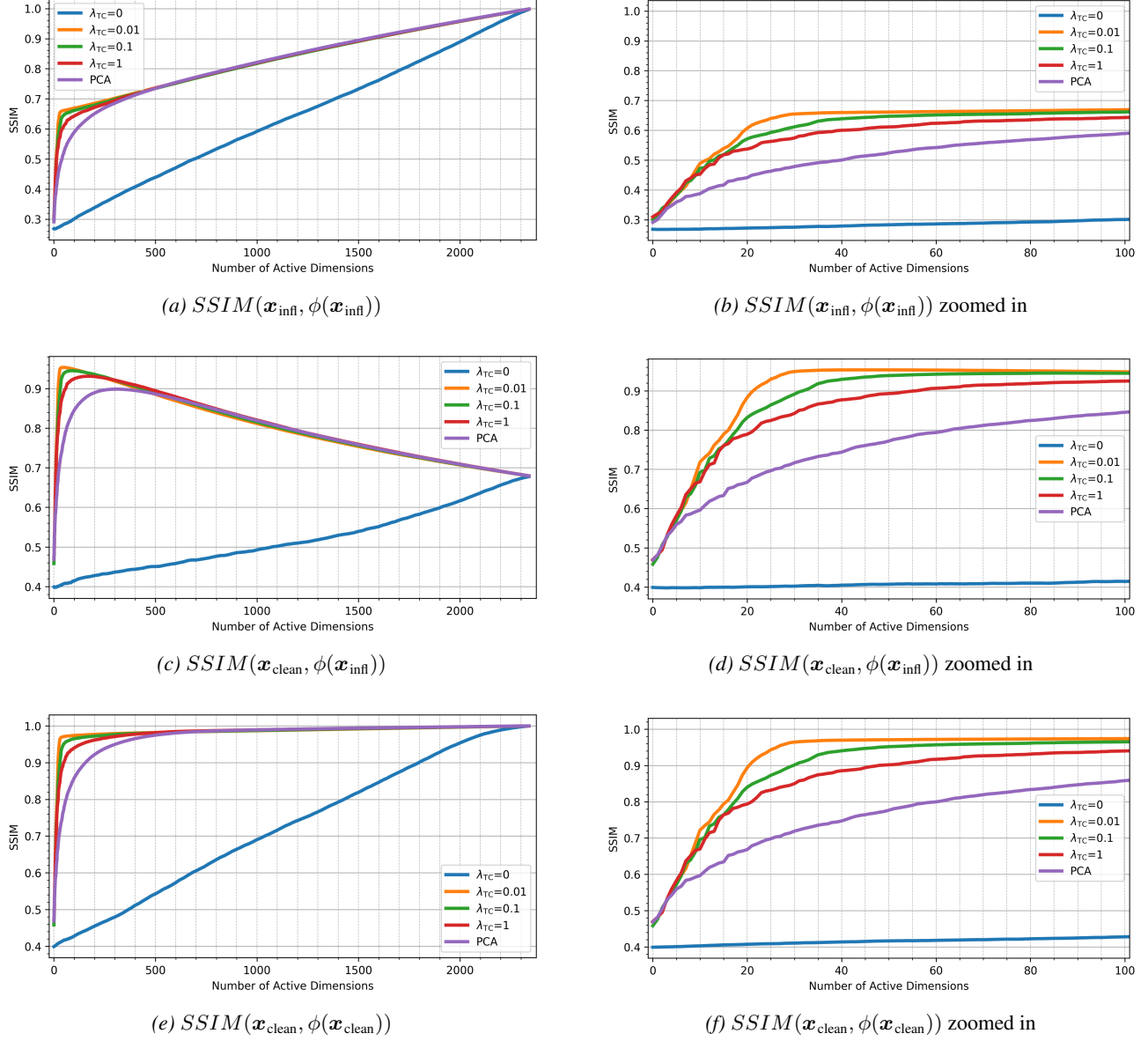


Figure E.16. Rate-distortion plots using SSIM as distortion metric.

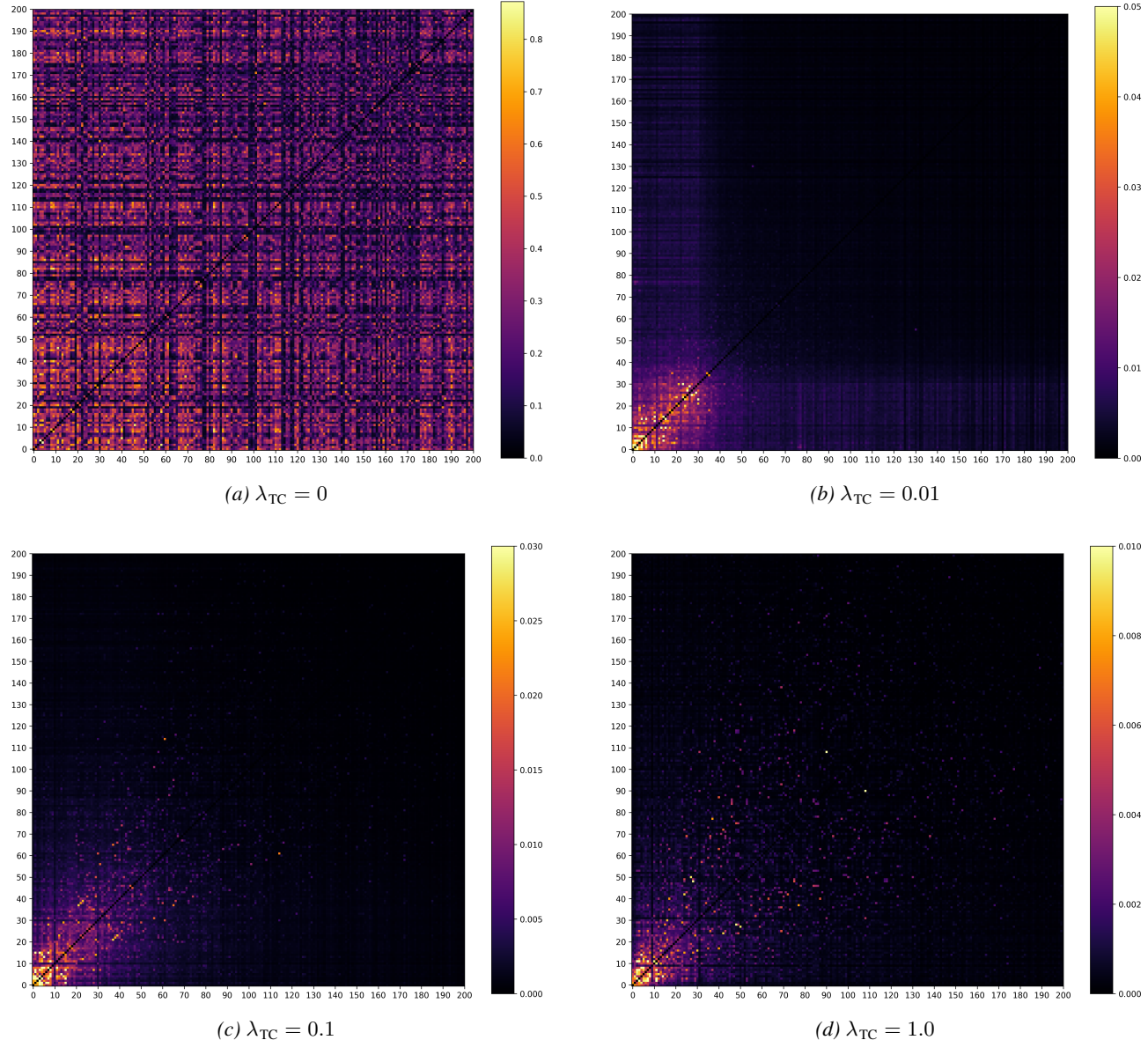


Figure E.17. Manifold Pairwise Mutual Information plots of EOFflows, plotted for the 200 most important latent dimensions.

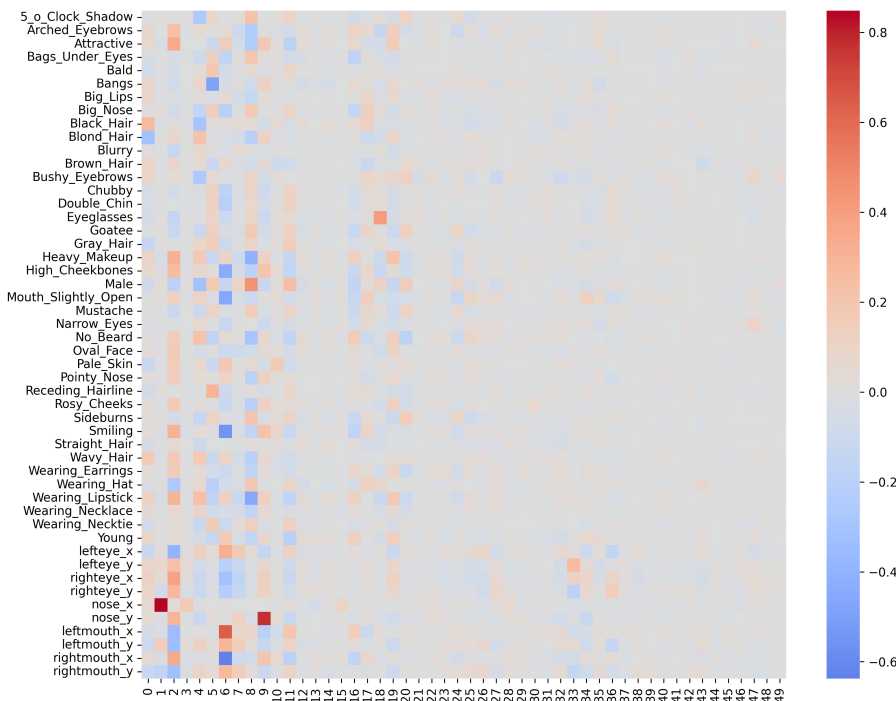


Figure E.18. Correlation matrix between attributes+landmarks of CelebA and feature activations of the 50 most important latent dimensions found by EOFlow with $\lambda_{TC} = 0.1$.